Diagnostic and Statistical Modelling Techniques Applied to an Aluminium Plasma Etch Process.

Thesis submitted by

James Robertson Hannah

for the degree of

Doctor of Philosophy

Edinburgh Microfabrication Facility,

Department of Electrical Engineering,

University of Edinburgh,

Scotland.

1992

Abstract

Dry etching processes are crucial to the fabrication of VLSI and ULSI circuits and are likely to continue so for the foreseeable future. However, the technique remains difficult to implement and is not well understood. To a great extent, this is a result of the use of novel machine configurations and chemical recipes which are employed far in advance of any real understanding of the interactions occurring within the process chamber. Historically, process development in this field has proceeded as a result of improvements in vacuum technology coupled to empirical one-dimensional trend analyses.

These traditional approaches to process development have become severely limited with the advent of ULSI. This project addressed the requirement for improved process characterisation by investigating diagnostic techniques and rigorous statistical modelling as applied to one of the most challenging leading edge processes: the $BCl_3/Cl_2/He$ dry etching of aluminium alloys.

Optical emission spectroscopy, electrostatic Langmuir probes and mass spectrometry were used to investigate the dry etch behaviour. During this research, a novel in-situ SIMS implementation of the mass spectrometer was used to investigate plasma generated positive ions. Details of detected ions and intensities during etching are presented.

A CCF experimental design was formulated from the major RIE machine parameters of rf power, system pressure and $\%Cl_2/BCl_3$. The final quadratic model covered 3 manipulated machine variables, 3 process parameters and 6 performance parameters. This is the first time that rigorous statistical modelling techniques have been applied to the $BCl_3/Cl_2/He$ based process or to an aluminium dry etch process in order to systematically characterise both the process and performance behaviour. This work presents these models, along with an estimate of each model's accuracy.

Declaration

I declare that this thesis has been completed by myself and that the research documented in this thesis is entirely my own except where indicated to the contrary.

James Robertson Hannah

Acknowledgements

I would like to thank absolutely everybody under the sun, and especially all those who have been remotely helpful during this period of mental torment in my life.

Particular thanks are definitely due to my parents who provided much needed encouragement and support during the course of this work. Perhaps my days as an eternal student are finally over! Much credit is also due to my supervisor, Bob Holwill, for his many useful project discussions, most notably when they coincided with lunch!

LaTeX help to format this thesis was consistently provided by Robin Smith. Also the good humoured support of all the EMF technicians, staff and PhD students with cleanroom processing and equipment is gratefully acknowledged.

Cheers to the many people who took me for a drink when it was most needed, including Steve Hudson, Iain Gardner, Tony O'Hara, Morag McKelvie, Chris Clarke, Sandy Alexander and Alex Watt. Dewi Williams provided displacement activities in the form of mountaineering. Hercules Neves cannot be thanked enough for his dedication to conversation and good food. Thanks to the many other people who helped me and have not been mentioned so far ... you know who you are!

Table of Contents

1. Overview 1

1.1 Background 1

1.2 Lithographic Process 3

1.2.1 Etching 4

1.3 Project Rationale 6

1.4 Thesis Structure 8

2. Reactive Plasma Etching **10**

2.1 Introduction 10

2.2 Plasma Properties 11

2.2.1 DC Plasma Excitation 13

2.2.2 AC Plasma Excitation 15

2.3 The General Reactive Plasma Etch Process 20

2.3.1 The Basic Mechanisms of Plasma Etching 21

2.3.2 Reactor Configurations 23

2.3.3 The Choice of Gas Chemistry 26

2.3.4 The Role of Gas Additives 27

2.3.5 The Etchant-Unsaturate Concept 29

2.3.6 Aluminium Etching 31

2.4 The Plasma Etch Parameter Space 34

2.4.1 Pressure 35

2.4.2 Flow Rate 37

2.4.3 Power 37

2.4.4 Excitation Frequency 38

2.4.5 Temperature 40

2.4.6 Chamber Dimensions 40

2.5 Plasma Etch Process Characterisation 42

2.5.1 Anisotropy 42

2.5.2 Selectivity 43

2.5.3 Uniformity 45

2.5.4 Loading Effect 45

2.5.5 Throughput 47

2.5.6 Defects, Impurities and Surface Roughening 47

2.5.7 Radiation Damage 48

2.6 Equipment Trends in Plasma Etching 50

2.7 Summary 51

3. Diagnostic Techniques for Plasma Characterisation **53**

3.1 Introduction 53

3.2 Optical Emission Spectroscopy 55

3.2.1 Actinometry 58

3.3 Mass Spectrometry 59

3.4 Langmuir Probes 62

3.5 Microwave Interferometry 67

3.6 Laser Induced Fluorescence 68

3.7 Optical Reflection 68

3.8 Other Techniques 69

3.9 Summary 70

4. Modelling Strategies for Plasma Etch Processes **71**

4.1 Introduction 71

4.2 The Choice of Model 72

4.3 Statistical Model Building 74

4.3.1 Statistical Process Models 77

4.4 Mechanistic Model Building 79

4.4.1 Mechanistic Process Models 79

4.5 Summary 80

5. Experimental Setup and Characterisation **81**

5.1 Introduction 81

5.2 RIE System Description 82

5.3 Optical Emission Spectroscopy 85

5.3.1 Intensity Variations with Machine Parameters 87

5.4 Mass Spectrometry: In-Situ SIMS 91

5.4.1 Tuning 94

5.4.2 Energy Distributions for Argon 97

5.4.3 Intensity Variations with Machine Parameters 99

5.5 Langmuir Probe 101

5.5.1 Plasma Potential Variations with Machine Parameters . . 108

5.6 Summary 110

6. Diagnostic Techniques in a Reactive Gas Chemistry 113

6.1 Introduction 113

6.2 Process Description 114

6.3 Optical Emission Spectroscopy 115

6.4 Mass Spectrometry: In-Situ SIMS 117

6.4.1 The Detection of Ionic Species 117

6.4.2 Aluminium Etch Monitoring 119

6.4.3 Energy Distributions During Etching 129

6.5 Langmuir Probe 130

6.5.1 Plasma Potential Variations with Machine Parameters . . 131

6.6 Summary 134

7. Statistical Process Model 142

7.1 Introduction 142

7.2 Statistical Design for Aluminium Etching 143

7.2.1 Experimental Process Range 144

7.3 Experimental Procedure 146

7.4 Process Models 147

7.4.1 DC Self Bias 148

7.4.2 Interface Times 149

7.5 Performance Models 150

7.5.1 Etch Rate 151

7.5.2 Directionality 152

7.5.3 Selectivity 153

7.6 Induction Time Variations 154

7.7 Summary 155

8. Conclusions **173**

Bibliography **178**

A. Statistical Notes **192**

List of Figures

1–1 Increasing complexity of microprocessors. 3

1–2 Microelectronic device process fabrication sequence. 5

1–3 Isotropic etch profile. 6

1–4 Trends in minimum lithographic resolution (squares) and *advanced* process minimum feature size (triangles) where CP is contact printing; PE represents Perkin Elmer Microalign; GCA represents the GCA 4800 10:1 direct step on wafer (DSW); IL is the ASM i-line DSW; ASM is the planned ASM excimer laser DSW; ASM2 represents the ultimate ASM performance; S1.0 is the SPECTRE objective of 1μm; S0.7 is the SPECTRE objective of 0.7μm; and J is the JESSI objective of 0.3μm. 8

2–1 Schematic view of a typical dc glow discharge at low pressure, showing the most prominent regions. 13

2–2 A schematic view of a rf plasma discharge where the power is supplied through a matching network. 16

2–3 The time resolved potentials which occur for rf plasmas. 18

2–4 The development of negative self bias when a rf signal is capacitively coupled to a plasma. 19

2–5 The four major processes by which dry etching takes place: sputtering; chemical etching; ion-induced energy driven etching; inhibitor protected-sidewall ion-enhanced etching. 22

2–6 Barrel etch reactor with capacitively coupled rf power. 24

2–7 The two most frequently implemented planar etch configurations: plasma etch and reactive-ion-etch. 25

2–8 The influence of oxygen on the normalised etch rate of silicon using a CF_4/O_2 chemistry. Also shown is the normalised intensity of the emission from electronically excited F atoms (703.7nm line) during Si etching. 31

2–9 The parameter problem associated with the plasma etch process, where T_e is the electron temperature; N is the plasma density; V_p is the plasma potential; $f(\varepsilon)$ is the electron energy distribution function; and τ is the gas particle residence time. 35

2–10 Approximate rf plasma equivalent circuit. 38

2–11 Approximate driven electrode and plasma potential waveforms for a glow discharge with grounded chamber walls. R is the ratio of powered electrode to wall area. 41

2–12 Ideal etch profiles for isotropic and fully anisotropic processes, when there is no mask erosion. 43

2–13 For a fully anisotropic process, some overetch is needed to remove residual material at steps. 44

3–1 The three stages involved in a typical mass separation: hot filament ionisation; mass separation using a magnetic sector; and detection with a Faraday cup. 61

3–2 Basic Langmuir probe measuring circuit. 64

3–3 Typical single probe IV characteristic. 65

4–1 A generalised approach to model building. 74

4–2 A contour plot of a typical response surface for a 2-factor process. 75

4–3 Central composite model with three variables. 77

5–1 The EG&G OMA spectrograph setup used for wide spectrum evaluations. 86

5–2 Schematic of the monochromator system used in this work. 88

5–3 Intensity of the 750.4nm argon atomic emission line as rf power is varied, at a pressure of 20mtorr and a flow rate of 6sccm. 89

5–4 Intensity of the 750.4nm argon atomic emission line as chamber pressure is varied, at a flow rate of 6sccm and a power of 50W. . . 90

5–5 Intensity of the argon 750.4nm emission line as the total argon flow rate was varied at a pressure of 20mtorr and a power of 50W. . . 91

5–6 Schematic layout of the QMS system attached to the RIE chamber. 92

5–7 Schematic layout of the QMS probe head. 96

5–8 The energy spectrum of argon positive ions at mass 40. 98

5–9 Intensity of the Ar^+ trace at mass 40, as the glow discharge pressure is varied at 5W power and 3sccm Ar flow rate. 100

5–10 Intensity of the Ar^+ trace at mass 40, as the plasma flow rate is varied at a chamber pressure of 20mtorr and a power of 5W. . . . 101

5–11 Intensity of the Ar^+ trace at mass 40 as the plasma rf power is varied, at a pressure of 20mtorr and a flow rate of 3sccm. 102

5–12 Schematic of a Langmuir probe. 103

5–13 The experimental driven rf feedback Langmuir probe measurement system. 104

5–14 The phase shifting circuit used for Langmuir probe rf feedback. . 105

5–15 Langmuir probe IV characteristics for an argon plasma at 10W power, 52mtorr and 6sccm flow rate. 107

5–16 Argon plasma potential determined from the gradient of the IV curve. 107

5–17 Argon plasma electron temperature. 108

5–18 Plasma potential variations with pressure at a flow rate of 3sccm argon and a forward power of 10W. 110

5–19 Average electron temperature variations with pressure at a flow rate of 3sccm argon and a forward power of 10W. 110

5–20 Plasma potential variations with argon flow rate at a pressure of 20mtorr and a forward power of 10W. 111

5–21 Plasma potential variations with power at a flow rate of 3sccm argon and a system pressure of 20mtorr. 112

6–1 A representation of the Al* emission line at 396.2nm during an etch process. 117

6–2 Positive ion characteristic of a $BCl_3/Cl_2/He$ plasma. 119

6–3 In-situ SIMS monitoring of an aluminium etch showing characteristic intensities during the induction period. 120

6–4 In-situ SIMS monitoring of an aluminium etch showing characteristic intensities during bulk aluminium etching. 120

6–5 In-situ SIMS monitoring of an aluminium etch showing characteristic intensities at the process endpoint (SiO_2 etching). 121

6–6 In-situ SIMS results for a test wafer from batch 1, which was etched using a $BCl_3/Cl_2/He$ plasma. 124

6–7 In-situ SIMS results for a test wafer from batch 2, which was etched using a $BCl_3/Cl_2/He$ plasma. 126

6–8 In-situ SIMS results for a test wafer from batch 2, which was etched using a $BCl_3/Cl_2/He$ plasma. 127

6–9 Depth profiling results of a batch 1 test wafer, using standard SIMS. 128

6–10 Depth profiling results of a batch 2 test wafer, using standard SIMS. 129

6–11 Energy profiles of $^{11}B^{+}$ ions during Al etching. 136

6–12 Energy profile of $^{27}Al^{+}$ ions during the bulk Al etch. 137

6–13 Driven Langmuir probe IV characteristic from a 200W, 60mtorr, BCl_3/Cl_2/He plasma. 137

6–14 Gradient of the Langmuir probe IV characteristic for a 200W, 60mtorr BCl_3/Cl_2/He plasma. 138

6–15 Electron temperature of a 200W, 60mtorr BCl_3/Cl_2/He plasma. . 139

6–16 Plasma potential variation with power in a 60mtorr, 21sccm BCl_3, 11sccm Cl_2, 28sccm He plasma. 139

6–17 Plasma potential variation with pressure in a 200W, 21sccm BCl_3, 11sccm Cl_2, 28sccm He plasma. 140

6–18 Plasma potential variation with BCl_3 flow rate in a 200W, 60mtorr, 11sccm Cl_2, 28sccm He plasma. 140

6–19 Plasma potential variation with Cl_2 flow rate in a 200W, 60mtorr, 21sccm BCl_3, 28sccm He plasma. 141

6–20 Plasma potential variation with He flow rate in a 200W, 60mtorr, 11sccm Cl_2, 21sccm BCl_3 plasma. 141

7–1 CCF design for the experimental characterisation of an aluminium etch process. 144

7–2 Aluminium etch experimental worksheet. 145

7–3 3D statistical model for V_{dcb} during the induction period. 157

7–4 Statistical model contourplots for V_{dcb} during the induction period. 158

7–5 3D statistical model for V_{dcb} during the bulk Al etch. 159

7–6 Statistical model contourplots for V_{dcb} during the bulk Al etch. . 160

7–7 3D statistical model for the induction time. 161

7–8 3D statistical model for the overall metal etch rate. 162

7–9 3D statistical model for the bulk Al etch rate. 163

7–10 3D statistical model for the photoresist etch rate. 164

7–11 Statistical model contourplots for the photoresist etch rate. 165

7–12 SEM etch profile of a highly anisotropic aluminium track. 166

7–13 SEM etch profile of a less anisotropic aluminium track. 166

7–14 Measurements taken on SEM Al track cross-section to estimate the process directionality. 167

7–15 3D statistical model for the etch directionality. 168

7–16 Statistical model contourplots for the etch directionality. 169

7–17 3D statistical model for the etch rate selectivity of bulk Al to photoresist. 170

7–18 3D statistical model for the etch rate selectivity of bulk Al to SiO_2. 171

7–19 RGA monitoring of the H_2O peak at mass 18 during a He plasma. 172

7–20 RGA monitoring of the H_2O peak at mass 18 during a $BCl_3/Cl_2/He$ plasma. 172

List of Tables

1–1 Trends in DRAM microfabrication. 2

2–1 Some typical parameters which are characteristic of a RIE glow discharge process. 26

2–2 Applications of halogen gases for reactive plasma etching in silicon based fabrication. 28

3–1 Common species and emission wavelengths which have been monitored to determine etch process endpoints, where A* indicates a species A in an excited state. 57

3–2 Species which have been employed for endpoint detection and plasma characterisation using mass spectrometry. 62

5–1 QMS variables for ion analysis mode, with some typical values for positive ion extraction 95

6–1 1st ionisation potentials of some plasma species. 122

7–1 Coefficients of process response variables where V_{dcb1} is the self bias during the induction period; V_{dcb2} is the self bias during the bulk Al etch; t_{ind} is the induction time; Pwr is the rf power; Pres is the system pressure and Cl is the $\%Cl_2/BCl_3$ ratio. 148

7–2 Coefficients of performance response variables where ER_{metal} is the overall metal etch rate; ER_{Al} is the bulk Al etch rate; ER_{pr} is the photoresist etch rate; Dir is the directionality; $S_{Al/pr}$ is the bulk Al to photoresist selectivity; S_{Al/SiO_2} is the bulk Al to SiO_2 selectivity; Pwr is the rf power; Pres is the system pressure and Cl is the $\%Cl_2/BCl_3$ ratio. 150

Chapter 1

Overview

1.1 Background

Integrated circuits were first produced in 1959 and the period to the present day has seen a dramatic expansion in the microelectronics industry. Process improvements in fabrication techniques have lead to a steady increase in microcircuit complexity which is illustrated in table 1.1 [1].

Initially the increase in circuit complexity was paradoxically accompanied by a reduction in the cost per circuit element to the customer. This was due to an overall increase in packing density (ie. the number of devices per unit area of silicon) leading to a lower production cost per circuit element which occurred because the overall production costs were determined by the combined area of silicon being processed which was not initially a function of circuit complexity. Another reason for this phenomenon was that IC sales increased dramatically as the technology advanced which also lead to a reduced cost function [2]. Now, however, the cost function is on the increase as can be seen from the cost/die in table 1.1. The driving forces behind this trend are:

- Capital costs are rising faster than sales revenues [3].
- Packaging costs and complexities have increased.
- IC design is a labour intensive activity which is becoming a more significant factor in the overall costings.

	Year				
	1985	1989	1993	1997	2000
DRAM size	256K	1M	4M	16M	64M
Wafer diameter (mm)	150	150	150	200	200
CD (μm)	1.25	1.0	0.7	0.5	0.3
Wafers/year (k)	100	80	70	50	20
Factory cost (M$)	100	250	720	1320	2500
Price/wafer (k$)	1.2	3.75	12.3	31.7	150
Die size (mm^2)	40	70	120	280	600
Yield (%)	90	85	80	70	70
Good die/wafer	400	215	118	78	36
Cost/die ($)	3	17.5	105	406	4200
Cost/bit (mc)	1	1.75	2.6	2.5	6.5

Table 1–1: Trends in DRAM microfabrication.

Also illustrated in table 1.1 are some of the technological trends which are prevalent in the silicon microfabrication industry: smaller feature sizes, larger die sizes and larger diameter wafers. The drive towards smaller feature sizes has resulted in an increase in circuit density as demonstrated in figure 1–1 [4]; a reduction in die area for identical circuit function which results in more ICs per area of silicon. Minimising feature sizes also results in a reduction in stray capacitances and resistances which leads to an improvement in switching speed coupled to a reduction in power consumption. Improved lithographic techniques have allowed the fabrication of larger die sizes which has resulted in greater functionality and hence a higher intrinsic value. There is also a trend towards larger diameter wafers which has produced enormous economic benefits. The number of die increases as the square of the diameter, whereas the increase in fabrication costs is roughly linear [2]. Moving from 150mm to 200mm wafers , when coupled with technological improvements, results in an approximate doubling of productivity [5].

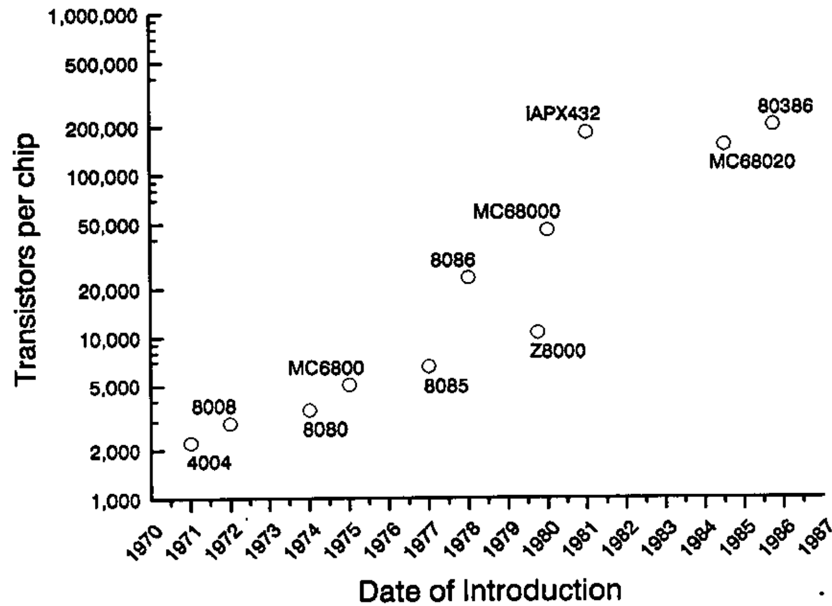

Figure 1–1: Increasing complexity of microprocessors.

1.2 Lithographic Process

An understanding of the basic fabrication sequence is necessary to understand the role of the etch process in the lithographic process. ICs are multilayer devices which are formed using a process sequence such as figure 1–2 [6]. At each iteration of the fabrication process a process layer has to be deposited and then patterned with all the patterns aligned to one another. For a MOS fabrication sequence, a finished device may consist of between 5 and 15 layers which implies 5 to 15 iterative cycles. Deposited materials range in function from conductors (Al, W, polySi) to insulators (SiO_2, Si_3N_4).

Lithography can be described as the process which defines the features and patterns which make up an IC. After a process layer has been deposited on the wafer, a thin film of photo-sensitive material known as photoresist is deposited. Each layer has an associated glass plate, or mask, on which the required design pattern has been previously defined in a thin layer of photographic emulsion or

chromium. The masking pattern is transferred to the photoresist by exposure to ultra-violet light. On development of positive photoresist, the photoresist remains on the wafer surface in the areas which were defined by the masking plate.

Material is removed from the areas which are not protected by the photoresist mask by a process known as etching. Etching can be described as the process of solid material removal from a substrate by means of an chemical reaction. In the semiconductor industry, the reactant which effects etching can be either a liquid or gaseous chemical agent. All wet chemical etch processes are known as *wet etching* and all gas or vapourised chemical based etch processes are known as *dry etching.*

1.2.1 Etching

Etching processes are widely used in IC fabrication in the following areas [7]:

- Etching for the removal of thin films from a substrate.
- Etching for analytical purposes.
- Etching for pattern transfer.

In the first two categories, wet etching is superior to dry etching and is the dominant process. It is in the area of etching for pattern transfer that dry etch processes have largely replaced wet etch processes. This is because most wet chemical processes are isotropic in nature and therefore result in a roughly equal rate of material removal in all directions as shown in figure 1–3. For linewidths of $4\mu m$ and larger this presents no problem. However, when the required linewidth approaches the film thickness dimension, then an anisotropic process is required. For VLSI and ULSI processing, the width and pitch of the material features must be very close to the mask dimensions, and this can only be achieved by an anisotropic process. Dry etch processes which are physical or chemical/physical in nature are the only acceptable choice at present.

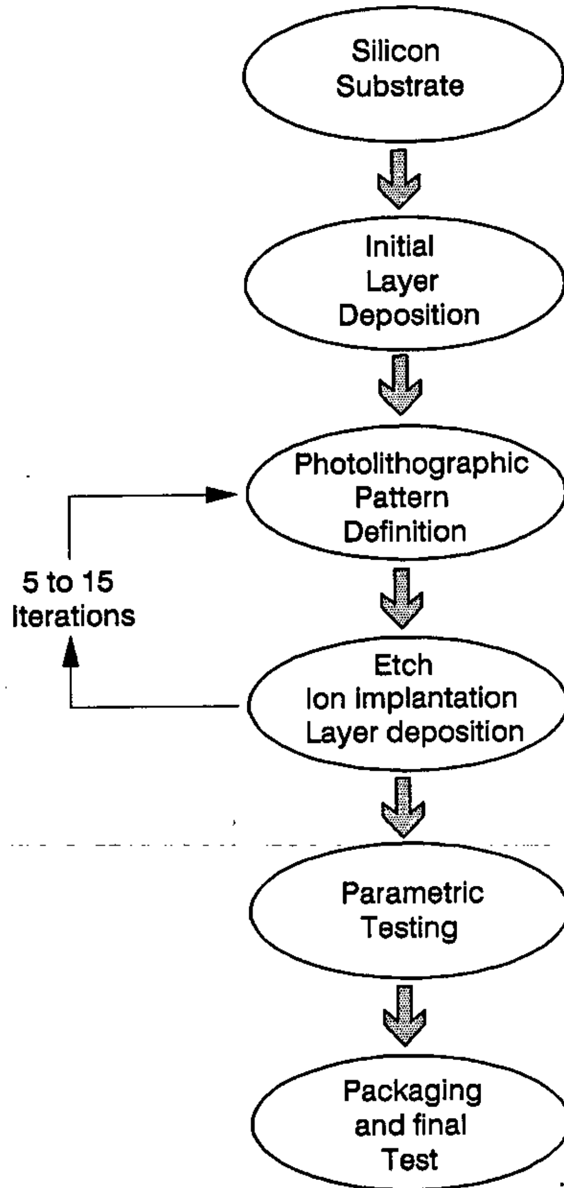

Figure 1–2: Microelectronic device process fabrication sequence.

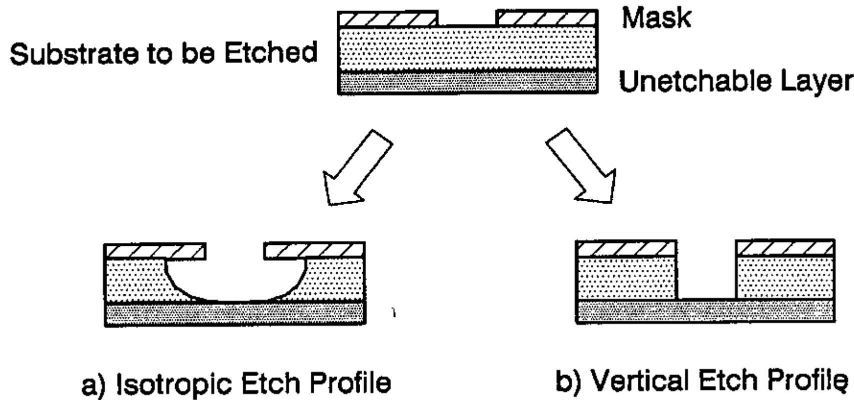

Figure 1–3: Isotropic etch profile.

1.3 Project Rationale

Although dry etching processes are crucial to the microfabrication of any complex semiconductor circuit, the technique remains difficult to implement and is not well understood. To a great extent, this is a result of the use of novel machine configurations and chemical recipes which are employed far in advance of any real understanding of the interactions occurring within the process chamber. The major problem with dry etching is the large parameter space of fundamental chemical and physical parameters, many of which are not easily accessible or alterable. This can lead to major problems when attempting to characterise or fault-find a specific process. To date, problem solving and process optimisation have been carried out on a largely empirical basis.

The problems associated with dry etching have lead to a gap opening up between state-of-the-art photoresist pattern definition and material pattern definition as illustrated in figure 1–4 [8]. This trend has lead to dry etching being identified by Sematech as one of the two key front end process modules which must undergo further development work in order to be incorporated in a 1Gbit DRAM fabrication sequence [9]. This is crucial for equipment vendors as new equipment for 1Gb processes with minimum feature sizes of $\approx 0.15\mu$m is being

considered now for incorporation into pilot processes which will begin sampling from 1997 [10].

In the field of dry etching, the patterning of Al and its alloys are among those that have presented the greatest challenges to the process engineer. Conversely, the Cl based processes which effect Al etching remain among the least well characterised and most poorly understood. The aim of this research work was to perform characterisation work on a leading edge dry etch process: the $BCl_3/Cl_2/He$ etching of Al. The project strategy called for two main approaches to be undertaken:

- Diagnostic techniques to be assessed.
- Empirical modelling to be carried out.

To link the two approaches, some of the diagnostic information was used as an input to the process model. This established a link between the final performance variables which are measured post-process and off-line and the actual process conditions.

This work is applicable both to the process engineer and to the equipment manufacturer. Process characterisation using statistical process control (SPC) techniques allows the identification and definition of process capability. This in turn allows variations in the process to be reduced which improves overall performance. This approach is one of the cornerstones of current Motorola policy in their goal of 6σ quality [11]. Process characterisation also allows an equipment manufacturer to implement a feedback and control system. When implemented properly, this would allow improved process repeatability which could compensate for small process fluctuations.

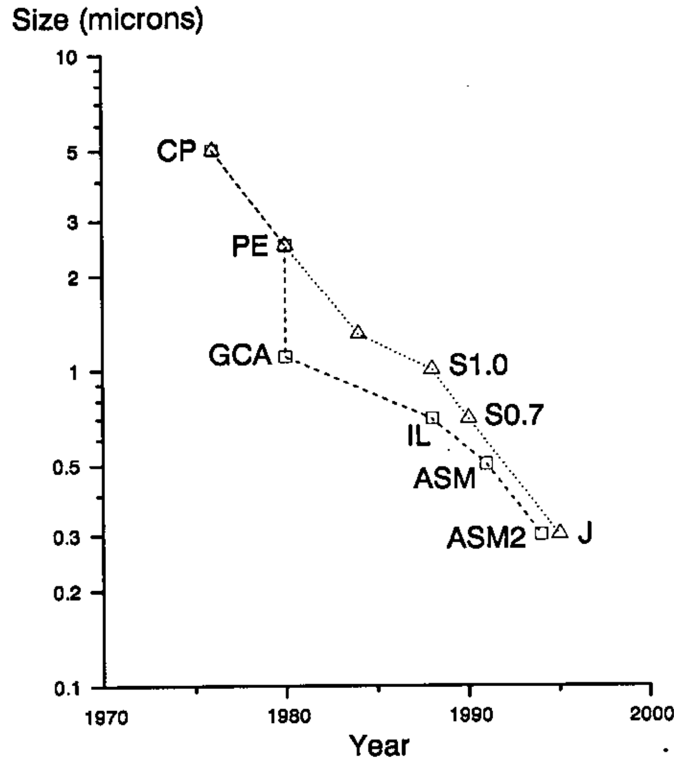

Figure 1–4: Trends in minimum lithographic resolution (squares) and *advanced* process minimum feature size (triangles) where CP is contact printing; PE represents Perkin Elmer Microalign; GCA represents the GCA 4800 10:1 direct step on wafer (DSW); IL is the ASM i-line DSW; ASM is the planned ASM excimer laser DSW; ASM2 represents the ultimate ASM performance; S1.0 is the SPECTRE objective of 1μm; S0.7 is the SPECTRE objective of 0.7μm; and J is the JESSI objective of 0.3μm.

1.4 Thesis Structure

Chapter 2: Reactive Plasma Etching. This chapter outlines the concepts and terminology which are necessary for a basic understanding of dry etch processes. It deals with plasma basics; the general etch process and shows the

parameter space influences which make process characterisation such a difficult problem.

Chapter 3: Diagnostic Techniques for Plasma Characterisation. This chapter reviews the techniques which have been applied to dry etch systems. It concludes that optical emission spectroscopy, mass spectrometry and Langmuir probes have been used most extensively to investigate a range of plasma behaviour.

Chapter 4: Modelling Strategies for Plasma Etch Processes. This chapter outlines the differences between empirical and mechanistic approaches for characterisation. It concludes that empirical models using orthogonal designs provide an efficient and rigorous solution to the problem of dry etching characterisation.

Chapter 5: Experimental Setup and Characterisation. A description of the assembly and test of all the equipment which was used in this research to monitor and carry out aluminium etching is given in this chapter. Preliminary results on argon plasmas using the techniques of OES, in-situ SIMS and Langmuir probes are presented.

Chapter 6: Diagnostic Techniques in a Reactive Gas Chemistry. A complex $BCl_3/Cl_2/He$ based chemistry for aluminium etching was developed and investigated using the diagnostic equipment. In-situ SIMS used the inherent sensitivity of the plasma positive ion distributions to monitor the etch progress. OES was used to monitor the behaviour of emissions from the Al atomic state. However, Langmuir probes proved unsuitable for routine process monitoring.

Chapter 7: Statistical Process Model. A novel empirical model was created which related both process and performance etch parameters to the machine variables of power, pressure and $\%Cl_2/BCl_3$. The process characteristics are presented, along with an estimate of each model's accuracy.

Chapter 2

Reactive Plasma Etching

2.1 Introduction

As outlined previously, all dry etch processes use gaseous or vapourised chemical sources. The most important subset of dry etch processes, for the semiconductor fabrication industry, can be referred to as *reactive plasma etching.* These processes rely on a plasma to convert the relatively inert input gases into reactive species which engage in etching.

There are many different physical phenomenon which are collectively referred to as plasmas. In the semiconductor industry the plasmas of interest can be defined as being hot, ionised gases. Plasma based processes are being increasingly used as a solution to challenges in material etch and deposition for advanced processes. This is particularly true for etch processes, where reactive plasmas are now routinely used for critical pattern definition instead of chemical wet etches.

One of the more confusing aspects of plasma based processes is the terminology. Names can often be misleading, and meanings for the same phrase can change from author to author. In this work, the terms 'plasma' and 'glow discharge' are interchangeable. 'Plasma etching' and 'dry etching' are also equivalent phrases and refer to the entire field of dry etch processing, unless otherwise indicated.

This chapter will outline the basic terminology and processes which are prevalent in the field of dry etching. Because of the importance of the plasma to the process, plasma properties are initially described. The general plasma etch process is also described along with the major process influences.

2.2 Plasma Properties

When an electric field of a sufficient magnitude is applied to a low pressure gas, the gas starts to break down. Unless the gas is at absolute zero, free electrons will already be present in the gas due to processes such as field emission or photoionisation. The free electron is accelerated in the applied electric field and gains kinetic energy. However, as it proceeds through the gas, it loses energy in collisions with gas atoms. Collisions can be either elastic or inelastic, with elastic encounters serving only to deflect the path of the electron with little energy loss. Ultimately, the electron energy can increase (e.g. of the order of tens of eVs) until it is high enough to excite or ionise neutral species by inelastic collision. Ionisation frees another electron which is then accelerated by the electric field, and the process continues. If the applied voltage exceeds the breakdown potential, then the gas rapidly becomes ionised throughout its volume by means of an avalanche process.

The most important inelastic, electron-impact reaction mechanisms for plasma formation can be described as excitation and relaxation; and ionisation and recombination [12]. For example, in an argon discharge this would involve:

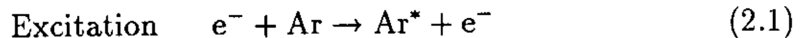

$$\text{Excitation} \quad e^- + Ar \rightarrow Ar^* + e^- \tag{2.1}$$

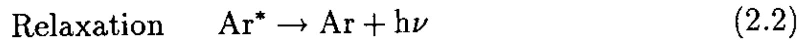

$$\text{Relaxation} \quad Ar^* \rightarrow Ar + h\nu \tag{2.2}$$

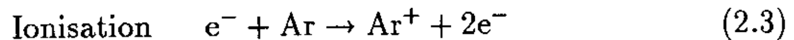

$$\text{Ionisation} \quad e^- + Ar \rightarrow Ar^+ + 2e^- \tag{2.3}$$

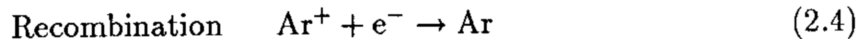

$$\text{Recombination} \quad Ar^+ + e^- \rightarrow Ar \tag{2.4}$$

where h is equal to Planck's constant and ν is the frequency of the emitted photon and Ar^* indicates an argon atom in an excited state.

Through these processes the discharge reaches a self-sustained steady state when ion/electron generation and loss processes are in equilibrium. The characteristic plasma glow is caused by emission of photons due to the relaxation of excited species within the plasma.

Electron densities for the plasmas of interest are in the range 10^9 to 10^{12}cm^{-3} [13]. As the density of gas molecules at 1 torr is approximately 10^{16}cm^{-3} it is obvious that these discharges are only weakly ionised. Average gas temperatures are near ambient despite mean electron temperatures of around 10^4 to 10^5 K.

An important feature of glow discharges is their ability to insulate themselves from outside influences using sheaths. It is useful at this stage to consider the effect of suspending a small electrically isolated substrate into the plasma. The substrate will be struck by both electron and ion fluxes. Due to the large mass difference between the electrons and ions, the electron flux density to the substrate is far greater than the ion flux density (by a factor of $\approx 10^3$). The substrate will immediately start to accumulate a negative charge, and hence a negative potential with respect to the plasma. This charge build-up disturbs the quasi-random motion of the charged particles in the vicinity of the substrate. The negative charge on the substrate starts to reduce the flux of negative charge to the substrate and attracts positive ions. This repulsion is sufficient to balance the fluxes of charged particles to the substrate. The area of positive space charge around the substrate is known as a *sheath* or *dark space*. Sheath thickness is related to the Debye length, λ_D, which is a measure of how a plasma will react to oppose a potential disturbance from a floating substrate. It has units of length and can be described as [12]:

$$\lambda_D = \left(\frac{kT_e \epsilon_O}{n_e e^2} \right)^{\frac{1}{2}} \tag{2.5}$$

where k is Boltzmann's constant; T_e is the electron temperature; ϵ_0 is the permittivity of free space; n_e is the electron density; and e is the charge on an electron. The Debye length shows how rapidly a potential disturbance is attenuated by the discharge, and over a length λ_D the perturbation is reduced to 0.37 of its original value.

2.2.1 DC Plasma Excitation

The simplest plasma is a glow discharge in which a dc potential is applied between two metal electrodes in a sealed chamber containing a low pressure gas. The discharge is spatially non-uniform and consists of a series of glowing and dark regions as shown in figure 2–1 [14].

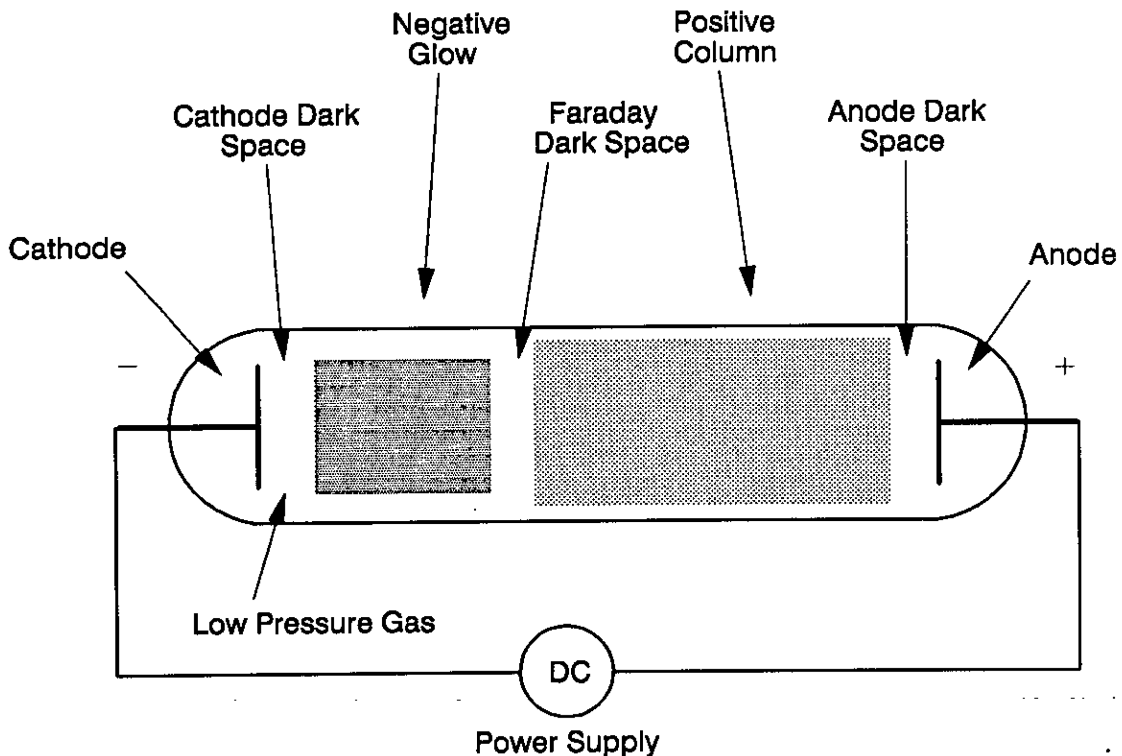

Figure 2–1: Schematic view of a typical dc glow discharge at low pressure, showing the most prominent regions.

Free electrons are accelerated in the electric field and excitation/relaxation and ionisation/recombination reactions occur in the gas, as described in section 2.2. Positive ions are then accelerated toward the cathode and cause ejection of secondary electrons on impact. These electrons are rapidly accelerated away from the cathode causing a space charge of less mobile positive charges to remain. Because few electronic excitations occur in this region, a visible glow is not observed. This area is the dark space or sheath and has a relatively low conductivity due to

the electron depletion which results in most of the applied voltage being dropped across it. When the secondary electrons reach a high enough energy, excitation and ionisation take place. The leading edge of the negative glow marks the point where the inelastic electron collisions begin. Negative glow width is a product of the distance over which the accelerated electrons dissipate their energy inelastically. On leaving this region, most of the electrons have energies too small to cause further ionisation and a further relatively dark area (Faraday dark space) is established. Finally there is a positive column where there are equal densities of ions and electrons. This positive column is considered by many researchers to be an 'ideal plasma.'

There are two major sheath regions at the electrodes in a dc discharge: the cathode sheath and the anode sheath. The cathode sheath may be as long as several centimetres and consists of the following regions:

1. A quasi-neutral 'pre-sheath' in which ions are accelerated towards the Debye region.

2. A Debye region which extends for a few Debye lengths and in which the electron density rapidly reduces to near zero.

3. A region of almost zero electron density, in which flows a space charge limited current. Positive ions carry the current in this region and there is a large voltage drop across the region.

The anode sheath is usually much thinner (by a factor of ≈ 10), and the electron density does not reduce to zero as in the anode sheath. A pre-sheath and a Debye region are the primary constituents of the anode sheath.

Both electrodes in a dc discharge must be conductors. If, during the discharge process, either electrode becomes covered with an insulating layer, then the surface of the insulator charges up capacitively. As the capacitor charges up, the net current through the plasma falls to zero, extinguishing the discharge.

DC glows exhibit three common characteristics of gaseous discharges:

1. Because electrons are much more mobile than ions, positive space charge tends to form adjacent to the negative electrode. In fact, the disparity in mobilities causes ion sheath formation around any surface which is in contact with the plasma.

2. The ion sheath is a relatively poor conductor and hence the largest voltage drops occur across the sheaths.

3. The mean electron energy is increased as the pressure is reduced, or more accurately as ε/p is increased, where ε is the electric field and p is the pressure. As the electron mean free path is proportional to p, ε/p is a scale of the energy gained by the electron in the field between collisions.

2.2.2 AC Plasma Excitation

If a low frequency alternating field ($< 10^4$Hz) is applied to the circuit shown in figure 2–2, then the effects discussed in the previous section will remain unchanged except for the reversal every half cycle of anode and cathode. Ion and electron distributions can both equilibrate with the changing field and the cathode and anode dark spaces also change position every half cycle. As the applied field frequency is increased, a point is reached when the period of oscillation is less than the time required for plasma equilibrium. Initially positive ions cannot be fully extracted from the cathode sheath areas before the field is reversed. As the frequency is increased further, the electrons are unable to travel to the anode during a half cycle. These electrons then oscillate in the inter-electrode gap and collide with gas molecules. Frequencies of >1MHz must typically be applied for oscillation of electrons to occur.

The rf generated discharge has fewer regions than the dc discharge. It consists of a negative glow insulated from the electrodes by dark spaces at the powered electrode and the earthed electrode. These dark space sheaths are similar in composition to the cathode sheath in a dc discharge, with regions of positive

space charge being formed. This is analogous to the case of a dc discharge which has only a small inter-electrode gap.

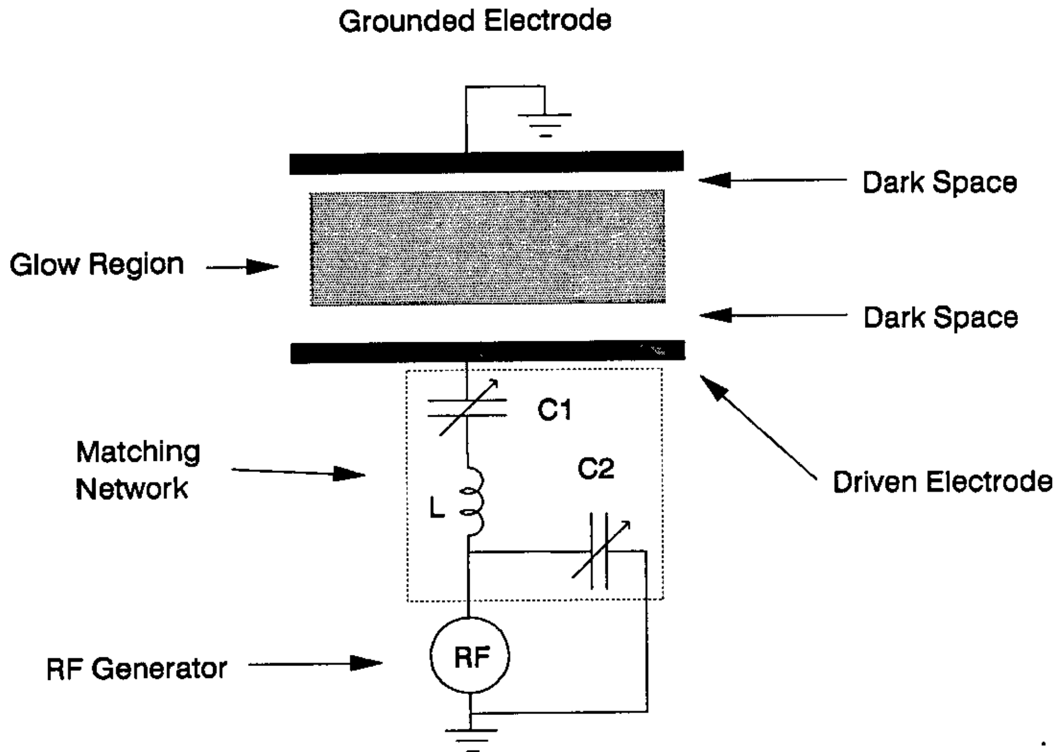

Figure 2–2: A schematic view of a rf plasma discharge where the power is supplied through a matching network.

The regions of positive space charge occur as a result of the differences in mobility of electrons and ions. This means that *self bias* voltages are set up between the chamber surfaces and the discharge. Differences in voltage between the plasma and both the grounded electrode and the driven electrode are affected by the chamber dimensions, the system pressure, the gas composition and the applied power and will be discussed further in section 2.4.

The largest self bias voltage is developed at the driven electrode. This is because there is an impedance matching network between the driven electrode and the rf power supply, as shown in figure 2–2. A dc isolating capacitor exists in the circuit between the rf supply and the plasma. A large dc self bias (V_{dcb})

develops between the powered electrode and the negative glow due to the action of this capacitor.

There are several advantages in the use of rf powered as opposed to dc powered discharges:

1. Electrons which are oscillating in the plasma can gain sufficient energy to cause ionisation. Rf discharges can therefore be maintained independently of the secondary electron yield from the chamber walls and electrodes.

2. Electron oscillations increase the probability of ionising collisions occurring with time. This leads to a more efficient method of plasma generation which can therefore operate down to a lower minimum pressure (1 mtorr).

3. The discharge will not extinguish if either electrode is totally covered with an insulator, as long as the capacitor formed by the insulator is large enough to couple energy into the plasma. This is significant as it allows the sputter etching and reactive sputter etching of insulators to take place [12].

It is important to consider the potentials which develop at various points in the rf discharge of figure 2–2, as this directly affects the energies of ions incident on surfaces immersed in the plasma [15]. Figure 2–3 shows the time resolved potentials, including the dc self bias voltages, which occur in a typical rf discharge. V_{dcb} is the self bias potential at the rf powered electrode, measured with respect to ground. V_p is the voltage in the bulk of the negative glow measured with respect to ground and known as the plasma potential. V_f is the potential relative to ground of an electrically floating surface such as a substrate or film isolated from ground by an insulating layer. Ions collide with the grounded surfaces with a maximum energy of eV_p. Collisions with the driven electrode are more energetic as the maximum possible energy of ions is $e(V_p - V_{dcb})$. V_{dcb} is typically of the order of 200V for most processes, with V_p usually of the order of 20V, and V_f around 5V. Depending on the reactor geometry, V_p can rise to several hundred volts [16,17]. These potentials are influenced by various parameters of

the discharge including the applied power and the chamber dimensions and will be explained in more detail in section 2.4.

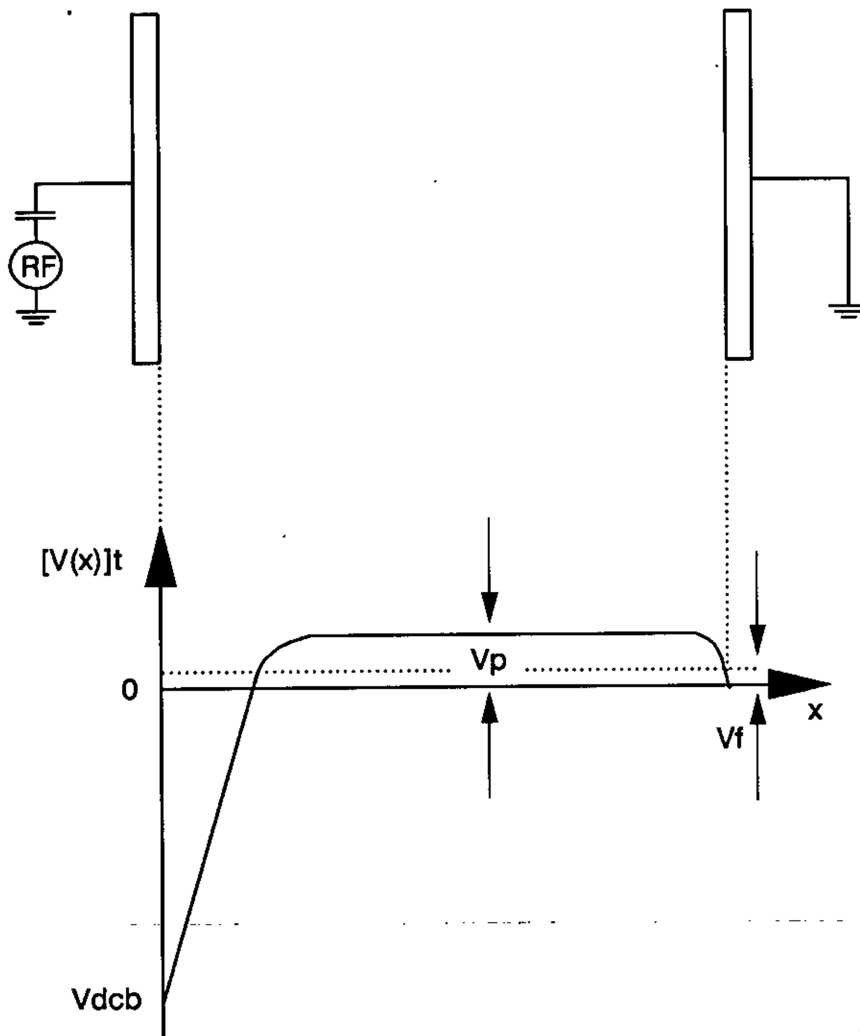

Figure 2–3: The time resolved potentials which occur for rf plasmas.

A self bias that is negative with respect to the plasma potential develops on any surface that is capacitively coupled to the glow discharge [18]. The difference in mobility of electrons and positive ions results in the static IV characteristics of the plasma resembling those of a leaky diode. If an rf signal is applied to this type of characteristic, a very large electron current flows during one half of the cycle, while a relatively small ion current flows during the other half of the cycle. If there is a capacitor, or a dielectric wall, between the rf generator and

the plasma, then no charge can be transferred through it. For stability to be achieved, equal numbers of ions and electrons must reach the surface during the cycle. As the ion flow cannot increase, the electron current must decrease. This effectively means that the powered electrode in a capacitively coupled discharge must charge negatively as shown in figure 2–4, until the stable condition shown is achieved. This oscillating negative signal has an average value of $-V_{dcb}$ on the powered electrode.

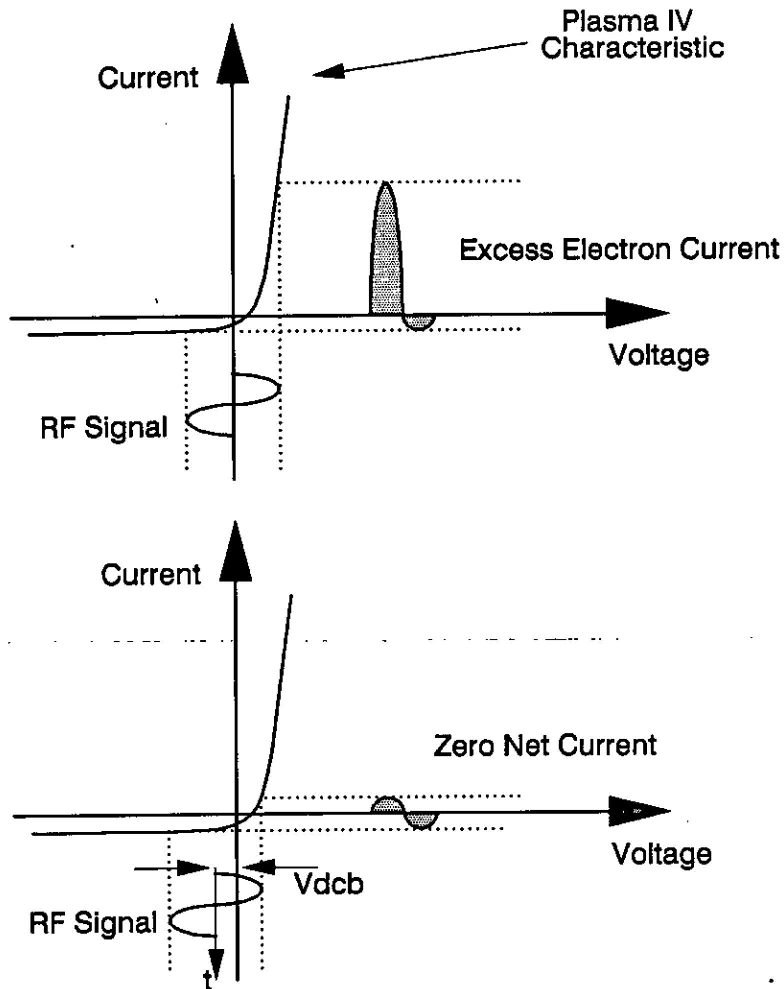

Figure 2–4: The development of negative self bias when a rf signal is capacitively coupled to a plasma.

2.3 The General Reactive Plasma Etch Process

Etching can be defined as the removal of a solid material from a substrate by means of a chemical reaction. The reactant which effects etching can be a liquid or gaseous chemical agent. In the microelectronics industry, all gaseous or vapourised chemical source etch processes are referred to as dry etching. The most widely used and important sub group of dry etching can be described as *reactive plasma etching.*

Many different types of reactions are possible in a glow discharge [19,20,21] but in order to successfully perform etching, the rf discharge must act as a source of species which engage in or catalyse etching. For these species to occur it is necessary that dissociation of the molecular feed gas takes place. Dissociation occurs as a result of electron impact reactions in the negative glow:

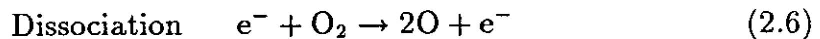

$$\text{Dissociation} \quad e^- + O_2 \rightarrow 2O + e^- \tag{2.6}$$

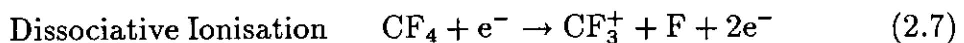

$$\text{Dissociative Ionisation} \quad CF_4 + e^- \rightarrow CF_3^+ + F + 2e^- \tag{2.7}$$

Fragmentation of the feed gas in this way is essential as the gases themselves are mostly unreactive with the substrate. Radicals created during dissociation processes are atoms, molecules or complexes which contain one or more unpaired electrons, such as O and F in the examples above [22]. Long and short lived radicals play a major role in the etch process due to their highly reactive nature. The resulting rf glow discharge is a mixture of ions, neutrals, radicals and electrons. If a semiconductor wafer is exposed to this reactive flux then some of the plasma species can combine with the substrate to form *volatile* products which evaporate, thereby etching the substrate. The reactive plasma etch process can therefore be summarised by the following sequence:

1. Dissociation of the feed gas(es).

2. Adsorption of the reactant to the surface.

3. Product formation.

4. Desorption and product removal.

Any one of these steps has the potential to be the slowest, and thereby become the limiting step in terms of the etch rate.

2.3.1 The Basic Mechanisms of Plasma Etching

Plasma etching is an extremely complicated process with many parameters contributing to the etch performance. Even at a basic level, these parameters encompass a wide range of interactions, many of which are not well understood. However the etching mechanisms can be grouped into four categories: sputtering; chemical etching; energy-driven ion-induced etching; inhibitor protected-sidewall ion-enhanced etching [23] as shown in figure 2–5.

During sputtering, particles (usually positive ions which are accelerated across the sheath) collide energetically with the substrate. If the energy transferred to the surface is greater than the atomic binding energy, then some surface atoms are ejected leading to net material removal. The sputtering yield is the number of target atoms ejected per incident ion, and is dependent on the relative masses of the atoms and the incident energy, and is typically less than one. This is a purely mechanical interaction.

Chemical etching occurs when gaseous active species encounter a surface and react with it to form a volatile product. The criterion of product volatility is essential to stop reaction products coating the surface, thus inhibiting the etch process by preventing etchants adsorbing to the surface. Chemical etching using plasmas is usually carried out by free neutral radicals and has no directionality, leading to isotropic profiles.

Fast directional etch rates (essential for $< 3\mu m$ feature definition) can occur for certain plasma/substrate combinations when there are fluxes of both neutral-

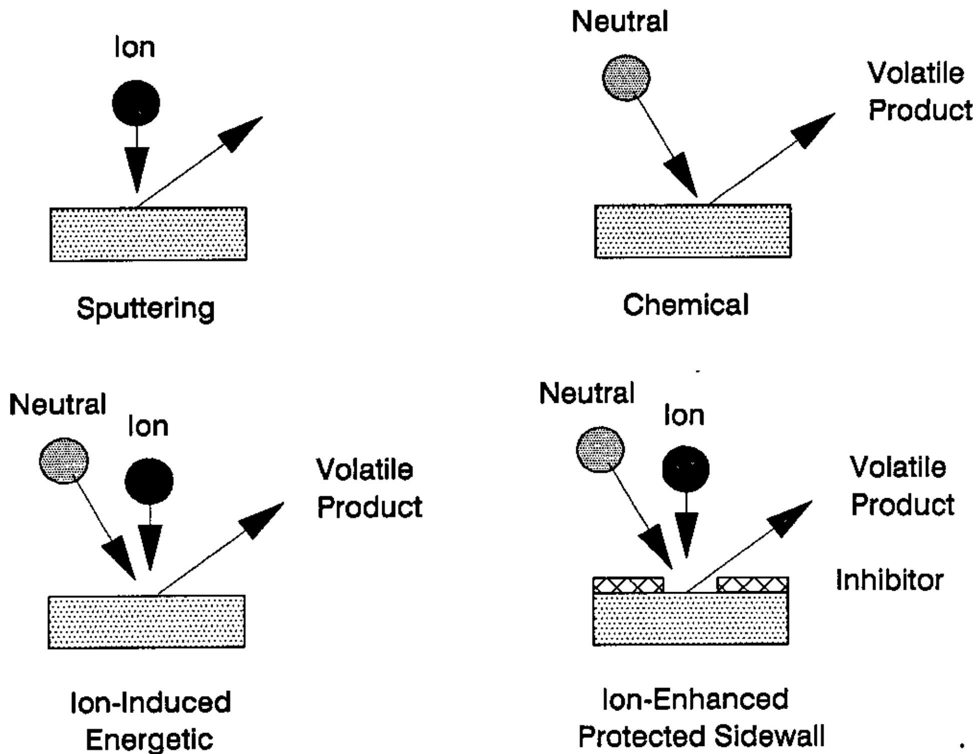

Figure 2–5: The four major processes by which dry etching takes place: sputtering; chemical etching; ion-induced energy driven etching; inhibitor protected-sidewall ion-enhanced etching.

s and ions to the surface. The effect is synergistic as ion bombardment in the presence of reactive etchant species often greatly exceeds the sum of the individual sputtering and chemical etch rates. Coburn demonstrated this effect by comparing the relative silicon etch rates achieved by XeF_2 gas; an Ar^+ ion beam; and the combination of ion beam and reactive gas. The etch rate of the reactive gas in combination with the argon ion beam was far greater than either of the individual etch rates (by a factor of ≈ 12) [24]. This ion enhanced reaction is generally considered to proceed by one of two types of mechanism [25].

In energy-driven ion-induced etching there is usually little or no etching when the substrate is exposed to neutral etchants alone. The rate limiting step in this case is the product formation. The ion bombardment component enhances the reaction rate by creating 'damage' sites on the surface of the substrate, by virtue

of the ion impact energy. Ion bombardment makes the substrate surface more reactive to the neutral radical flux. 'Damage' includes the formation of reactive dangling bonds, disruption of lattice structure and formation of dislocations.

Ion bombardment plays a different role in inhibitor protected-sidewall ion-enhanced etching. Neutral etchant species from the plasma can spontaneously etch the surface, but etch resistant polymers are also deposited on the surface during the reaction. This 'protective' inhibitor film can only be removed from horizontal surfaces that are receiving a vertical bombardment component from energetic ions. Vertical walls of masked features retain their protective film because they only interact with the small number of ions which are scattered as they cross the sheath. Sidewall film depositions allow the etch profile to become highly directional. The protective film may be formed by involatile reaction products from either the masking material or the substrate, or from film forming precursors that adsorb during the etch process. Etch rates are limited with this process due to the action of the protective film in preventing reactants adsorbing to the surface and products desorbing from the surface.

2.3.2 Reactor Configurations

Dry etching was first used in the 1960s in semiconductor applications for the stripping of photoresists [26]. This process used a rf glow discharge to dissociate molecular oxygen into reactive oxygen radicals and worked at room temperature. The configuration employed for this task is called a barrel etcher, or barrel asher, and has a cylindrical chamber as shown in figure 2–6. The wafers to be etched are placed in batches in the centre of the chamber and are screened from the discharge by a perforated metal cylinder (etch tunnel). The reactor chamber can be made of silica or aluminium and rf power is usually applied by encircling the vessel with an rf coil or by placing metal electrodes on either side of the chamber.

Etching arises due to the action of long lived neutral radicals which diffuse from the plasma to the wafer surface. Radiation damage from energetic ions is prevented by the shielding action of the etch tunnel. Etch profiles are isotropic

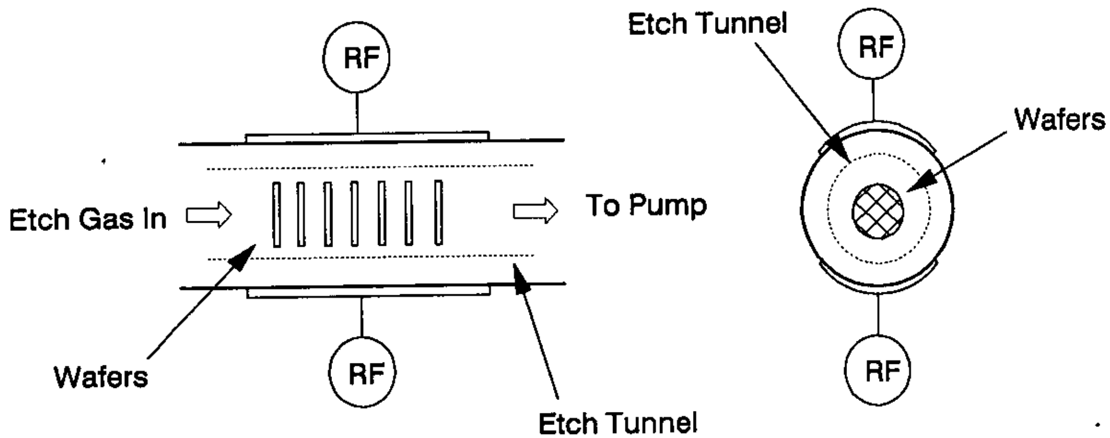

Figure 2–6: Barrel etch reactor with capacitively coupled rf power.

because the radicals involved are travelling in random directions. Operating pressures for barrel etchers range from 0.3 to 5 torr.

For more directional etching a planar geometry of reactor is used. The directional etch is caused by the addition of ion bombardment to the substrate as discussed in section 2.3.1. Planar systems are also called parallel plate systems, surface loaded systems, diode systems or Reinberg reactors [27]. The general arrangement of a planar system is shown in figure 2–7 along with the two most common configurations.

In the *plasma etch* configuration, two flat electrodes form parallel capacitor plates with a spacing of between 10 and 50 mm. Wafers are placed on the lower grounded electrode and the upper electrode is connected to the rf supply. Gas pressure is held constant in the range 0.1 to 1 torr. Wafers are not isolated from the plasma and short lived radicals contribute to the etching. The electrodes assume a negative potential with respect to the discharge and positive ions are accelerated towards the grounded wafers with a maximum energy of eV_p. Some physical etching takes place, but due to the relatively high pressure, the effect is limited. However, with the correct choice of gas, chamber dimensions, pressure and power, the etch can achieve a near vertical profile. This is achieved by

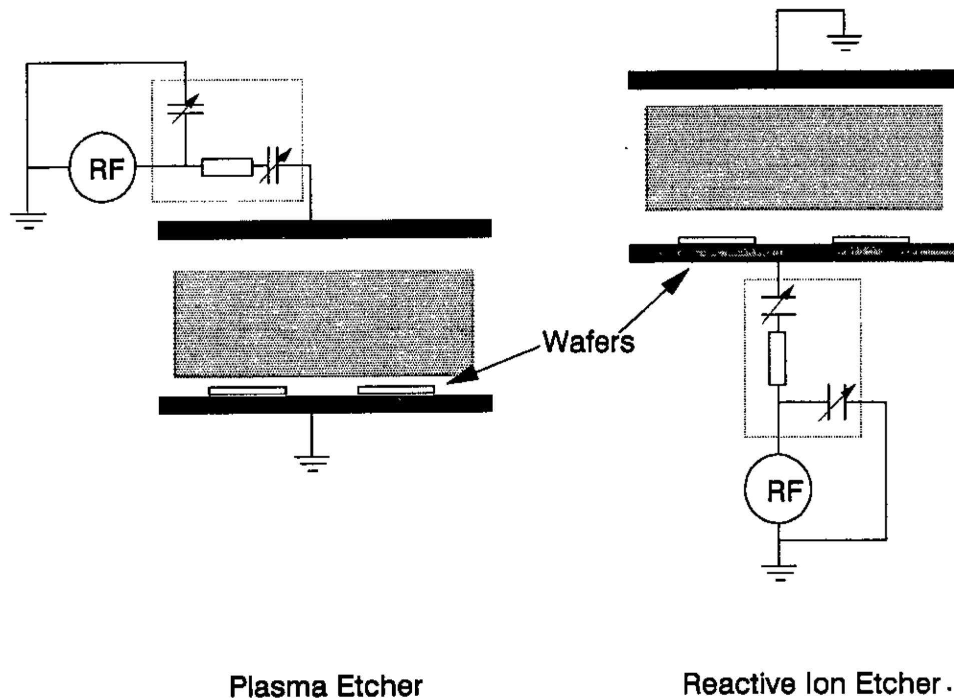

Figure 2–7: The two most frequently implemented planar etch configurations: plasma etch and reactive-ion-etch.

increasing the plasma potential, so that the ion bombardment energy to the grounded wafers is increased.

In the second planar etch configuration, the wafers are placed on the driven electrode. This is known as *reactive-ion-etching*(RIE) and is the most widely used process for pattern transfer in the semiconductor industry. Due to the self bias effect on the dc blocking capacitor the potential of the driven electrode, and hence the wafers, is more negative than in plasma etch mode. The maximum energy of positive ions is now $e(V_p - V_{dcb})$ as indicated in figure 2–2. RIE therefore has a high physical component and achieves more anisotropic profiles. Pressures for RIE are usually 10 to 100 mtorr with substrate voltages in the range 200 to 500V [16]. Some typical parameters which are representative of RIE are given in table 2–1 [28].

Many other plasma etch configurations are possible, but they are not widely

Pressure	< 100mtorr
Frequency	13.56 MHz
Power Density at Electrode	$0.1 \rightarrow 1$ Wcm^{-2}
DC Bias	50-500 V
Ion Density	10^{16} m^{-3}
Degree of Ionisation	10^{-4}
Electron Temperature	1-10 eV
Vibrational Temperature	0.1 eV
Rotational Temperature	0.05 eV
Translational Temperature	0.05 eV
Ion Plasma Frequency	3 MHz
Electron Plasma Frequency	1 GHz
Debye Length	$10^{-4} \rightarrow 10^{-2}$ m

Table 2–1: Some typical parameters which are characteristic of a RIE glow discharge process.

used in the semiconductor industry. A summary of these techniques are available in the literature [29,30].

2.3.3 The Choice of Gas Chemistry

Although ions play an important role in RIE processes, they are not the agent that reacts with the substrate to form gaseous products. Ions add directionality and increase the etch rate, but it is essential that the chemical component of the process forms a potentially volatile product. The actual chemical reactions occurring during plasma etching are not well understood, but some of the basic reactions and products can be summarised.

Four main groups of reactants are used to etch almost all the materials in silicon based wafer fabrication. They all rely on the discharge to produce reactive halogen based radicals or oxygen, as follows:

1. Chlorine and chlorine containing radicals are commonly used to etch aluminium, silicon and polysilicon [31,32,33,34,35].

2. Fluorine and fluorine containing radicals are employed in the etching of silicon dioxide, silicon nitride, silicon, titanium and tungsten [36,37,38,39, 40,41,42,43].

3. Bromine and bromine containing radicals have been successfully, although infrequently, used to plasma etch polysilicon, silicon nitride and some refractory metals [44].

4. Oxygen radicals are produced from molecular oxygen to remove hydrogen and carbon based films, such as photoresists [26].

A list of the halogen based gases which have been used in the silicon fabrication industry is given in table 2–2.

2.3.4 The Role of Gas Additives

Various gases can be added to the etchants mentioned in table 2–2 because they have useful effects on the outcome of the process. They can be qualitatively grouped into the following categories: native oxide etchants; scavengers; inert gas additions; and surface inhibitors.

Often, native oxides can cover the surface of a substrate and prevent the onset of etching. These oxides can prove to be very difficult to remove. Additions of small amounts of oxide etchants can get round this problem. Examples of this type approach include the action of C_2F_6 for Si etching; and BCl_3 or $SiCl_4$ for Al etching.

Oxidants can be added to gas mixtures in order to perform a scavenging role by increasing the etchant concentration or by suppressing polymer formation. This behaviour is often referred to as the etchant-unsaturate concept and is discussed further in section 2.3.5. Gases such as BCl_3 and $SiCl_4$ can also scavenge adsorbed

	Silicon	Silicon Dioxide	Silicon Nitride	Metals	Metal Silicides	Organic Materials
Fluorine:						
CF_4	yes	yes	yes	yes	yes	yes
C_2F_6	yes	yes	yes	yes	yes	yes
CHF_3	yes	yes	yes			yes
NF_3	yes	yes		yes	yes	yes
SF_6	yes	yes	yes	yes	yes	yes
SiF_4	yes				yes	
Chlorine:						
CCl_4	yes			yes	yes	
$CHCl_3$	yes			yes		
Cl_2	yes			yes	yes	
HCl	yes			yes	yes	
BCl_3	yes			yes	yes	
$SiCl_4$	yes			yes		
Chlorofluoro-carbon:						
$CFCl_3$	yes			yes	yes	
CF_2Cl_2	yes		yes	yes	yes	
CF_3Cl	yes			yes	yes	
C_2F_5Cl	yes				yes	
Bromine:						
CF_3Br	yes		yes	yes	yes	
HBr	yes			yes		
Br_2	yes			yes		

Table 2–2: Applications of halogen gases for reactive plasma etching in silicon based fabrication.

water vapour and oxygen from the chamber as the discharge is struck, which aids process repeatability.

Inert gas additions are often used to stabilise and homogenise plasmas which can otherwise restrict or oscillate in the reaction chamber. Some gases can increase thermal cooling by either having a higher thermal conductivity than the etchant species (eg. helium), or by increasing the total gas pressure. A further function is the ability of noble gas ions to increase the sputter based components of the etch process [45].

Often, carbon containing gases such as CCl_4 are added as surface inhibitors. Protective film precursors such as CCl_x can form polymers which in the presence of ion bombardment can promote anisotropic etching if the major mechanism involved is inhibitor protected-sidewall ion-enhanced etching.

2.3.5 The Etchant-Unsaturate Concept

Halocarbons mixed with oxidants such as O_2 and Cl_2 form the chemical basis for almost all plasma processes. To help understand the effects of feed gas composition in these plasmas, an etchant-unsaturate concept was proposed [46]. In this reaction scheme, unsaturated fluoro- and chlorocarbon polymer precursors derived from CF_2 or CCl_2 plasma generated radicals are saturated during reactions with reactive atoms and molecules. The most reactive species combine preferentially and form chemically stable compounds. By assigning an order to this reactivity, a qualitative prediction of the dominant atomic etchants can be obtained as a function of the halocarbon and oxidant gas composition. While the reactive plasma model is most easily understood in terms of a specific chemistry, a general representation of the reaction scheme can be presented as follows:

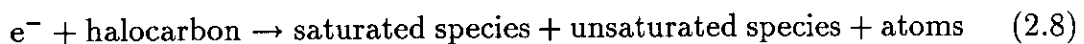

$$e^- + \text{halocarbon} \rightarrow \text{saturated species} + \text{unsaturated species} + \text{atoms} \qquad (2.8)$$

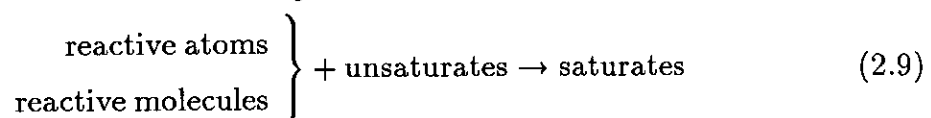

$$\left.\begin{array}{r}\text{reactive atoms}\\ \text{reactive molecules}\end{array}\right\} + \text{unsaturates} \rightarrow \text{saturates} \qquad (2.9)$$

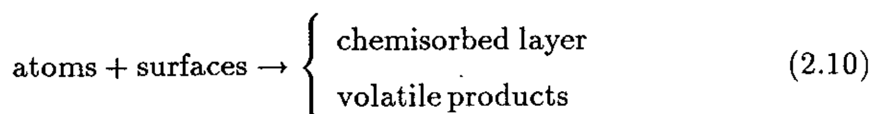

$$\text{atoms} + \text{surfaces} \rightarrow \begin{cases} \text{chemisorbed layer} \\ \text{volatile products} \end{cases} \tag{2.10}$$

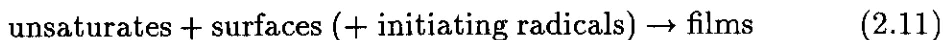

$$\text{unsaturates} + \text{surfaces (+ initiating radicals)} \rightarrow \text{films} \tag{2.11}$$

The relative reactivities of atoms and molecules in these saturation reactions can be assigned a reactive order: $F \approx O > Cl > Br$; and $F_2 > Cl_2 > Br_2$. Thus the predominant etchant species and reaction products can be predicted as a function of feed gas composition. For example, if CF_3Br is used as the feed gas, both Br and F atoms are formed during electron impact dissociation of the halocarbon. However, due to the high reactivity of F with CF_2 radicals and unsaturates such as C_2F_4, there is usually a negligible steady-state concentration of F atoms. A similar situation exists for heavily chlorinated plasmas (such as CCl_4), with Cl, CCl_2 and C_2Cl_4 behaving similarly. As the most reactive atoms (F, O) cannot co-exist with unsaturates at appreciable concentrations, then either the atoms or the unsaturates must be severely depleted. Etching takes place when atomic etchants predominate and polymer formation occurs when unsaturates are present in excess and are adsorbed onto the substrate surface. Polymerisation of unsaturates is inhibited by surfaces that react with the unsaturates to form volatile products [47] (eg. fluorocarbon radicals with SiO_2).

This behaviour can be illustrated by the action of O_2 in CF_4 plasmas [48]. O_2 removes CF_x radicals from the gas phase and prevents their recombination with F atoms, thereby increasing the F atom concentration. As F atoms are the main Si etchants, there is a consequent etch rate increase as shown in figure 2–8.

The addition of O_2 to chlorocarbon plasmas results in different effects dependent upon the discharge gases employed. When O_2 is added to CCl_4 there is an immediate decrease in the aluminium etch rate. Etching stops completely with larger concentrations of O_2. With BCl_3, small O_2 additions ($< 5\%$ volume) increase the aluminium etch rate, while large concentrations of oxygen impede the etch process and deposit boron oxides within the etch chamber. It is suggested that in CCl_4 etching, oxygen reacts either with the aluminium (inhibiting the etch) or with the carbon species. However with BCl_3, oxygen (or water vapour)

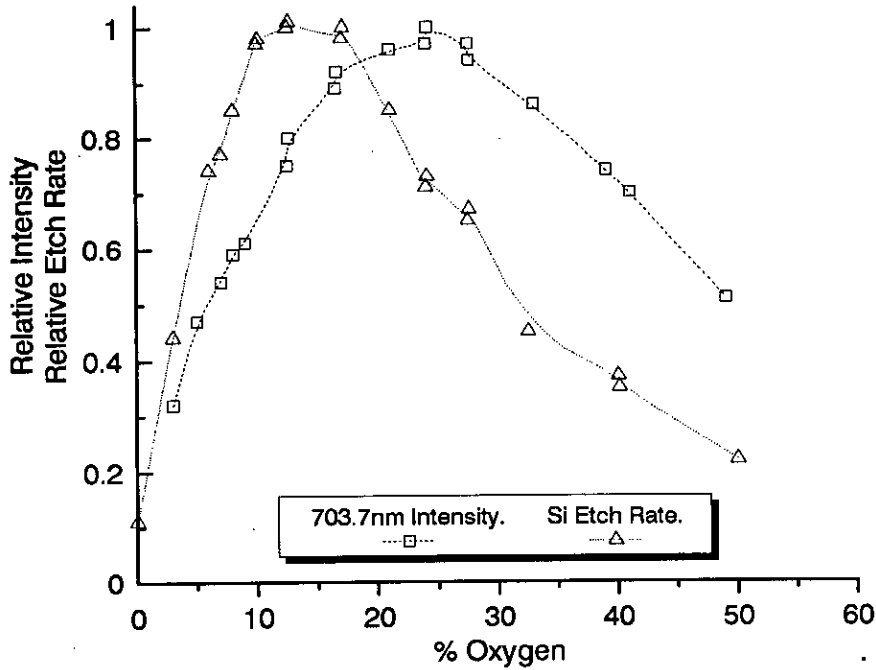

Figure 2–8: The influence of oxygen on the normalised etch rate of silicon using a CF_4/O_2 chemistry. Also shown is the normalised intensity of the emission from electronically excited F atoms (703.7nm line) during Si etching.

reacts preferentially with boron to form oxides or oxychlorides. This releases extra Cl atoms from the BCl_3 which increases the etch rate, at least for small oxygen additions [49].

Oxidant additions to a plasma will therefore change the relative concentrations of halogen atoms and unsaturates. The most reactive oxidants will react preferentially with unsaturates which will increase the concentration of less reactive halogen atoms and also suppress polymer formation.

2.3.6 Aluminium Etching

Aluminium and aluminium alloy films are widely used in the semiconductor industry as interconnect layers in integrated circuits. Aluminium metallisation is

preferred because of the ease of processing; low resistivity; and the ability to reduce native SiO_2, which is always present on Si wafers, so that low contact resistances are obtained. Dilute amounts ($\approx 1\%$) of Si are added to Al to help prevent junction spiking, with copper ($\approx 4\%$) being added to help improve the resistance of the interconnect to electromigration [50]. These additives, especially copper, greatly increase the complexity and the difficulty of metallisation etching.

The etching of Al and its alloys are among those that have presented the greatest challenges for fine linewidth definition using reactive plasma etch techniques. Major problems have included: long and frequently erratic induction times; toxic or corrosive etch products and etchants; polymer formation; reproducibility problems due to water vapour contamination of the process chamber; resist degradation and erosion leading to loss of linewidth control; and incomplete etching of non-Al constituents.

Aluminium etching consists of two distinct phases with an initial induction period followed by a bulk aluminium etch. The induction period occurs because two processes must be completed before bulk Al etching can start. Oxygen and water vapour must be scavenged from the vacuum chamber, and the unreactive, native oxide layer (≈ 30Å) must be removed. The former are present in large amounts on the reactor walls and electrodes, as they are easily adsorbed by either anodised Al or by the reaction products and polymers which coat the earthed surfaces. This can be minimised by using a load-lock to prevent exposure of the reactor to atmosphere between runs, and by using a gas additive such as BCl_3 or $SiCl_4$ that can scavenge water and oxygen. Native aluminium oxide can be etched by sputter ion bombardment of the surface and by supplying chemical species which are capable of reacting with the oxide. Oxide clearing radicals include CCl_x [31], BCl_x and $SiCl_x$ [23]. The need for an ion bombardment component is the primary reason that aluminium has not been successfully etched in a barrel reactor [49].

Etching of aluminium, in common with most metals, is dominated by product volatility limitations. The fluoride, Al_2F_6, is almost refractory with a very high

boiling point, and can be treated as involatile for the purposes of etching, although some research has shown that Al and its alloys can be sputter etched using a SiF_4/O_2 mixture [51]. For this reason, chlorine containing gases are used to etch aluminium, although bromine containing gases have also been used [52]. Once the native oxide has been removed, the Al can be etched in pure Cl_2, without the need for a plasma [53]. The major products in the reaction have been proposed as $AlCl_3$ at higher temperatures (T=200°C) and Al_2Cl_6 at lower temperatures (T=30°C) [54]. Because $SiCl_4$ is reasonably volatile, Si containing Al films can be readily etched in chlorine plasmas. However copper or copper chloride residues can often remain on the substrate surface after processing. Removal rates of copper products can be enhanced by elevating the substrate temperature, but this can necessitate the use of inorganic masking materials.

Following etching, aluminium films often corrode on exposure to atmospheric conditions due to the hydrolysis of chlorine or chlorine containing residues which remain on the substrate, the sidewalls or in the photoresist. Post etch treatments such as rinsing in water or concentrated nitric acid can be employed to remove these residues [49]. Because the unreactive, protective, native oxide has been removed during the etch, the chlorine species can react with the bulk Al, leading to corrosion. Various methods have been proposed to deal with this problem. Photoresist adsorbs large quantities of chlorine, mainly in the form of the etch product $AlCl_3$, which is a Lewis acid. Stripping the photoresist in an oxygen plasma before exposure to atmosphere removes much of the chlorine and is also thought to replace some of the chlorine chemisorbed on the aluminium with oxygen, but is not sufficient to totally prevent corrosion. Rinsing in de-ionised water can also remove most of the chlorine, but is again not sufficient to totally avert corrosion [23]. Low temperature oxidations in dry oxygen can reduce corrosion by restoring the passivating aluminium oxide layer [55]. Another method involves exposure to a fluorine based plasma, which is thought to replace chemisorbed chlorine into non-hygroscopic fluorine residues [56]. A further nitric acid rinse can be used to remove the fluoride residues and regrow the protective oxide.

2.4 The Plasma Etch Parameter Space

One of the major obstacles to the routine implementation of plasma etching is the extensive parameter space that is associated with the process, and the difficulty involved in directly measuring most of the fundamental variables. To a certain extent, these parameters can be characterised, as shown in figure 2–9. Ideally, etching processes would be controlled at an atomic level by manipulating basic chemical and physical variables.

Some authors in the field of electrical discharges have examined the plasma from a fundamental point of view as a series of quasi-dimensionless similarity variables [57]. These variables include the ratio of electric field to number density: ε/N (described in section 2.2.1 as ε/p, since $p \propto N$); the ratio of driving frequency to density: f/N; and the reactor aspect ratios. The state of the plasma and its products can be uniquely defined by a full set of these similarity ratios. However from a process engineering point of view, the usefulness of ratios is limited as the relationships are determined entirely by the apparatus and plasma gas. The process engineer cannot then set these variables directly. Also, common process plasmas may not actually have well defined ratios, with ε/N in particular sometimes varying by a factor of ten. Because of these problems, the machine parameters or *discharge variables* are often used for control. These parameters include pressure, input power, flow rates, temperature, excitation frequency, chamber dimensions and feed gas composition. Attributing specific process characteristics to individual parameters can be too simplistic because all plasma parameters are inter-related. However, some general trends and effects can be isolated. Feed gas composition has been dealt with in the preceding section, and the other discharge variables will now be reviewed.

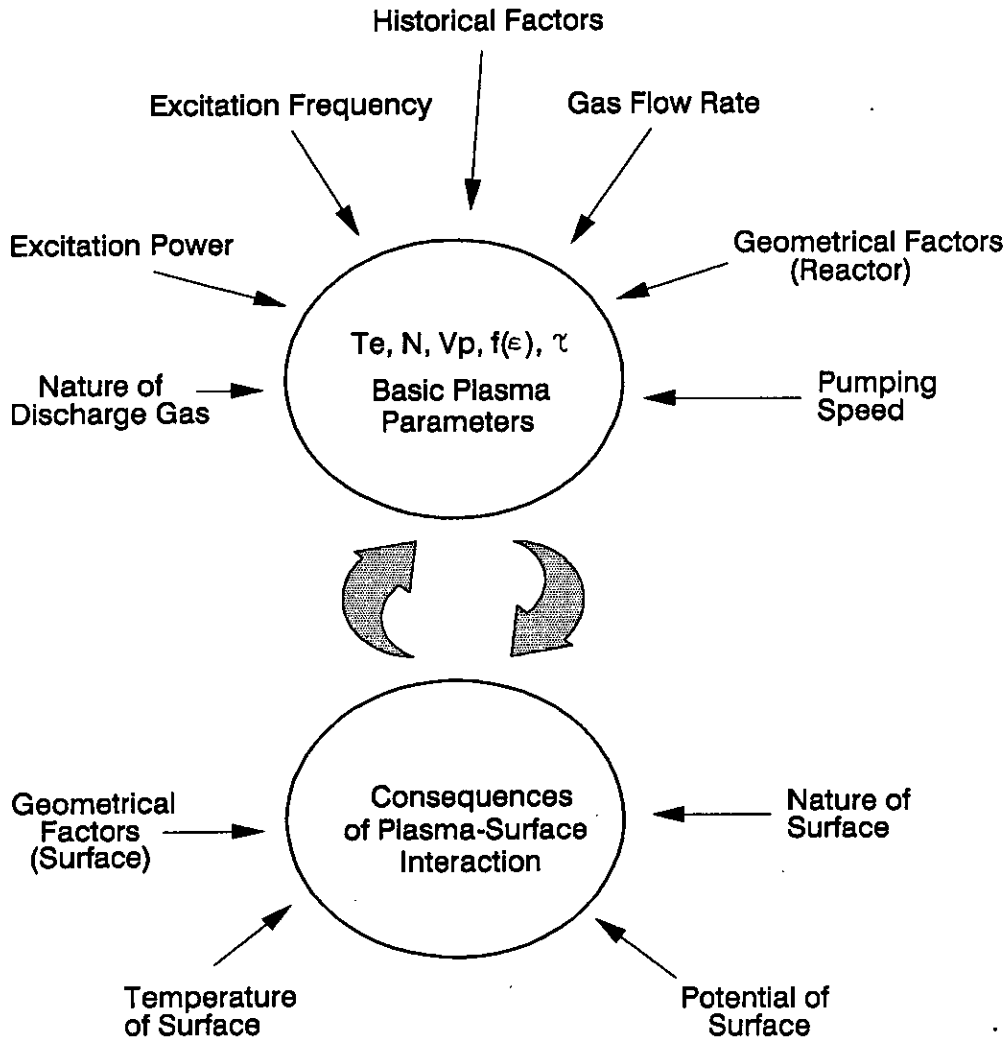

Figure 2–9: The parameter problem associated with the plasma etch process, where T_e is the electron temperature; N is the plasma density; V_p is the plasma potential; $f(\varepsilon)$ is the electron energy distribution function; and τ is the gas particle residence time.

2.4.1 Pressure

Pressure directly influences the energy distributions of ions, neutrals and electrons by affecting particle densities, mean free paths and collision rates. For example, the energy with which an ion impacts with a surface is not only dependent upon the sheath field, rf frequency and ion mass, but also the rate at which the ions collide with neutrals as they traverse the sheath. If the ion mean free path is

greater than the sheath thickness, then ions which enter the sheath will accelerate under the influence of the entire sheath field, and will impact the surface with a narrow and highly energetic velocity distribution. If the mean free path is much smaller than the sheath thickness, then the velocity distribution will have a much lower mean value and will have a greater variance.

The electron energy distribution function $f(\varepsilon)$ is also affected by pressure. Electron-neutral collisions result in the formation of ion-electron pairs. If the electron-impact mean free path for ionisation is small in comparison to the sheath thickness, then substantial ionisation can occur within the sheath region. This will alter the ion energy distribution at the electrode surface, and the sheath thickness [58]. Collisions involving ions which are close to the substrate will also influence the directionality of the etch with less anisotropic etches being observed.

In general the ion and electron collision mean free paths can be expected to scale inversely with pressure. As the physical thickness of the positive ion sheath is related to the electron mean free path, it also increases with decreasing gas pressure [15].

With all other parameters being held constant in the 5-50 mtorr range, then the etch rate generally increases with increasing pressure. This is due to an increase in both ionised and reactive neutral species. However, some researchers have observed that while the concentrations of active species do increase with increasing pressure, these concentrations are constant with residence time [59]. The residence time of a system is the average length of time a molecule spends in the chamber, neglecting any chemical interactions which may occur, and can be expressed as:

$$\tau = \frac{pV}{Q} \tag{2.12}$$

where p is the pressure, V is the volume of the system and Q is the gas flow rate. Therefore the observed etch rate increase with pressure could actually be an etch rate increase with residence time.

2.4.2 Flow Rate

Because of the effects of changing pressure on the physical properties of the plasma, the best way to vary the residence time is to vary the gas flow rate at a constant pressure. This has the *minimum* effect on the other plasma parameters. As the residence time changes for a given power density, then it can be reasoned that the less time the feed gas spends in the chamber, the less extensive will be the degree of dissociation. At high flow rates, radical densities will decrease with increasing flow rates. At low flow rates or long residence times, the extent of dissociation may reach an upper limit and an equilibrium may be reached such that radical concentrations become flow independent. Chapman et al [60] show that the overall dependence of the surface reaction rate on residence time, or flow rate, will display a maximum point.

2.4.3 Power

Increasing the applied power increases the sheath potential and increases the concentration of reactive neutrals and ions by affecting f(ε). Increases in the sheath potentials can occur due to increases in both the plasma potential and decreases in the negative dc self bias for the powered electrode for a typical grounded wall etch chamber. Due to these effects, etch rates generally increase with increasing power. However, in some modes of operation such as RIE, increasing power can also result in excessive ion bombardment, lower selectivity, photoresist degradation and an aggravation of the loading effect leading to etch non-uniformities (discussed further in section 2.5. Etch rate also increases with increasing rf power due to increased dissociation occurring within the plasma, which leads to greater levels of reactant [61].

Overall power is often used as an etch criterion, but since the electrode structure and discharge characteristics define the area and volume over which the discharge extends, more meaningful power based parameters are the power density or the dc self bias voltage.

2.4.4 Excitation Frequency

Excitation frequency is a key parameter affecting both the chemical and electrical properties of the plasma. The ion bombardment energy is affected because the discharge potential V_p increases as the frequency is lowered, leading to greater sheath potentials. The peak voltage which must be applied across the discharge to maintain constant power also increases as the frequency is reduced. From the equivalent circuit model of a rf discharge in figure 2–10 it can be seen that this outcome is a result of the change in sheath character from being predominantly capacitive at high frequency to being predominantly resistive at low frequencies.

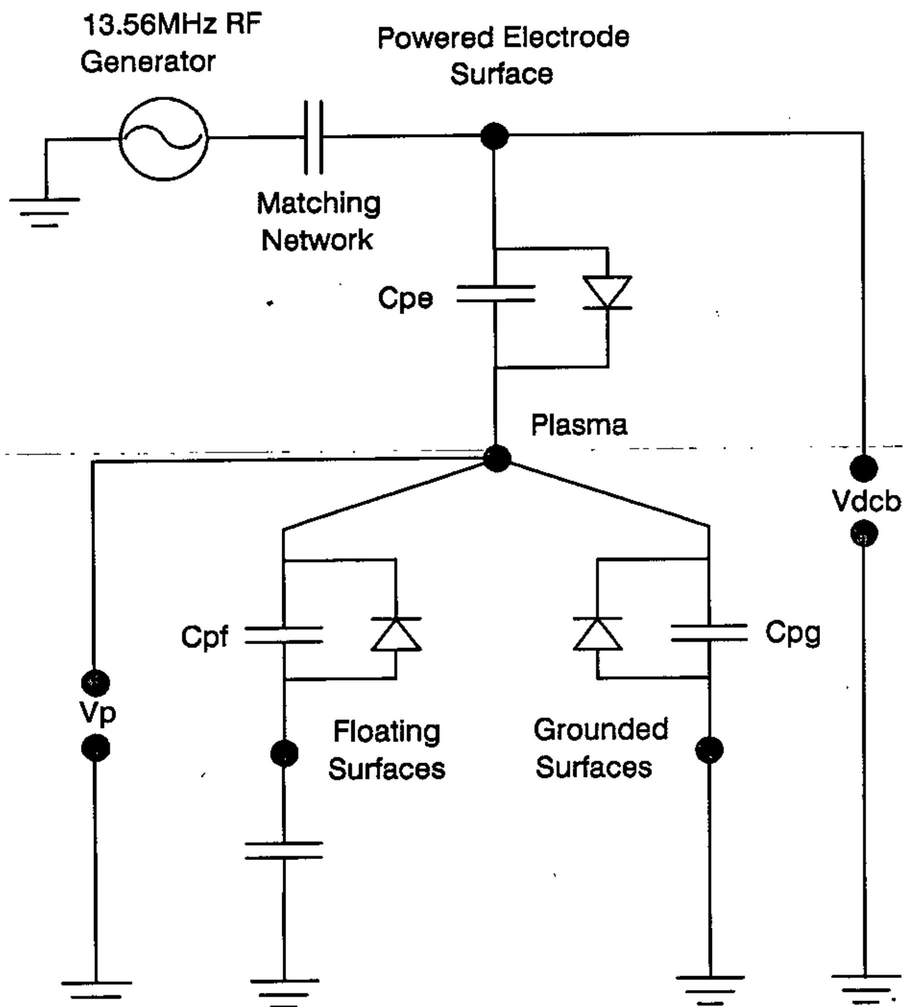

Figure 2–10: Approximate rf plasma equivalent circuit.

Frequency also affects the ion bombardment energy distribution with the energy of ions being distributed to higher energies at low frequency than at high frequency. To understand this phenomena it is necessary to introduce the concept of an *ion transit frequency* (ITF). At the ITF ions cross the sheath in a time equal to one applied field half cycle. At high rf generator frequencies (operation above the ITF), ions cross the field slowly compared to the applied field oscillation, and arrive at the electrode with an energy proportional to an average value of the sheath potential. At low rf generation frequencies (operation below the ITF), ions cross the sheath quickly compared to the field oscillation and gain a maximum energy which is equal to the instantaneous applied field, leading to a greater distribution of ion energies [53]. An example of this effect is the etching of Si in CCl_4 which decreased by more than an order of magnitude as the discharge frequency was raised above 7 MHz, whereas the etch rate of Al in CCl_4 increased by a factor of four over the same range of frequency increase [62]. Cl_2 etching of Si is thought to be energy-driven ion-induced whereas Cl_2 etching of Al is thought to be inhibitor protected-sidewall ion-enhanced. In the case of Si the etch rate depends mostly on the ion energy and in the case of Al the etch rate depends mostly on the density of reactive species.

The shape of $f(\varepsilon)$ is also influenced by the frequency. This means that the dominant electron-molecule interactions can be affected and hence the chemical composition of the discharge can be altered. This can be demonstrated by looking at undercutting effects, which are a result of chemical interactions, becoming enhanced at higher excitation frequencies. Undercutting of highly n-doped polysilicon in a Cl_2 discharge is negligible at low frequency, but substantial undercutting is observed at high frequency [53].

Most commercial plasma systems today operate at a frequency of 13.56 MHz, because this is a licenced US Federal Communications Commission (FCC) industrial frequency for which rf generators are readily available, instead of being an optimal discharge parameter. Similarly, microwave based systems operate at 2.45 GHz which is another FCC frequency. Low frequency generators (200-800 kHz)

are often a result of a manufacturers previous products and are not optimised for etching, as the intentional use of frequency as a process parameter is a novel development.

2.4.5 Temperature

Temperature influences the etch rate, selectivity, surface texture and the degree of anisotropy. Changes in surface temperature affect the reaction rate and the rate at which products leave the surface of the wafer. Possible etch product boiling points (eg. $AlCl_3$ at 177.8°C) or vapour pressure curves can be useful in the initial selection of an etch chemistry. Chemical etching rates can be raised by increasing temperature to the point where it has an etch rate comparable with ion-enhanced processes, leading to decreased anisotropy.

Typical RIE processes and heats of reaction can produce temperature rises of the order of 100 to 200°C in a 75mm wafer [63]. The applied power and the etch rate are therefore limited in practice by the thermal stability of the masking material. Heat can be transferred from the wafer to the electrode or to inert gases such as helium. Because cooling reduces the rate of removal of volatile product species, a trade-off must occur that minimises resist deformation, while maintaining chamber temperatures that prevent product condensation on the reactor walls. Chamber walls and electrodes often incorporate independent temperature control through the use of heat/chill circuits in order to enhance the process stability.

2.4.6 Chamber Dimensions

The dimensions of the reactor chamber play an important role in the determination of the plasma potential V_p, the self bias potentials, and therefore the ion bombardment energy which is incident on the reactor walls and electrodes. The relationship between the plasma potential and the driven electrode potential, V_{dcb}, as a function of time with the area ratio R as a parameter are shown in

figure 2–11 [64]. R is equal to $\frac{A_e}{A_d}$ where A_e and A_d are the earthed electrode and driven electrode areas respectively. If the system consists of two electrodes of equal area, then V_p will be very large and both electrodes will be subject to energetic ion bombardment to approximately the same extent, as the sheath voltage drop across all the sheaths will be equal to V_p. A typical RIE system will feature $0 < R < 1$.

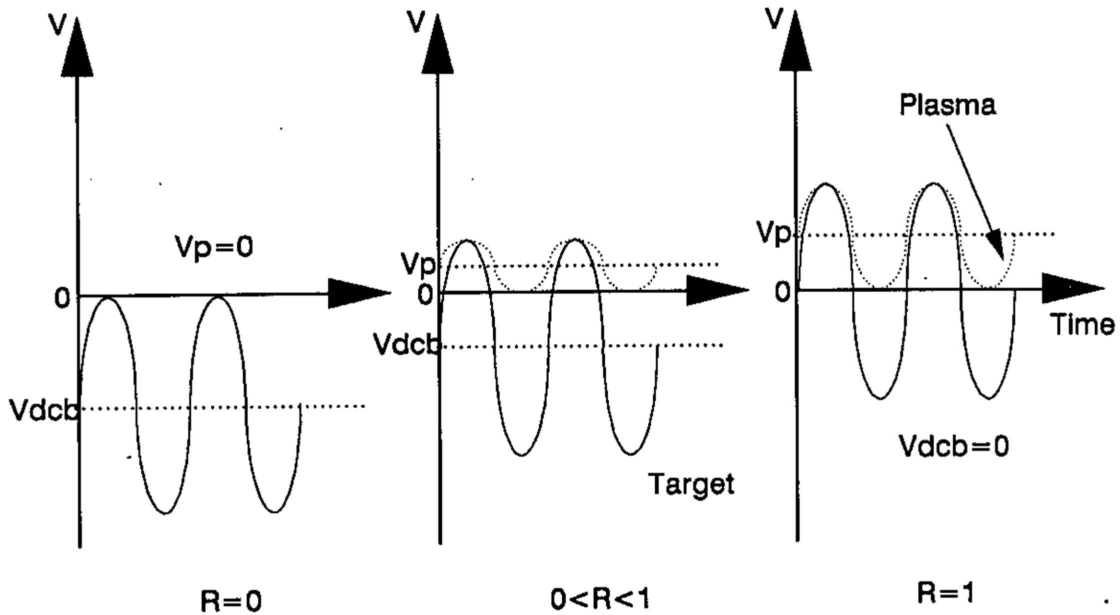

Figure 2–11: Approximate driven electrode and plasma potential waveforms for a glow discharge with grounded chamber walls. R is the ratio of powered electrode to wall area.

This behaviour is due to the capacitive nature of the ion sheaths. From the approximate equivalent circuit for a discharge shown previously in figure 2–10 it follows that V_p is determined by the relative magnitudes of the sheath capacitances. This is effectively capacitive voltage division which in turn depends on the relative areas of the cathode electrode and other surfaces in contact with the plasma. An early theory of plasma characteristics predicts [65]:

$$\frac{V_d}{V_e} = \left(\frac{A_e}{A_d}\right)^4 \tag{2.13}$$

where V_e and V_d are the voltage drops across the earthed and driven electrode sheaths respectively. This model was originally developed for sputtering systems operating at a few mtorr, and some problems occur when applying this relation in higher pressure scenarios, as outlined in the literature [12]. In fact, for the plasmas which are used in etch processes, there is evidence to suggest that the voltage ratio varies as the first, and not the fourth power of the area ratio [64].

2.5 Plasma Etch Process Characterisation

The size and final profile of an etched feature are often regarded as the most important properties of the process. However, there are many other characteristics which can affect the outcome of the process, and many of these must be taken into account when considering the economic viability of the manufacturing process.

2.5.1 Anisotropy

Anisotropy is a measure of the directionality of the etch process. In wet chemical etch processes, the etch has no preferred direction and has a horizontal etch rate that is equal to the vertical etch rate. This leads to rounded profiles which undercut the original mask, and is known as *isotropic* etching, as shown in figure 2–12a. By definition, any profile which is not isotropic must be anisotropic, with a perfectly anisotropic feature having no horizontal component as shown in figure 2–12b. As feature linewidths become comparable with feature heights in size, the loss of linewidth due to isotropic processes cannot be tolerated and directional processes must be employed. This occurs when the thickness of the layer to be etched approaches the linewidth required (approximately $< 4\mu m$).

The ion bombardment mechanisms which are responsible for anisotropic etching have already been discussed in section 2.3.1. It is important to note that although fully anisotropic etches are required for true pattern transfer, their use

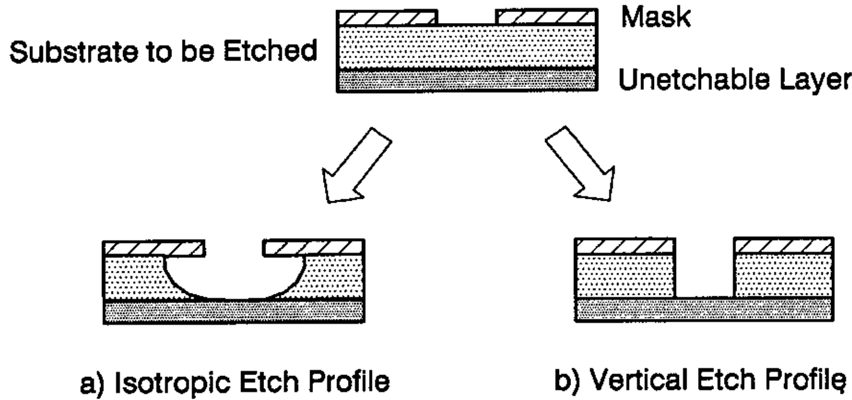

Figure 2–12: Ideal etch profiles for isotropic and fully anisotropic processes, when there is no mask erosion.

is not without some problems. When etching materials which are deposited over substrates with steep surface topography, some overetch is essential to compensate for the effectively thicker material at the step edges as shown in figure 2–13. Overetching is a term used to describe the action of continuing an etch process for longer than is necessary to just complete the etch at one point on the wafer. This overetch can, when coupled with poor selectivity (described in section 2.5.2), lead to device destruction. The steep walls of fully anisotropically etched features can also cause severe problems for subsequent step coverage. To prevent void formation on metal deposition, for example, contact holes should have a tapered profile.

2.5.2 Selectivity

The selectivity of a process is a measure of the etch rate of layer to be etched relative to other materials which are in contact with the etchant flux. Selectivity is usually expressed simply as a ratio of these two rates:

$$\mathrm{S_{ab}} = \frac{\mathrm{ER_a}}{\mathrm{ER_b}} \tag{2.14}$$

where $\mathrm{ER_a}$ is the etch rate of the layer to be etched, and $\mathrm{ER_b}$ is the etch rate of a second material. If a process has similar etch rates for two materials in

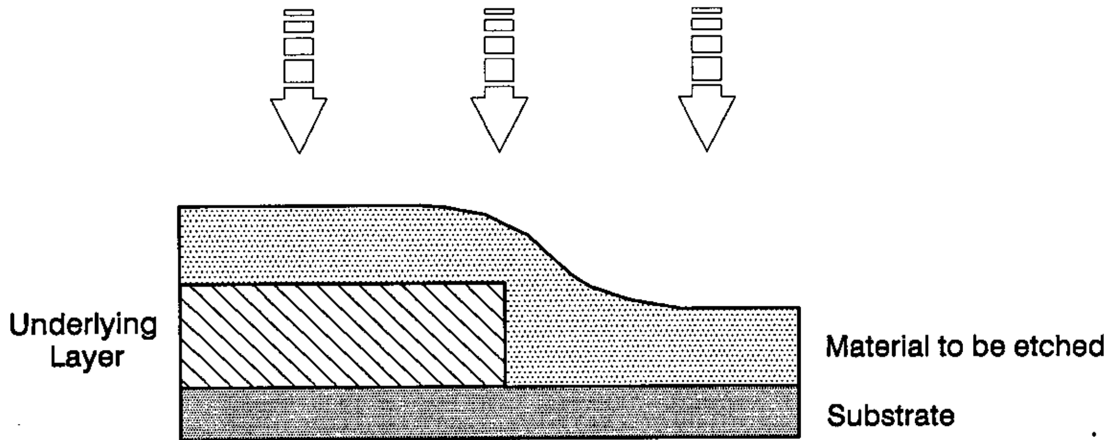

Figure 2–13: For a fully anisotropic process, some overetch is needed to remove residual material at steps.

contact with a plasma, then that process can be described as having low or poor selectivity. Large comparative etch rates for a material layer compared to the masking layer, for example, would imply a highly selective process.

In section 2.5.1, both the mask and the substrate were treated as unetchable materials. In plasma etch processes this is rarely the case and all materials exposed to the plasma have a finite etch rate. Selectivity with respect to the mask affects feature size control. Selectivity with respect to the substrate affects overall performance and yield. The substrate in this case may be either the silicon substrate or an underlying film which has been grown or deposited on a previous level of the fabrication.

Ideally, a high selectivity would be coupled with a highly directional etch profile, but this is not easy to attain in practice. High selectivities are characteristic of systems in which chemical processes dominate and ion based mechanisms are minimised. Ion-induced and ion-enhanced mechanisms add directionality but result in non-selective material removal.

2.5.3 Uniformity

Uniformity is a measure of the consistency of an etching process. *Intrawafer* uniformity refers to the rates measured within a single wafer, while *interwafer* uniformity is a measure of the rates measured wafer to wafer. In the case of batch processes, a further distinction can be made between interwafer uniformities from the same batch, and cross batch uniformities. This parameter is usually determined by measuring the relative etch rates at selected sites. The major causes of non-uniformity are electric field gradients along the plasma sheath and differences in the concentrations of reactive species in the plasma.

Etch non-uniformities which can be modulated by changing the residence time are usually indicative of a non-uniform gas composition. This is usually minimised in the reactor design stage by using distributed gas rings or showerhead designs to introduce the gas. Problems with uniformity that are attributed to electric field gradients can prove more difficult to solve. Often, alterations to the reactor design and geometry may be the only way to reduce the problem [66].

2.5.4 Loading Effect

During reactive etching, the etch rate is sometimes found to decrease as the amount of etchable surface is increased. This is a phenomenon which is known as the *loading effect*, and it has an adverse effect on both the uniformity and reproducibility of etching. Loading occurs when the active etch species react rapidly with the material to be etched, but have a long lifetime when there is no etchable material. The primary loss mechanism for the reactive species is etching, and so the greater the material area, the greater is the depletion of etchant species. The generation rate of active species is fixed by the discharge variables, and is largely independent of the amount of etchable material present. The average value of etchant species concentration is therefore the difference between the rates of generation and loss, and must decrease as etchable surface area increases.

Mogab [67] expressed this quantitatively for the case of a single etchant species as follows:

$$\mathrm{ER} = \frac{\beta \tau \mathrm{G}}{1 + \mathrm{K} \beta \tau \mathrm{A}} \tag{2.15}$$

where ER is the etch rate; β is a reaction rate coefficient which is related to the affinity of the etching material for the active species created in the plasma; A is the etchable area; τ is the lifetime of the etchant species in the absence of etchable material; G is the generation rate of active etchant species; and K is a constant which is dependent on the reactor geometry and material. According to equation 2.15, there will be no major loading effect as long as $\mathrm{K}\beta\tau\mathrm{A} \ll 1$. If the gas chemistry and conditions are selected such that the reactive species lifetime is kept small, then this condition will be satisfied. Obtaining accurate values for some of these coefficients for specific equipments and operating conditions can prove difficult.

Mogab [67] showed experimentally that the concentration of active species is non-uniform, except when the etchable material is symmetrically distributed. Concentrations of etchants were found to be slightly higher near a wafer which was not surrounded by other wafers. From equation 2.15 it can be seen that this is simply a manifestation of loading, where there is decreased competition for active species. This same effect can lead to an etch rate dependence on feature size, with small isolated features etching more rapidly than large less isolated features on a wafer. This is known as a 'microscopic loading effect.'

The presence of a loading effect has major implications for feature size control if the process contains a horizontal etch component. As the process endpoint is reached, the etchable area decreases very rapidly, resulting in an accelerated etch rate at the endpoint and during the overetch period. This makes feature size control very difficult as there is an increased horizontal etch rate as the surface clears.

2.5.5 Throughput

The number of wafers etched per unit time is known as the *throughput* of the system. Throughput is governed by the machine uptime and reliability, and also by the average etch time per wafer.

Average etch time per wafer depends on the number of wafers which are etched per cycle. A typical cycle may involve loading, pumpdown, wafer pre-treatment, etching, post-treatment, venting and unloading. For large batch processes, the cycle time can be long, allowing lower etch rates. For single wafer processes, all operations have to be of extremely short duration to achieve the same throughput as a batch process. Etching must therefore be carried out at higher rates using higher power densities.

If the technology exists, then only economic factors can determine an acceptable throughput. A typical requirement for a batch etcher would be to process 60 wafers/hour with etch rates of 100 to 600 Å/min. Single wafer etchers must achieve etch rates which are 10 to 20 times faster for equivalent throughput, although other factors such as capital cost and cleanroom footprint must also be considered. The implications of throughput with reference to equipment trends will be discussed further in section 2.6.

2.5.6 Defects, Impurities and Surface Roughening

An ideal etching system would replicate exactly the masking layer pattern in the material layer; stop at the underlying layer; and leave no residue on the surface. During the process, small particulates can fall onto the surface and act as masks to the etch. These masks will then form localised features or defects. Acceptable defect densities for the entire pattern transfer process are typically less than 1 defect/cm^2.

A major source of defects is the flaking of material which has previously been deposited on the chamber walls. Many RIE processes etch the wafer surface which is subject to a high sheath potential, while depositing etch products and polymers

onto the chamber walls which are only subject to low sheath potentials. If the chamber is not load locked and must be vented to atmosphere between batches, high velocity gases passing over the walls can cause particulate flaking. Frequent chamber cleans or the introduction of a load lock can reduce this problem.

Chemical alteration of the surface etching rate can cause roughening of surfaces during etching. During an aluminium etch for example, surface oxides etch at rates which are much lower than for the bulk film. Small variations in the thickness of the surface oxide can therefore cause significant roughening of the surface due to the large disparity in etch rates. This effectively means that a greater period of overetch is required to remove the film completely. Contaminants such as water in the process chamber can result in the formation of surface oxides which can lead to process variations and surface roughening.

Sputtering of etch resistant material from the electrodes onto the film can also result in regions with low etching rates and surface roughening. A common example of this occurs when Si is etched on an Al electrode in fluorine based chemistries. Non-volatile compounds are sputtered from the electrode onto the wafer surface. These deposits mask further etching and appear as 'black grass' on the wafer surface. This type of problem can be reduced by using electrode coatings such as Ardel and Lexan [1] (a high temperature polymer), which produce mainly volatile compounds under ion bombardment [68].

In general, processes which have a large ion bombardment component produce rough surfaces, and chemical etch processes typically produce smoother surfaces.

2.5.7 Radiation Damage

During the plasma etch process, wafers are exposed to various different types of high energy radiation including ions, electrons, ultra-violet light and soft x-rays.

[1] Lexan is a trademark of the General Electric Company

This creates a potentially hostile environment for electrically sensitive process layers. The gate oxide and the Si/SiO_2 interface in a FET fabrication process are particularly susceptible to these types of damaging radiation [68,69,70,71,72].

The damage can take several forms:

1. Energetic ion impact can result in atomic displacement. The penetration depth of this type of damage is a function of the mass of the ion and is usually < 25Å from the surface for RIE processes.

2. Primary ionisation of the lattice occurs when Si-O bonds are broken and electron-hole pairs created. UV photons and soft x-rays are the main causes of this effect.

3. Secondary ionisation occurs when the electrons caused by primary ionisation or atomic displacement interact with defects in the Si-O lattice.

These damage mechanisms are responsible for the production of trapped positive charge and neutral traps within the dielectric, which can degrade the quality of the final device. The former defects can cause shifts in threshold flat-band voltages, with neutral traps being able to trap energetic electrons. Annealing can remove the majority of these traps, but trapped impurities within the lattice can only be removed by wet etching. In FET fabrication, the sensitive gate oxide is usually protected from radiation by the gate electrode which is typically polysilicon. The radiation is not energetic enough to penetrate the polysilicon and so most of the damage is confined to the perimeter of the electrode.

2.6 Equipment Trends in Plasma Etching

The factors which will have the greatest influence on the future of reactive plasma etching will be driven by two major requirements: the need for much finer linewidth definition; and the trend towards larger diameter wafers. The 0.7 to 0.8μm features needed for today's 4 Mbit DRAMs can be defined using currently available machines such as RIE. However, the 256 Mbit DRAMs which are expected to appear around 1998 will require linewidths of 0.25 to 0.3μm and these cannot be defined on a *production basis* using current technology.

For current production processes, the main debate revolves around whether single wafer etchers should be used instead of batch etchers. Single wafer machines started to become an economically viable option as wafer sizes increased to above 100mm. When coupled with extremely fast etch processes, single wafer systems offer some advantages:

1. Wafer to wafer variability is reduced.
2. End-point detection (see chapter 3) can be carried out on each wafer. When allied with a suitable control system, it is possible to compensate for previous process variation.
3. Malfunction destroys only one wafer.
4. Automation is easier.
5. A smaller cleanroom footprint is achieved.

The major problem with single wafer machines is throughput. To compensate for single wafer processing, extremely fast processes are used where the power density is high (typically 5 Wcm^{-2}) compared to batch systems (typically 0.25 Wcm^{-2}). This can result in lower selectivity, resist damage and consequent

degradation of pattern quality, as well as increasing the possibility of radiation damage and impurity contamination.

There are several candidates which look promising for the small feature definitions required for new generations of DRAMs. These include electron cyclotron resonance (ECR), helicon plasma sources, distributed ECR (DECR), rotating field magnetrons and the helical resonator. Some of these operate at rf frequencies, but are capable of maintaining high density plasmas and performing highly anisotropic etching. A full description of these techniques is beyond the scope of this review but is available in the literature [73].

Another limitation on currently implemented production equipment is the interdependence of the plasma parameters. Variation of one process parameter alters many other plasma variables as discussed in section 2.4. This inherent inflexibility limits process optimisation. Some machine configurations partially separate the dual plasma source functions of species generation and ion bombardment. These machines include the triode [29] and ECR based machines [74]. Using this type of approach the dc self bias can be set semi-independently of the active species generation, leading to greater control of the ion bombardment potential.

2.7 Summary

In conclusion, the major problems with dry etching centre on the sensitivity of the plasma, coupled to a basic lack of understanding of the fundamental physical and chemical variables. For control purposes, the machine parameters or discharge variables, such as power, pressure... etc. are used to alter the fundamental variables. However, because the fundamental variables are inter-related and interdependent, characterisation of the process with respect to discharge parameters is not straight-forward.

EX BIBL. UNIV. EDINBURGEN.

In this chapter, some of the concepts necessary for an insight into plasma etch processes were also presented. Included were dc and ac plasma properties; a description of the reactive etch process; the parameters which influence the process outcome; and the characteristics which can define the etch process outcome. Finally, the techniques and trends which are likely to influence the future of plasma etching were briefly described.

Chapter 3

Diagnostic Techniques for Plasma Characterisation

3.1 Introduction

Traditionally, the plasma etch processes which are employed in the microelectronics industry have relied on a stable and well-characterised process for repeatable automatic operation. Due to the inherent complexity of the process, few processes had this stability. Even fewer machines actually had the required sophistication of control system to ensure repeatable operation, with process termination being determined using an etch timer or by eyeball from the operator. As the economic and process requirements for modern production systems become more stringent, it will become necessary to feed more and more discharge information back to an automatic controller. In this way, the balance between the competing chemical and physical processes that constitute the plasma can be monitored. For these reasons, it is necessary to employ reliable diagnostic methods, both to initially provide a basic understanding of the plasma and also to operate as a useful monitor for practical processes.

The most sophisticated of the current generation of production plasma etchers can generally be specified with some built-in plasma diagnostics. These are

usually configured as end-point detectors for processes which require a minimum of overetch to protect the underlying layer and reduce undercutting. Most of the analysis methods used, such as optical emission spectroscopy, yield an average parameter value for the discharge. It is therefore essential for the process uniformity to be high, so that clear interface points can be recognised and defined as endpoints. Many more commercial companies are producing equipment specifically for use in the field of plasma analysis. As diagnostic equipment production shifts from the academic environment to the commercial environment, the cost of implementation will decrease. This should lead to a more widespread use of diagnostic techniques and also their realisation as real time process monitors, as well as end-point detectors.

The overall objective of plasma diagnostics is to deduce information regarding the state of the glow discharge from practical observations of physical processes and their effects. Plasma diagnostic techniques are often extremely complex and sometimes require large amounts of physical data before any conclusions can be reached. Much of the research and development work on diagnostic techniques has been driven by the goal of obtaining economically significant amounts of power from thermonuclear fusion. Many of the techniques currently being applied to semiconductor plasma processes were developed from analysis of simple dc discharges or from fusion research.

Diagnostic strategies generally measure one of the following physical processes:

1. Electromagnetic emission from bound electrons. In this case the line radiation from atoms and ions that are not fully ionised is analysed.

2. Electromagnetic emission from free electrons. Plasma properties are deduced from the observation of radiation emitted from free electrons. This includes cyclotron (synchrotron) emission, bremsstrahlung, and Čerenkov processes.

3. Plasma particle flux measurements. These are measurements based on di-

rectly sensing the the flux of plasma particles using various types of probes which are directly in contact with the plasma.

4. Plasma refractive index. These techniques are based on the measurement of the plasma refractive index by transmitting appropriate electromagnetic waves through the plasma.

5. Magnetic measurements. In this case, the magnetic field is measured directly at various places inside and outside the plasma using coils and probes of assorted types.

6. Scattering of electromagnetic waves. When subject to incident radiation, the radiation which is scattered by the plasma is analysed.

7. Ion processes. Measurements of phenomena occurring to heavy non-electron species, such as charge exchange reactions and nuclear reactions.

A complete description of the theory that is involved in the various diagnostic implementations mentioned above is available in the literature [75]. The following sections describe the most commonly used diagnostic techniques which have been applied to plasma etch systems.

3.2 Optical Emission Spectroscopy

Optical emission spectroscopy (OES) is the most widely used optical method used for plasma monitoring and characterisation. This method relies on the detection of emissions of line radiation from plasma species as they 'relax' from excited electronic states. Excitation is usually achieved by electron impact reactions within the plasma. As the electron bound to the atom, molecule or ion undergoes relaxation, it falls to a lower energy level and emits the difference in energy as line radiation. The line radiation is a characteristic of both the plasma species involved and the energy level transition [76]. In an atom, each change of electronic

state gives rise to an emission line, whereas in a molecule each change of electronic state gives rise to a band system. The various bands of the system arise from differences in the vibrational state of the molecule and in general involve much smaller energy intervals than the electronic changes. Identification of species from observed emission lines can prove problematic because the band systems often overlap in a multi-species system such as a complex plasma. A summary of previously identified optical data is available in the literature [77] to aid species identification.

OES techniques are relatively simple to implement, and their widespread use can be partially attributed to the fact that the technique is almost completely non-invasive. This means that the interaction between plasma parameters is not disrupted. However, information from the discharge is limited to those species which emit light and very little can be obtained on the polyatomic and ionic species which often play important roles in plasma etch processes[78].

The most common implementation of OES is as an end-point detector. For end point detection to be successful some variation in the reactant or product concentrations must be optically detectable. A more sensitive end-point is usually obtained if a characteristic reaction product can be monitored, as the reactant species may only change concentration by 10-20% during a complete etch process. Table 3–1 shows some of the most common emission lines which have been used to determine etch end-points in the Si based wafer fabrication process.

OES also has an important role to play in the fundamental characterisation of plasma based processes. Observed line radiations are characteristic of the thermodynamic state and composition within the discharge chamber. This type of diagnostic has therefore been used by many plasma researchers in the field in order to produce fundamental models which can approximate the chemical and physical interactions of some plasma etch processes. For example, OES techniques have been applied in the investigation of the reactive ion etching of Si using a CF_4/O_2 discharge. In particular, OES has greatly increased the present understanding of the role of oxygen in this process [81]. Other workers have

Material Etched	Species Monitored	Wavelength (nm)	Reference
Si, polySi	F^*	703.8	[79]
	SiF^*	777.0	[79]
SiN, Si_3N_4	F^*	703.8	[79]
	CN^*	387.1	[79]
	N_2^*	337.1	[79]
	N^*	674	[78]
SiO, SiO_2	CO^*	483.5	[79]
	CO^*	519.5	[79]
Al	$AlCl^*$	261.4	[80]
	Al^*	396.2	[80]
Resist	CO^*	483.5	[79]
	CO^*	519.5	[79]
	OH^*	308.9	[78]
	H^*	656.3	[78]

Table 3–1: Common species and emission wavelengths which have been monitored to determine etch-process endpoints, where A^* indicates a species A in an excited state.

employed OES techniques to allow real time photoresist selectivity measurements to be estimated [82]. Some studies have also obtained estimates of the discharge electron temperature by measuring the intensities of two emission lines from the same excited species [83]. OES can also be used for quantitative chemical analysis of the discharge and for depth profiling of diffused or ion-implanted samples [84]. OES is also useful for *fingerprinting* of the process chamber under normal operating conditions. If a problem occurs at a later date, then another spectrum can be recorded and compared with the standard [79].

Using OES, it is usually straightforward to follow qualitative changes in dis-

charge properties as a function of the machine parameters. However, the majority of the plasma species are in the ground electronic state. To infer information about the ground state species from the emissions of excited species, a technique called *actinometry* was proposed [85].

3.2.1 Actinometry

Actinometry involves the use of optical emission intensity ratios to provide an estimate of ground state species concentrations. The emission intensity of the species of interest is divided by the emission intensity from an inert gas (the actinometer) which has been added to the discharge as a minority component. By ratioing the intensity signal in this way, actinometry can correct for the fact that variations in emission intensity may be due to changes in excitation rate caused by a shift in f(ε), instead of an actual change in species concentration. For actinometry to be able to relate species of interest X to the actinometer A, then the following conditions must hold [86]:

1. The excited species X^* and A^* must occur as a result of electron impact excitation of the ground state species.

2. The excited species must decay as a result of photon emission.

3. The electron impact cross sections and for X and A must have similar thresholds and shapes as a function of electron energy.

Actinometry can fail when mechanisms such as dissociative excitation compose a significant proportion of the production of excited species. Gottscho and Donnelly [87] examined emission line shapes from F^*, Ar^* and Cl^*. They found that for F^* in CF_4 based discharges, Ar could be used confidently as an actinometer to determine F concentrations. However, they found that Cl^* and Ar^* line shapes became substantially broadened during some parts of the rf cycle. They attributed this broadening to additional excitation mechanisms. Actinometry can

therefore only be applied to Cl based systems with great care and may not give a valid measure of the ground state concentration.

3.3 Mass Spectrometry

Mass spectrometers are used to measure the ratio of mass to electric charge of a molecule or atom. They can be used in several ways to monitor glow discharges:

1. Analysis of the discharge gas without line of sight to the chamber. This includes sampling of the exhaust gas with the spectrometer mounted in the pumping line between the chamber and the pumping system; and sampling through a controlled leak valve from the chamber. This setup is relatively simple to install but does not allow reactive species detection. There is a time lag involved between the chamber process reactions and neutral species detection, with the result that endpoints tend to be irreproducible or non-existent. Some researchers have reduced the time delay and increased the sensitivity by sampling through a small quartz capillary tube which was directly attached to the spectrometer probe head. Reactive species could be detected using this technique despite its markedly invasive nature [88].

2. Line of sight sampling of neutral species. This setup allows the detection of reactive species, but is not very sensitive. The major disadvantage is that mounting the apparatus is very complex in terms of cost and modifications to the etching machine [89]. Line of sight neutral sampling is most often used to provide information for basic studies of plasma chemistry.

3. Direct sampling of positive ions which have been created in the glow discharge, which is also known as in-situ SIMS. This is a very high sensitivity technique which has previously been used for ion-molecule reaction studies and to characterise the discharge [90]. However, the apparatus required is complex and the ions sampled are not representative of the neutral species concentrations [91].

Mass spectrometry usually consists of three stages: ionisation, mass separation and detection. Various methods have been used for each of these stages. The most sophisticated spectrometers are capable of differentiating small fractional mass differences. More commonly implemented are systems which can resolve peaks which are 1 amu apart. These systems are often referred to as *residual gas analysers* (RGA).

A schematic view of the stages involved in mass analysis is shown in figure 3–1. Ion production is almost always implemented by electron impact ionisation. Electrons from a hot filament cross the chamber to an anode and collide with gas molecules as they cross. This creates positive ions. The next stage of the analysis is mass separation of the ions, using either a magnetic sector or a rf quadrupole. The magnetic sector technique accelerates the ions through a uniform magnetic field which then separates the different mass to charge ratios. The quadrupole technique uses four electrodes to filter the different masses. One pair of electrodes in the quadrupole acts as a low pass filter, while the other set acts as a high pass filter. The end result is a band pass filter. A more comprehensive review of these techniques is beyond the scope of this work but is available in the literature [92]. Detection is typically carried out using a combination Faraday cup - electron multiplier arrangement.

Each gas species has a unique mass/charge ratio, while the peak amplitudes are dependent on the gas and instrumental conditions. The different peaks which can be obtained from a gas sample are created primarily by isotopic mass differences, multiple ionisation and dissociative ionisation. The particular species which are monitored during the process depend on the etching equipment used; the way in which the mass spectrometer has been employed; the gas chemistry; and the layer(s) to be etched. A brief summary of some of the species which are useful for characterisation and endpoint detection is given in table 3–2.

Obtaining quantitative results from mass spectrometry is very difficult due to the complexity of both the process and the equipment. However, some useful qualitative ideas have been formulated using this technique. An analysis of

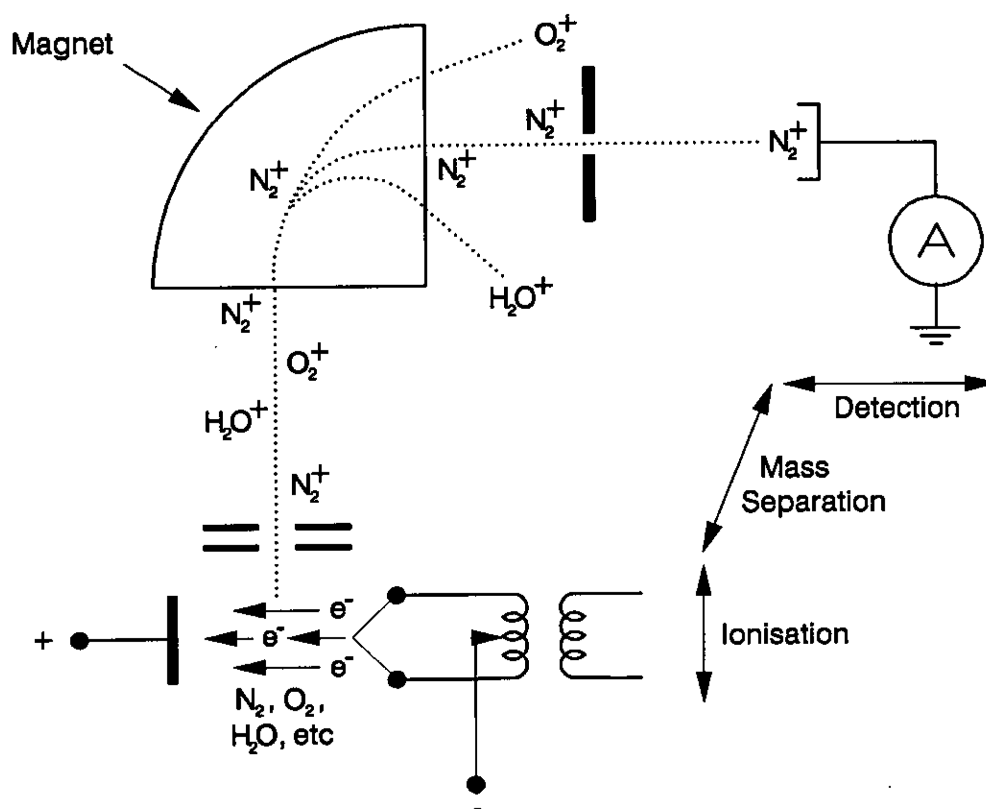

Figure 3–1: The three stages involved in a typical mass separation: hot filament ionisation; mass separation using a magnetic sector; and detection with a Faraday cup.

the CF_4 based etching of a Si/SiO_2 system lead to the formulation of the fluorine:carbon ratio approach to the qualitative characterisation of fluorocarbon based plasma-assisted etching [91]. Mass spectrometry is not always the best technique to use for process and discharge characterisation, and OES can yield more information. For example, the RGA approach has also been applied to the etching of Al in a BCl_3 chemistry, without yielding any information on Al containing species [94].

Mass spectrometry appears to have a similar sensitivity to OES but can provide more information on ions, radicals and polyatomic molecules within the discharge. One of the major advantages is that when operating as a neutral sam-

Etch Process	Species Monitored	Mass/Charge Ratio	Reference
Si_3N_4 on Si	CN^+	26	[88]
	CNF^+	45	[88]
	$SiNF^+$	61	[88]
SiO_2 on Si	Cl_2^+	70	[88]
TiW on Si	$SiCl_3^+$	133	[88]
Si	SiF_3^+	85	[78]
polySi	SiF_3^+	85	[78]
Si_3N_4	SiF_3^+	85	[78,93]
	N^+	14	[78,93]
	N_2^+	28	[93]
SiO_2	SiF_3^+	85	[78,93]
	O^+	16	[78]
	CO_2^+	44	[78]
	Si^+	28	[78]
photoresist	CO_2^+	44	[93]

Table 3–2: Species which have been employed for endpoint detection and plasma characterisation using mass spectrometry.

pler, mass spectrometry allows process control and monitoring to be implemented before the discharge has been struck.

3.4 Langmuir Probes

One of the most prominent figures in plasma research who did much of the early pioneering work was Irving Langmuir. The technique of electrostatic probes and the associated theory was developed by Langmuir and Mott-Smith in 1924 and has since become known as the Langmuir probe method.

An electrostatic or Langmuir probe is a piece of conducting material that is inserted into a plasma on a mechanical support and provides an electrical connection from the probe to external voltage biasing circuitry. The probe potential is varied over a range which normally includes the plasma potential. Electric current collected by the probe is monitored as a function of applied voltage. The shape of the resulting curve is dependent on the composition and the thermodynamic state of the plasma, and therefore contains information which can be used to characterise the discharge. Experimentally this is a very simple technique, but the theory needed to understand the IV curve more than compensates for this ease of implementation by being exceedingly complex. There are a number of comprehensive reviews which deal with the extensive theory required for a full understanding of electrostatic probe operation including Chen [95], Swift and Schwar [96] and Laframboise [97]. A full review of this theory is outwith the scope of this work, and only the necessary equations for parameter extraction will be outlined. In principle, information about the plasma potential; electron and ion densities; and electron temperature can all be obtained.

Consider the IV characteristic of a small metal probe which is immersed in a low pressure plasma, with the return current passing through the large reference electrode as shown in figure 3–2. A typical IV characteristic is shown in figure 3–3. It can be seen from the IV curve that there are basically three distinct regions of operation: the ion saturation region; the transition region; and the electron saturation region.

Assume that the probe is biased to the plasma potential V_p in a quasi-neutral plasma that consists of ions and electrons which both have a Maxwellian energy distribution defined by a temperature T. For the thin sheath collisionless regime the currents involved are [98]:

$$I_e = \frac{1}{4} A_p N e \left(\frac{8kT_e}{\pi m_e} \right)^{\frac{1}{2}} \tag{3.1}$$

$$I_+ = \frac{1}{4} A_p N e \left(\frac{8kT_+}{\pi M_+} \right)^{\frac{1}{2}} \tag{3.2}$$

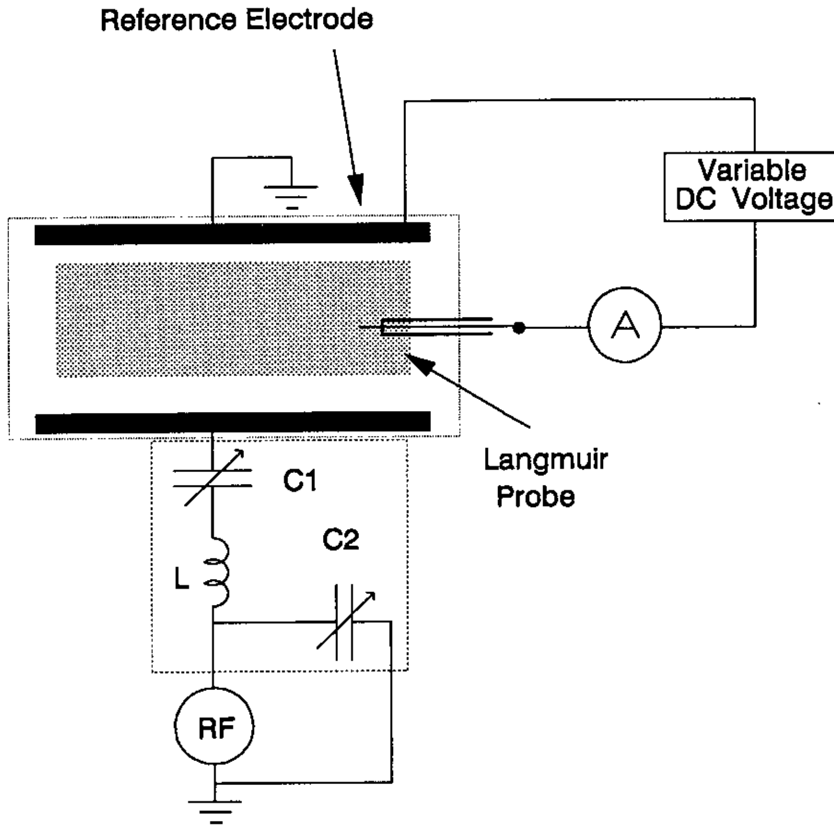

Figure 3–2: Basic Langmuir probe measuring circuit.

I_e and I_+ are the electron and ion currents respectively; A_p is the area of the collecting probe; N is the plasma density; e is the electron and ion charge; k is Boltzmann's constant; m_e is the electron mass; and M_+ is the ion mass. The current at the plasma potential is due almost entirely to electrons, because of the large mass difference between ions and electrons. When the probe is biased positively with respect to the discharge, the positive ions are repelled and electrons are attracted. There is a negative charge buildup near the probe surface which cancels the positive charge on the probe. This is the *electron saturation* region.

If the probe bias is decreased below V_p, positive ions are attracted to the probe. The ion concentration near the probe gradually increases and a positive sheath forms around the probe. As the potential applied to the probe reduces, the ionic component of the current gradually increases and the *transition region* of the characteristic is obtained. At the floating potential, V_f, the ion and electron

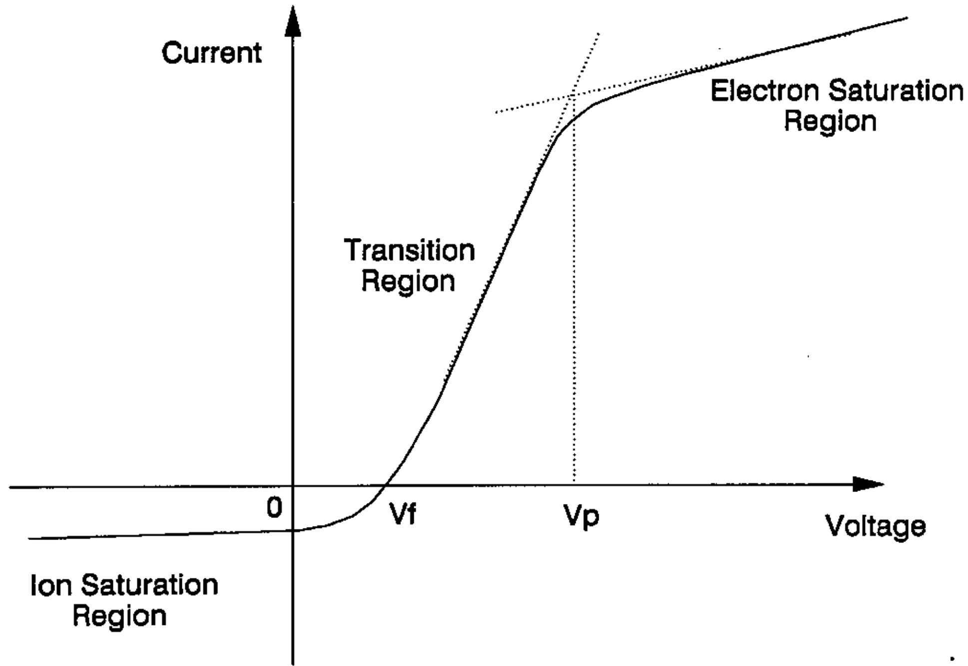

Figure 3–3: Typical single probe IV characteristic.

currents are equal and the resultant net current to the probe is zero. If the probe bias is reduced even further, then the current becomes entirely due to positive ions and the *ion saturation* region is obtained.

Excessive perturbation of the plasma can occur as a result of the probe collecting current in the electron saturation region. This is due to excessive electron currents being drawn from the discharge ($I_e \approx 100 I_+$) [99]. During operation in the more stable ion saturation and transition regions, the following parameters can be extracted from a plot of collected current against applied voltage:

1. Plasma Potential. This point can be extracted by looking for a maximum point on a plot of $\frac{\mathrm{dV_a}}{\mathrm{dI}}$ against $\mathrm{V_a}$ where $\mathrm{V_a}$ is the applied probe voltage.

2. Electron Temperature. In the transition region, the electron current is given by [98]:

$$I_e = \frac{1}{4} A_p N e \left(\frac{8kT_e}{\pi m_e}\right)^{\frac{1}{2}} \exp\left(\frac{-e(V_p - V_a)}{kT_e}\right) \tag{3.3}$$

A graph of $\ln(I_e)$ against $(V_p - V_a)$ should be linear with a slope proportional to T_e in electronvolts. I_e is obtained in a practical system by deducting the value of ion current from the total collected current.

3. Plasma Density. Once T_e and V_p have been computed, the plasma density can be calculated by looking at the current collected by the probe at V_p [100]. The current at this point is almost entirely due to electron flux, and so from equation 3.1:

$$N = \frac{-I_e}{eA_p \left(\frac{kT_e}{2\pi m_e} \right)^{\frac{1}{2}}} \tag{3.4}$$

The circuit shown in figure 3–2 shows how Langmuir probe measurements could basically be made. However there are problems involved with the implementation of practical measuring systems for reactive rf plasmas. Material deposition can occur on the probe which can alter the response characteristics. These contaminants can be removed by biasing the probe to a high negative voltage which allows localised sputtering of the probe end to occur. When making measurements in a rf plasma, a rf voltage will form across the probe-plasma junction. The IV characteristic, which is an average of many rf cycles, can be distorted by this ac component [101], and plasma loading may occur [102]. Two main experimental approaches have evolved to cope with this problem: the blocking filter technique [103,104]; and the driven rf probe technique [102,105].

The blocking filter technique uses two decoupling LC chokes in series with the probe to prevent rf currents distorting the IV characteristic. The filters are tuned to have resonant frequencies equal to the frequencies of the rf current, and are positioned as close to the probe as possible.

A second technique involves the use of a driven rf Langmuir probe. In this case, a second rf signal is added to the probe at a suitable phase and amplitude to null out the rf component between plasma and probe. The correct degree of feedback is obtained by observing the floating potential of the probe. Any rf

component on the characteristic will drive the floating potential negative, so the circuit is adjusted for maximum absolute floating potential.

Much research has been carried out on discharges using plasma probe techniques in order to gain basic information regarding the fundamental state of the plasma. Historically many researchers have concentrated on characterising the positive column in a dc discharge of a monotonic gas - often thought of as an 'ideal plasma.' Much of the research on rf discharges has also been carried out on simple gas chemistries such as pure argon [106,107]. Some researchers have also used electrostatic probes to characterise CF_4 and CHF_3 based chemistries to help characterise the role of ions in Si based etching processes [101,108]. An investigation into SF_6 and CCl_4 based discharges indicated that negative ions were present in the discharge [109].

Langmuir probe theory is very complex and difficult to implement. However, information regarding the important discharge parameter V_p can only be obtained using some type of probe. Despite the invasive nature of the technique, it can yield very useful information.

3.5 Microwave Interferometry

Another technique which has been proposed to measure the plasma density is microwave interferometry. This has the advantage of being far less invasive than Langmuir probes. When a microwave beam of a known frequency is passed through a typical etching plasma, a phase shift is introduced to the beam. The detected signal amplitude depends on the relative phases of the two paths of the interferometer and varies with the average plasma density in the transmission path. This type of system is known as a microwave phase shift interferometer [110], and requires initial calibration to an accurate measure of the plasma density such as a Langmuir probe system.

3.6 Laser Induced Fluorescence

To obtain more quantitative information about plasma processes, an optical technique such as *laser induced fluorescence* (LIF) can be employed. LIF has the advantage that it can directly detect ions, molecules and atoms which are in the electronic ground state. LIF combines the high spatial and spectral resolution of a laser technique with a high sensitivity, which allows the detection of low concentrations of reactive radicals and ions [86].

This method uses a tunable dye laser beam to pass through a discharge chamber and resonantly excite atoms or molecules, which subsequently fluoresce. A significant limitation of this approach is that the targeted species must fluoresce with a reasonable quantum efficiency. This is not necessarily true for the larger polyatomic molecules which are present in plasmas. Background light must also be kept to a minimum when using LIF, and discharge emissions as well as scattered laser light can cause problems. A LIF spectrometer also relies on a laser source of an appropriate wavelength being available to match the spectroscopic transition of the species to be detected. This is not always possible.

3.7 Optical Reflection

Optical reflection makes use of either the differences in reflectivity of an incident light source at a material layer boundary, or it looks at the interference effects in the thin film being etched. In the optical reflection mode, the change in reflectivity is monitored as a function of time. As the boundary point is reached, there is a change in the intensity of the reflected signal. The magnitude of the change is proportional to the ratio of the two material layers which are encountered. If a film is transparent, then the reflected intensity varies approximately sinusoidally as the interference conditions vary with decreasing film thickness. The periodicity

of the reflected signal against time plot varies with both the etch rate and the refractive index of the film being etched.

This type of diagnostic implementation is highly suitable for endpoint detection and various different forms of this technique have been successfully used. Both coherent and non-coherent light sources have been employed with in-situ *laser interferometry* emerging as one of the most common systems [111,112]. An in-situ ellipsometric version has also been reported [78].

3.8 Other Techniques

Many other techniques have been used to monitor and endpoint plasma processes. These include discharge impedance monitoring [113]; optogalvanic spectroscopy [114]; pressure monitoring [115]; absorption spectroscopy [86] and chemiluminescence [115].

Discharge impedance monitoring is useful for endpoint detection as it monitors the change in impedance across the plasma as layer boundaries are reached. Optogalvanic spectroscopy monitors the change in discharge characteristics (current, voltage, electron density) which are induced by the absorption of light. One of the simplest endpoint techniques is the monitoring of chamber pressure, although the usefulness of this technique has been reduced by the easy availability and widespread use of constant pressure control systems. Absorbance spectroscopy in the infra-red, visible or ultra-violet can allow detection of ground state species. Information regarding absorbance coefficients can be obtained from species that do not fluoresce or give rise to an optogalvanic effect, but the sensitivity is limited. Chemiluminescence is a downstream technique which detects the emission of light from the reaction products of a chemical reaction, and is used primarily to study heterogeneous reaction mechanisms.

3.9 Summary

In this chapter, the diagnostic techniques which have been implemented for plasma characterisation were described. The most extensively used methods rely on optical emission spectroscopy, mass spectroscopy and electrostatic Langmuir probes. Between them, these three approaches can infer information about neutral and charged particles within the plasma as well as accessing some of the fundamental plasma variables. Various other approaches which can yield end-point and characteristic information were also reviewed. This field is of major importance because as the plasma etch processes develop in complexity and diagnostic equipment reduces in cost, this type of equipment will become increasingly incorporated into advanced dry etch systems.

Chapter 4

Modelling Strategies for Plasma Etch Processes

4.1 Introduction

To achieve the sub 1μm linewidths that are required for ULSI, process characterisation is essential. Historically much of the improvement in plasma etching has been due to improved vacuum technology and an improvement in the rudimentary understanding of plasma chemistry [116]. These approaches are no longer sufficient for reproducible fine line definition and rigorous empirical modelling techniques must be employed. The first stage for successful process control is process characterisation or modelling. This allows feedback between the daily operating characteristics of the process to be compared with the model and allows monitoring and assessment to be carried out. In this way, process drifts can be identified and suitable action taken, which improves yield and therefore increases efficiency. Successful modelling also allows the equipment manufacturer to use the model as a framework for a fully automated feedback and control strategy.

4.2 The Choice of Model

Scientific research can be described as a process of guided learning. This learning process is advanced by *iteration* until a successful outcome is achieved. An initial hypothesis leads by a course of deduction to certain consequences which can be compared with data. When the consequences and data fail to agree, then the hypothesis must be modified and a second iterative cycle initiated. The consequences of the modified hypothesis are then worked out and again compared with data to check their accuracy. This can lead to further modifications and gain of knowledge until an accurate hypothesis, or model, is obtained. The learning process can therefore be described as a feedback loop in which the discrepancy between data and the consequences of the proposed model leads to a modified model, etc.

The choice of modelling strategy can be divided into *statistical* design and *mechanistic* design. Assume that in a course of study of some physical phenomenon, enough of the physical mechanism was discovered to *deduce* the form of the relationship linking the output, η, to the inputs via an expression:

$$\eta = f(\xi, \theta) \tag{4.1}$$

where $\xi = (\xi_1, \xi_2, ...)$ is a set of input variables measuring, for example, power, pressure, gas flows, etc. and $\theta = (\theta_1, \theta_2, ...)$ represents a set of physical parameters measuring, for example, V_p, $f(\varepsilon)$, T_e, n_i, n_e, reaction rate coefficients, radical and neutral concentrations, etc. Then it is possible to say that equation 4.1 represented a mechanistic model. Accurate mechanistic models represent the ideal solution for researchers, as they require a complete knowledge of the chemical and physical interactions which occur within a process.

Often, the necessary physical knowledge of the system is absent or incomplete, and no mechanistic model is available. This is generally the case in plasma based processes due to the size and complexity of the parameter space, and the

difficulties involved in measuring most of the fundamental coefficients as outlined in section 2.4. In these circumstances, it can often be assumed that the relationship between η and ξ would be smooth. If this is true, then $f(\xi, \theta)$ can be locally approximated by an interpolation function $g(\xi, \beta)$, such as a polynomial. The elements of set β would be the coefficients of the interpolation function, and would be related to, but distinct from, the parameters, θ, of the physical system. This statistical model could therefore be represented as:

$$\eta \simeq g(\xi, \beta) \tag{4.2}$$

This technique is applicable when the input variables are quantitative within an operating area of interest and the experimental error is not too large compared to the range covered by the observed responses.

The purely mechanistic model and the purely statistical model represent extremes. Mechanistic models are appropriate to a system in which a great deal is accurately known about the system. Statistical (also known as empirical or parametric) models are appropriate to systems in which nothing can be assumed except that the response surface was locally smooth. In most real investigations the situation is somewhere in the middle.

The approach that is generally taken for complex process characterisation is outlined in figure 4–1. At the WHICH stage the objective is to determine which of all the possible input variables have a significant and important effect in terms of the response variable. This stage is often referred to as screening. At the HOW stage the intention is to learn more about the pattern of response behaviour as changes are made in the significant variables. This phase results in the formation of a statistical model. At the WHY stage, an attempt is made to determine the fundamental mechanistic reasons for the behaviour which has been observed in the previous stage.

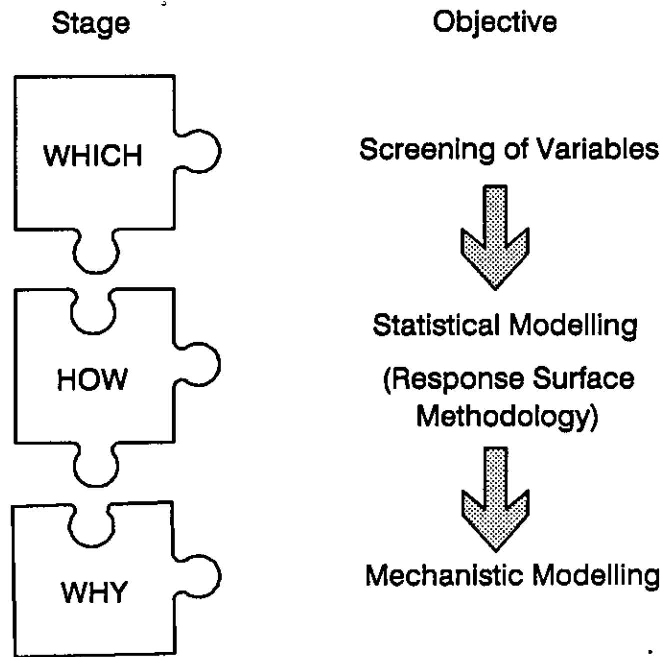

Figure 4–1: A generalised approach to model building.

4.3 Statistical Model Building

Much of the empirical process characterisation and optimisation work that has traditionally been carried out has used a single factor approach. In this case, the effect of each individual parameter on the process is evaluated while all other factors are held constant. If there is interaction between parameters then this type of procedure may not always succeed in optimising a process as shown in figure 4–2. Any change in either parameter from the starting point will result in a lower response. In some cases, conclusions based on single parameter at a time characterisations are over generalised and subsequently found to be invalid.

Response Surface Methodology (RSM) is now a common technique [117,118] applied to the characterisation of a full dimensional operating space. Many different types of experimental designs are available to the researcher who requires to investigate response surfaces. At one extreme is a full factorial design with all the settings of every factor appearing in all possible combinations with the settings

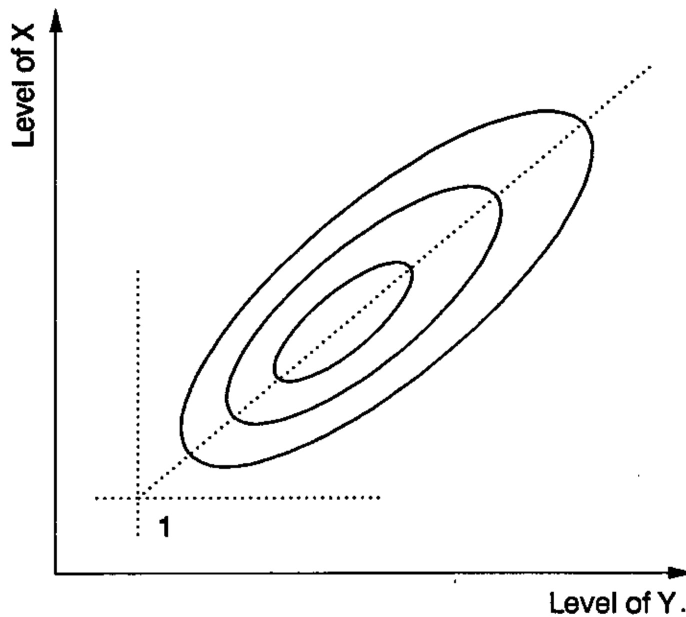

Figure 4–2: A contour plot of a typical response surface for a 2-factor process.

of all the other factors. The results are analysed to understand the correlations between the parameters and the resulting responses. This type of approach is most commonly used when the factors have only two levels. The total number of runs is then a power of two where the value of the power equals the number of factors. When the number of different factors increases beyond four or five, this type of design becomes very expensive and time consuming to run. However, this approach has the advantage that it estimates all of the main effects, and the interactions (multiple factor effects) of any order are statistically independent.

To reduce the number of runs in an experiment, a design other than full factorial must be used. These designs use subsets of the full dimensional search to characterise the process, and include orthogonal designs. A review of the history of orthogonal design is available in the literature [119]. In general, the purpose of orthogonal design is to efficiently, and rigorously, study the relationship between process parameters and their response functions by selecting certain representative combinations of the input parameter level settings. These level settings fit into certain orthogonal tables. By following the orthogonal tables, the maximum

amount of information about the response characteristics can be obtained for the least number of experiments. Many different types of these classical experimental designs exist including fractional factorial designs; Plackett-Burman designs; Box-Behnken designs; central composite designs; and D-optimal designs [120]. These designs allow a major reduction in the number of experimental runs but do not allow independent estimation of all the possible interactions. The resolution of a design is a measure of which effects are 'confounded'. For example, a resolution V design confounds main effects with four factor interactions and two factor interactions with three factor interactions. This confounding process is the trade-off that is paid for the reduced experimental matrix. When the two factor interactions are confounded with the three factor interactions, it is impossible to distinguish which of the specific interactions which are confounded together is responsible for an observed effect. If necessary, further experimentation can be employed to remove any confusion.

Construction of a statistical model is generally a two stage procedure, as shown in figure 4–1: *screening of variables* and *response surface methodology.* At the beginning of an investigation there are often a long list of variables $\xi_1, \xi_2, \ldots$ which could be important in the determination of η. The list of variables can either be reduced using 'expert knowledge' gained from previous experience or, more reliably, by employing a preliminary statistical screening design. For example, this could involve using a two-level fractional factorial design to identify variables which are worthy of further study.

The most influential variables, identified at the screening stage, can then be used to form an experimental design such as the central composite design for three variables shown in figure 4–3. When the experiment is completed, the data obtained is sufficient to describe the process response over the entire dimensional space represented, according to a second degree equation of the form:

$$\eta \simeq \beta_0 + \beta_1\xi_1 + \beta_2\xi_2 + \beta_3\xi_3 + \beta_4\xi_1\xi_2 + \beta_5\xi_1\xi_3 + \beta_6\xi_2\xi_3 + \beta_7\xi_1^2 + \beta_8\xi_2^2 + \beta_9\xi_3^2 \quad (4.3)$$

where ξ_1, ξ_2 and ξ_3 are the input variables and β_0 to β_9 are the weighting coefficients. A complete array would require a minimum of 14 experiments using this

design. The coefficients in the equation could be solved using only 11 experiments but this would not be possible using an orthogonal approach. Regression analysis techniques are often employed to estimate the weighting levels for the polynomial. The resultant 'fitted' polynomial can be used to visualise the response surface of the output within the entire operating space. Process monitoring, optimisation and control can then be carried out on the basis of the statistical model.

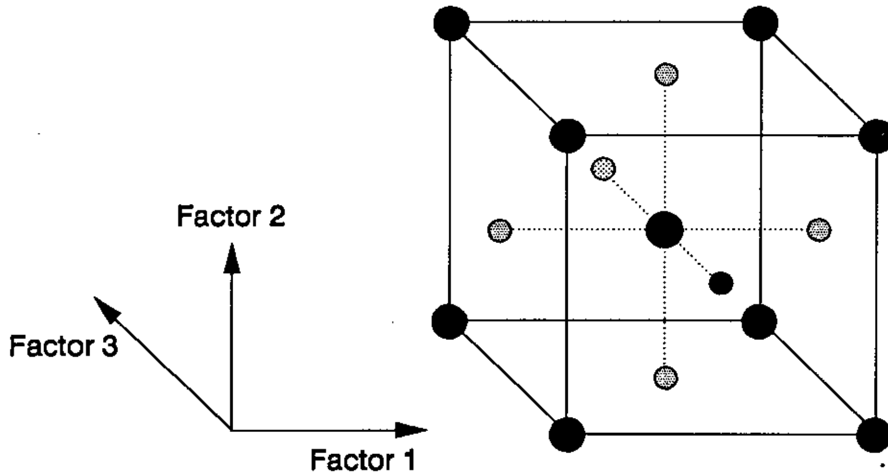

Figure 4–3: Central composite model with three variables.

4.3.1 Statistical Process Models

The complex processes and narrow tolerances which are characteristic of the silicon wafer fabrication industry have provided many opportunities for statistical modelling techniques to be implemented. Typical applications have included the modelling of the aluminium sputter etch rate and uniformity for more reliable metallisation [121]; and the characterisation of a low pressure chemical vapour deposition system for un-doped polysilicon [122]. It has also been applied to the optimisation of photoresist processing and optical stepper development [119]; and electron cyclotron resonance CVD silicon oxide planarisation [123]. However, it is in the field of plasma etch processing where statistical modelling techniques have the potential to provide the largest advances in operational knowledge.

Bergeron and Duncan first applied statistical design techniques to optimise the anisotropic etching of polysilicon in a C_2F_5Cl/O_2 glow discharge [124]. A radial-flow, parallel plate reactor, operated in the plasma etch mode, was used as the basis for this work. Power, pressure, O_2 percentage and temperature were used as the inputs in a central composite design. It was demonstrated that the polysilicon edge slope could be reproducibly varied from nearly complete isotropy to almost vertical sidewalls and that the model provided a good approximation to this behaviour.

Mocella et al used RSM techniques to model the etch rate of polysilicon in a CF_3Cl/Ar glow discharge [125]. Power, pressure and gas composition were selected as inputs to a design which fitted a cubic polynomial to the etch rate response. This required a 3-factor, 7-level design which employed 37 experimental runs. Etch rate models accounted for approximately 97% of the observed results.

The problem of optimising a nitride etch process on a single wafer plasma etcher was addressed by Yin et al [119]. This process used C_2F_6 as the sole reactant and varied the total flow of the C_2F_6; the applied power; the chamber pressure; and the inter-electrode spacing. A 4-factor, 3-level design was employed to model the etch rate, uniformity and selectivity of the process.

Feng et al employed a preliminary screening design to reduce the variable parameter space from six to the three most influential parameters [126]. A radial flow, batch RIE system employing a CF_4/O_2 chemistry to etch SiO_2 was used as the basis for this study. Applied power, percentage of O_2 and system pressure emerged as the most influential parameters which controlled the process. The total gas flow rate, etch time and position of the sample on the electrode were eliminated during the screening stage. A 3-factor, 3-level Box-Behnken design was used to model the etch rate using a quadratic polynomial. The average error between the model and the practical operating characteristics was around 5%.

Riley et al have used statistical techniques to characterise the etch rate and uniformity of a SF_6 based process for tungsten etchback in a magnetron enhanced, single wafer etcher [127]. The reactive ion etching characteristics of InP

in CH_4/H_2 have also been investigated using RSM techniques [128]. McLaughlin et al have used RSM to analyse the etching of Si and SiO_2 in CF_4/O_2 and CF_4/H_2 chemistries for the purpose of real-time monitoring and process control [129].

4.4 Mechanistic Model Building

Mechanistic modelling techniques are now being extensively applied by many semiconductor equipment manufacturers in order to optimise systems before hardware is constructed. Novel equipment and processing concepts can be simulated, analysed and optimised in areas such as vertical CVD furnaces, rapid thermal processes, plasma-enhanced CVD and lithography tools. However, this type of approach has not met with the same degree of success when applied to the field of plasma etching. A large parameter space coupled with complex physical/chemical interactions within the discharge chamber have meant that the gap in knowledge between state of the art equipment and the latest models has not reduced. Some research has indicated that it may need at least fifteen years more research before models can be generated which are useful to the equipment manufacturer or process engineer [130].

4.4.1 Mechanistic Process Models

Because of the complex nature of the process involved, most physical models have concentrated on modelling specific aspects of the glow discharge using chemistries such as Ar or pure CF_4. Dalvie et al present a good review of the steps that are necessary in order to successfully model a plasma etch process [131]. The two major areas which are of interest in plasma reactor modelling are the discharge structure as a function of electrical parameters; and the transport and reaction of neutral species governing the etch performance. Advances towards achieving complete discharge models have been made by using discrete Monte-Carlo techniques [101]. However, at the time of publication, there were no models developed

which were sufficiently simple and accurate to be included in transport and reaction predictions of etch rates. Many authors [132,133] have therefore proposed models which predict that process performance may be derived by making assumptions about the magnitude and form of the electron densities and energies within the discharge.

4.5 Summary

In this chapter, some of the problems which face researchers engaged in the field of plasma etch modelling are outlined. Although mechanistic models provide the ideal solution to current process problems, they are not yet accurate enough to provide a realistic representation of the plasma/materials interactions. Statistical techniques have been proposed as a solution to fill this gap in knowledge between the latest processing equipment and the current level of understanding of the physical and chemical interactions occurring in the process chamber. Factorial designs result in a rigorous characterisation of the process throughout the operating region. This empirical approach approximates the chamber reactions with a continuous polynomial and fits experimental results in order to obtain weighting coefficients for this equation. Orthogonal designs can be employed to reduce the total amount of experimentation that is required, allowing more efficient process characterisation and control.

Chapter 5

Experimental Setup and Characterisation

5.1 Introduction

The assembly and test of all the equipment which would be required to monitor and accomplish aluminium etching is described. Initially this involved the extensive re-design and conversion of an existing batch oxide RIE machine to cope with the highly reactive chlorine chemistries which are necessary for aluminium etching. In the previous chapter, various plasma monitoring and diagnostic techniques were described. From this wide range of diagnostic techniques, three systems were selected which provided a broad spectrum of plasma information: optical spectroscopy, mass spectrometry and electrostatic Langmuir probes.

After interfacing these systems to the RIE machine, the diagnostics were initially characterised using a 'basic' argon glow discharge to minimise the effects of molecular interactions. Argon plasmas have been used for many years by researchers to investigate the fundamental characteristics of plasmas and published data exists with which to check the results of this particular experimental setup.

5.2 RIE System Description

The etch equipment that was used in this project was based on a Vacutec 1500 series RIE machine. The batch reaction chamber on this system was 37cm in diameter; centre pumped and capable of processing up to eight 75mm wafers. Wafers were loaded manually into the reaction chamber. The chamber and electrode were fabricated of aluminium and had a fixed electrode spacing. The powered electrode was cooled, using chilled re-circulating water.

The ability to maintain constant pressure at a range of flow rates is an important requirement in a dry etching machine. In this system, a butterfly valve was employed to vary the effective pumping speed at the centre of the reaction chamber. The valve was connected to a closed loop control circuit which altered the position of the butterfly valve to minimise the difference between the reference set-point and the actual pressure. Actual chamber pressure was measured using a Vacuum General CML series capacitance manometer.

Rf power was applied to the bottom electrode via a matching network. The rf generator was an ENI ACG-6 which could supply up to 600W of power at 13.56MHz. Impedance matching of the rf generator to the reactor was accomplished by a Vacutec Plasmatch network. Differences in impedance between generator and load result in rf power being reflected back to the generator. The matching network detects the amplitude and phase of the reflected wave. An error signal is generated which drives servo motors on two variable capacitors until the phase shift and amplitude signals are minimised. The network consists of one fixed value inductor and two variable capacitors in a basic 'L' configuration. The connection between the matching network and the powered electrode was a silver plated copper strip which was enclosed in an aluminium housing to prevent rf leakage.

Up to five different process gases can be used to perform etching operation, with each line is regulated by a Vacuum General UFC series mass flow controller

(MFC). The gases are combined in a stainless steel mixer tank on the reactor side of the gas jungle. The gas mixture is then introduced to the chamber through a gas distribution ring, located at the periphery of the lower driven electrode.

System operation is effected by means of a manual process controller. This unit controls the valve settings, the enabling of gas lines, purging and pumping. Process recipe times have to be implemented manually.

Chamber pumping was carried out by an Edwards E2M40 two stage rotary pump. The pumping speed was increased by the addition of an Edwards EH250 roots blower mounted above the rotary pump.

The Vacutec RIE machine is a small batch reactor which is intended for research and development applications. In this original configuration, the system was used to etch silicon dioxide and silicon nitride in a CF_4/O_2 plasma chemistry. However, for the purposes of this research project, the original system needed redesigned for several reasons:

1. In order to etch aluminium, a reactive chlorine based chemistry would have to be used. This type of recipe is extremely corrosive, highly toxic and therefore places specific demands on the system.

2. Diagnostic equipment required interfacing to the RIE.

Many of the major components of the RIE system were altered in order to perform aluminium etching characterisation. Specific modifications that were carried out were:

1. The reactor chamber was re-designed so that only the lid opened when wafers were loaded and unloaded. This allowed the mass spectrometer to be permanently mounted to the earthed chamber sidewall.

2. A Conflat 114 flange for the mass spectrometer was added to the chamber sidewall.

3. Three new viewing ports were added to the chamber sidewall to effect Langmuir probe and OES access.

4. The chamber sidewall was securely attached to the reactor base-plate. This arrangement meant that one extra large 'O' ring seal was required in the system.

5. The aluminium electrode was replaced with an anodised aluminium electrode. This electrode material is more resistant to the chlorine chemistry and therefore reduces the amount of chamber contamination.

6. Four extra process gases were added to the system: BCl_3, Cl_2, Ar and He.

7. Two MFCs were replaced with Kalrez [1] sealed, corrosion resistant versions in order to cope with BCl_3 and Cl_2.

8. A load locked fume cover was designed and fabricated to cover the etch cabinet so that toxic residues from the chamber were isolated from the operator. The fume cover was continuously purged with nitrogen, and pumped so that it was maintained at a lower pressure than the surrounding clean room. A nitrogen purged load lock was also incorporated for wafer transfer to and from the etcher.

9. The Vacuum General CML series capacitance manometer was replaced with a high temperature Vacuum General CMH capacitance manometer. Temperature changes within the RIE cabinet were observed to influence the system pressure reading, and a gauge which remained at a constant higher temperature of 35°C removed this source of error.

---

[1] Kalrez is a trademark of E. I. Dupont Co.

5.3 Optical Emission Spectroscopy

Two different systems were used in the course of this work to perform optical emission spectroscopy. To study a wide range of wavelengths, an EG&G 1460 optical multi-channel analyser (OMA) was used. Once a particular wavelength of interest had been identified, a Bentham M300 monochromator could be employed for intensity measurements.

The schematic layout of the EG&G OMA is shown in figure 5–1. Radiation from the plasma chamber is transmitted along an optical fibre link to the spectrograph, and strikes the collimating mirror. The collimating mirror is aligned to reflect the light to a diffraction grating. The grating then disperses the electromagnetic radiation into its constituent wavelengths. The light is directed to the focussing window and into the detector. The spectrum is incident on a silicon diode array detector which converts the intensities into electrical signals. A trickle of dry nitrogen gas is fed into the detector for cooling and to keep condensation from forming on the silicon diode array. A detector controller translates the electrical signals into digital data which is transmitted to the 1460 system processor. The system processor controls the data acquisition process as well as providing analysis and data storage facilities.

The specific setup for the experimental system used a 300 grooves/mm grating, blazed at 650nm, which gave an effective wavelength detection spectrum of 300 to 800nm. A 25μm slit size was fitted to the entrance aperture of the spectrograph to give a resolution of approximately 0.5nm.

System calibration for the OMA was achieved using a standard argon/mercury low pressure glow discharge tube. Initially a quadratic fit of the following four optical intensity peaks was carried out: 363.6, 575.0, 577.2 and 801.3nm. The relative intensities and absolute wavelengths of these peaks were obtained from a calibration chart which was characteristic of the argon/mercury discharge tube. This particular calibration method was found to result in errors of up to 10nm

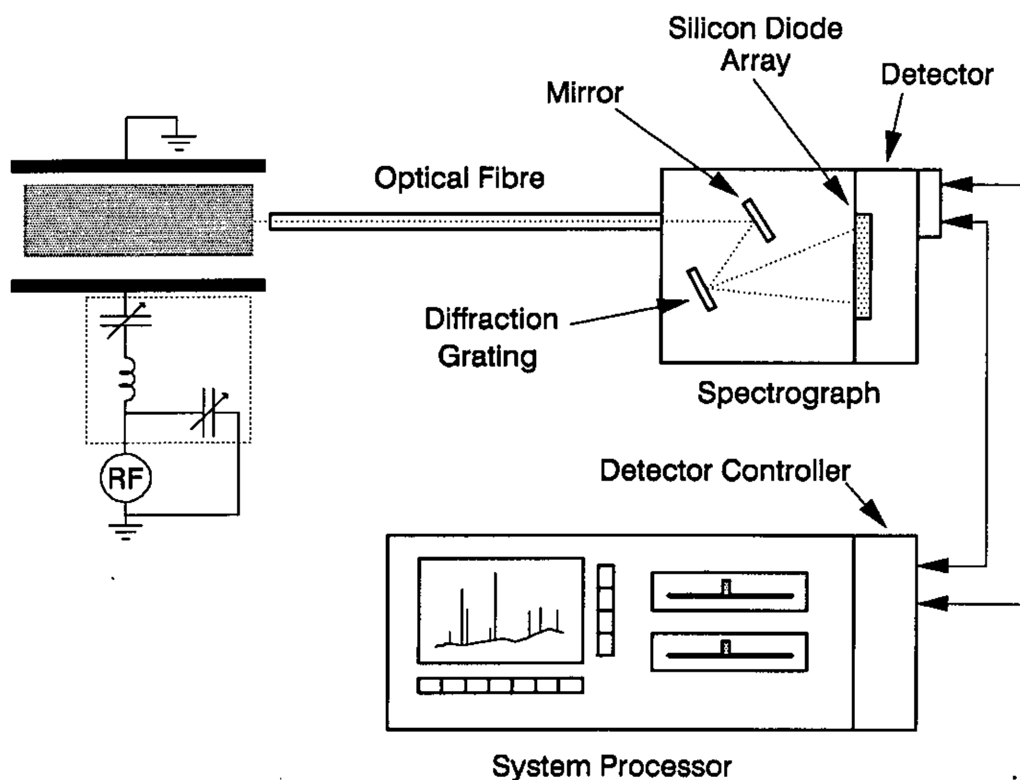

Figure 5–1: The EG&G OMA spectrograph setup used for wide spectrum evaluations.

at the high end of the wavelength spectrum. A more accurate calibration was obtained when a cubic fit was carried out on the following six peaks: 316.0, 435.8, 546.1, 579.0, 696.5 and 794.8nm. This method resulted in a maximum error across the mercury/argon spectrum of 1.3nm.

A useful feature of the OMA 1460 is the ability to isolate and analyse the emissions which are being generated purely from the source under investigation. Before any plasma processes were investigated, the OMA was used to obtain a background spectrum. This reference spectrum was then stored and could be automatically removed from any experimental results. Specific wavelengths and intensity changes could be observed more easily using this technique.

A second system was also used to investigate the optical intensities of single wavelengths. This setup used a Bentham M300E monochromator. The

monochromator was a symmetrical Czesney-Turner design with a focal length of 300mm. Wavelength dispersion was again carried out using a diffraction grating. Wavelength selection was performed manually by a micrometer which rotated the diffraction grating relative to the incident light. The micrometer enabled wavelengths to be selected in 0.05nm steps. A variable gain photo-multiplier tube was used to convert the light into an electrical signal. Power for the photo-multiplier tube was provided by a 1000V power supply. The value of electrical current at each selected wavelength was measured using an integral high sensitivity ammeter and displayed on a digital front panel display. Permanent recording of the spectrum intensities was accomplished by monitoring the output using a chart recorder. A schematic of this system is shown in figure 5–2

This system used a 1200 grooves/mm diffraction. Overall, there was a resolution of 0.5nm, due to the inherent misfocus in the monochromator. Initially the monochromator aperture was closed off to light and the zero point for the photo-multiplier tube was adjusted to zero. System calibration was performed using an argon/mercury low pressure glow discharge tube. The major emission peaks in the mercury spectrum were measured and the wavelength accuracy was within the system resolution throughout the range.

5.3.1 Intensity Variations with Machine Parameters

In order to check the performance of the optical system, intensity monitoring was carried out on argon glow discharges in the Vacutec RIE. Argon atomic emission intensities were investigated with the monochromator tuned to the 750.4nm line. The effects of the machine parameters on the important atomic excitation and relaxation reactions occurring within the plasma chamber are outlined. A full 3-dimensional characterisation of the argon discharges was not necessary for this stage of the project, so a one dimensional characterisation was performed around the major machine dependent variables of power, pressure and flow rate.

For a total argon gas flow of 6sccm (standard cubic centimetres per minute) and a constant chamber pressure of 20mtorr, the rf power was varied. The applied

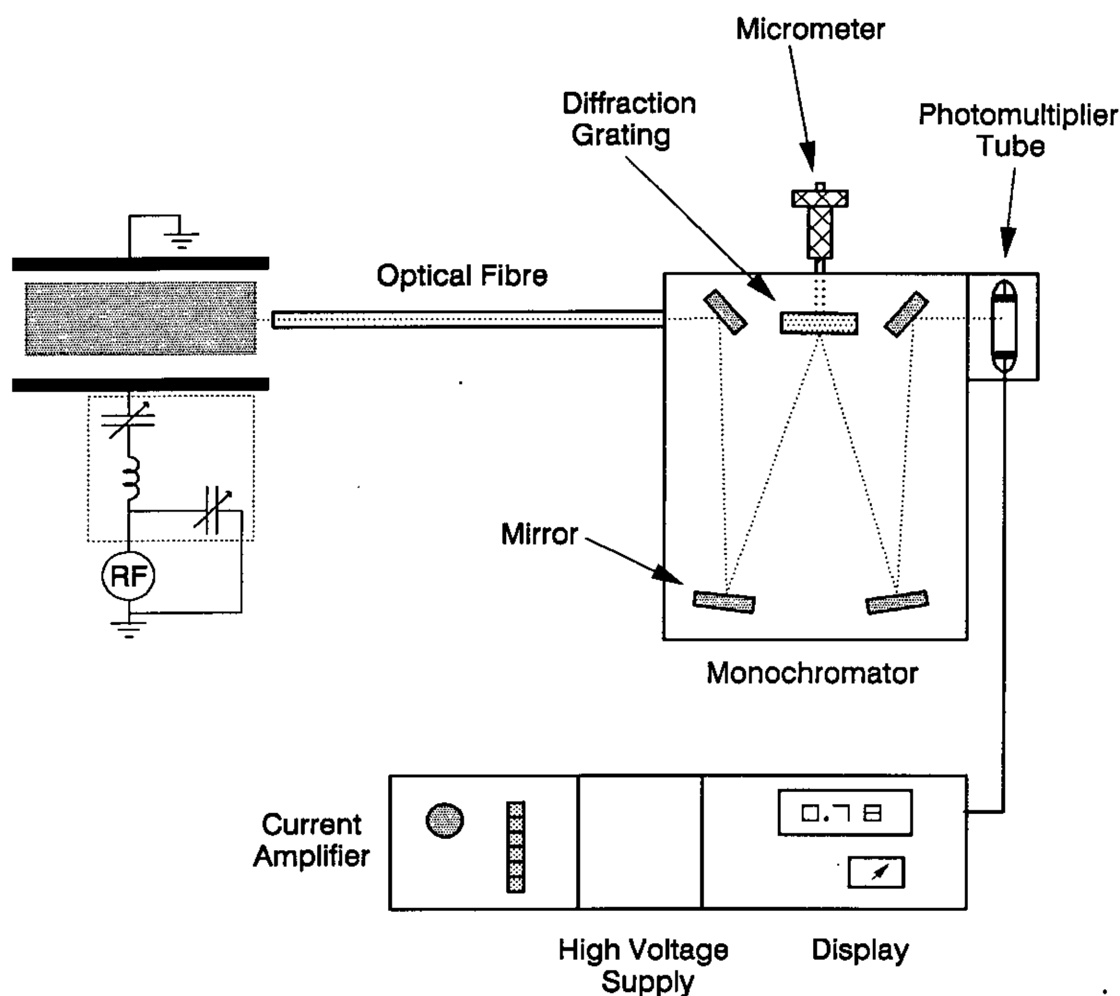

Figure 5-2: Schematic of the monochromator system used in this work.

power range was 10 to 200W and the argon atomic intensities were noted at each level. The results from this experiment are shown in figure 5–3.

It can be seen that as more energy is applied to the plasma, more photons are emitted by the atomic argon. The Ar intensity has a non-linear dependence on the rf power, which is in agreement with the results of Coburn and Chen [85] who investigated Ar emissions within a $Ar/CF_4/O_2$ plasma. This behaviour is consistent with the fact that excited Ar atoms are formed from a single electron collision ($e^- + Ar \rightarrow Ar^* + e^-$), with a species whose density is constant as rf power is varied.

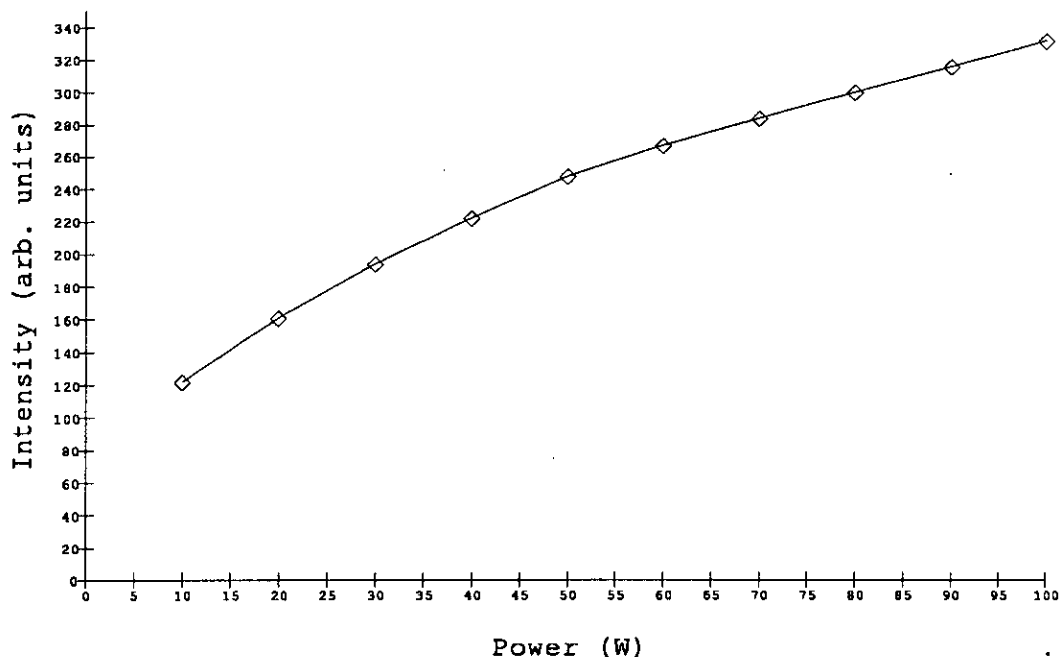

Figure 5–3: Intensity of the 750.4nm argon atomic emission line as rf power is varied, at a pressure of 20mtorr and a flow rate of 6sccm.

For a constant argon flow rate of 6sccm and a constant rf power of 50W, the system pressure was varied. The pressure range investigated was 12 to 100 mtorr and the atomic argon intensities were recorded at each setting. The results from this experiment are shown in figure 5–4.

Figure 5–4 shows that at this argon wavelength, there is little dependence on pressure. This trend is unexpected as the glow discharge emissions generally increase with increasing pressure, in this low pressure system. Ar* relaxation at 750.4nm corresponds to an energy of 13.48eV [87]. This behaviour could therefore indicate that the pressure has little effect on the electron energy distribution at this particular energy level.

For a constant rf power of 50W and a pressure of 20mtorr, the total argon flow rate was varied. The flow rate range investigated was 1 to 10 sccm, and the argon atomic intensities were recorded at each set-point. The results from this experiment are shown in figure 5–5.

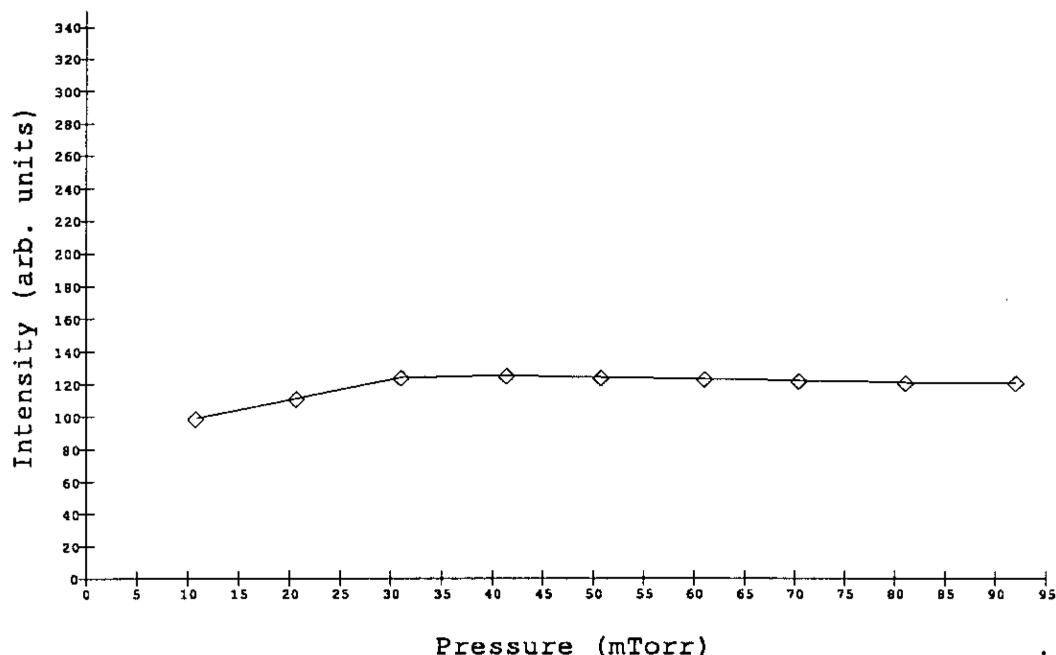

Figure 5–4: Intensity of the 750.4nm argon atomic emission line as chamber pressure is varied, at a flow rate of 6sccm and a power of 50W.

This characteristic shows a marked rise in intensity as the argon flow rate increases at the lower end of the range. Thereafter a gradual rise in intensity is observed, but at a reduced gradient. Changing the flow rate in this way should only affect the residence time of the molecules in the chamber, which would have only a minimal effect on the optical intensities. However, from figure 5–5 it is clear that varying flow rates across such a wide range in this experimental arrangement has affected other discharge parameters, such as the electron energy distribution function, which could account for the larger rises in intensity at this wavelength.

It can be seen from figures 5–3, 5–4 and 5–5 that the RIE machine parameter which had the greatest influence on the 750.4nm emission line from this argon plasma was the power setting. It was also of interest to note that, of the range of machine parameters under study, flow rate changes produced a greater range of variation than pressure changes.

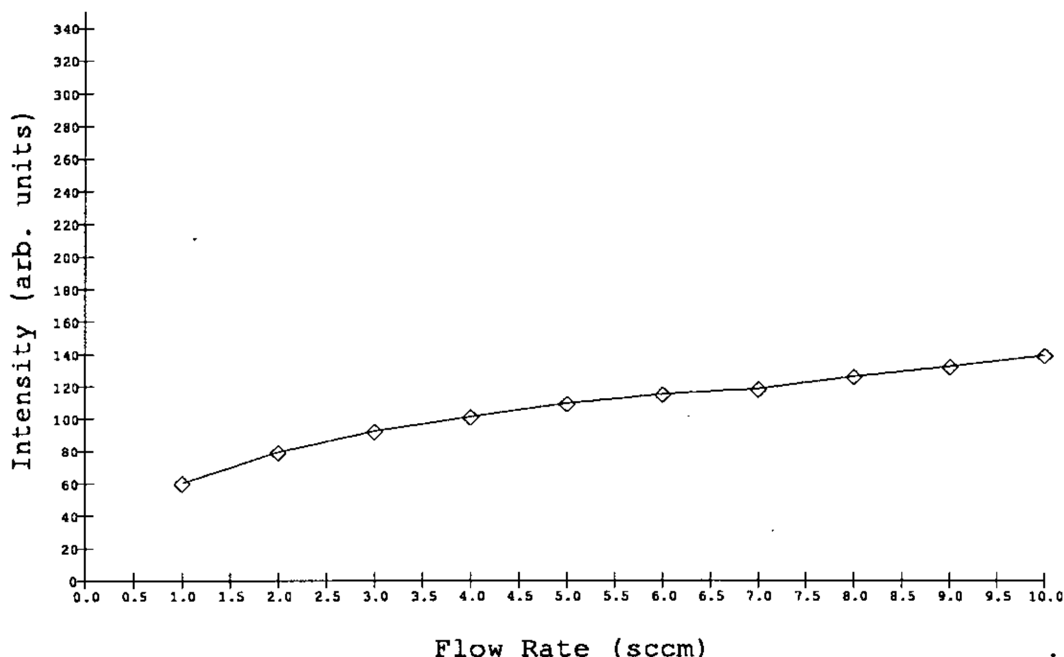

Figure 5–5: Intensity of the argon 750.4nm emission line as the total argon flow rate was varied at a pressure of 20mtorr and a power of 50W.

5.4 Mass Spectrometry: In-Situ SIMS

Mass analysis was performed using a Hiden Analytical quadrupole mass spectrometer (QMS). This is a computer controlled instrument intended primarily for plasma analysis and diagnostics. A schematic layout of this plasma diagnostic system is shown in figure 5–6. The particular arrangement which was employed on this project had a mass range of 0 to 300 amu and was capable of scanning ion energies in the range 0 to 50eV.

The probe head was sidewall mounted via a CF114 flange on the RIE chamber and differentially pumped through a 500μm diameter orifice by a turbomolecular pump. The flow rate of gas and effective pumping speed give a pressure in the QMS head of 10^{-6}torr, for a chamber pressure of less than 100mtorr. A Penning gauge mounted at 90° to the manifold provided a measure of the differential pumping action and was connected to the Hiden controller to provide

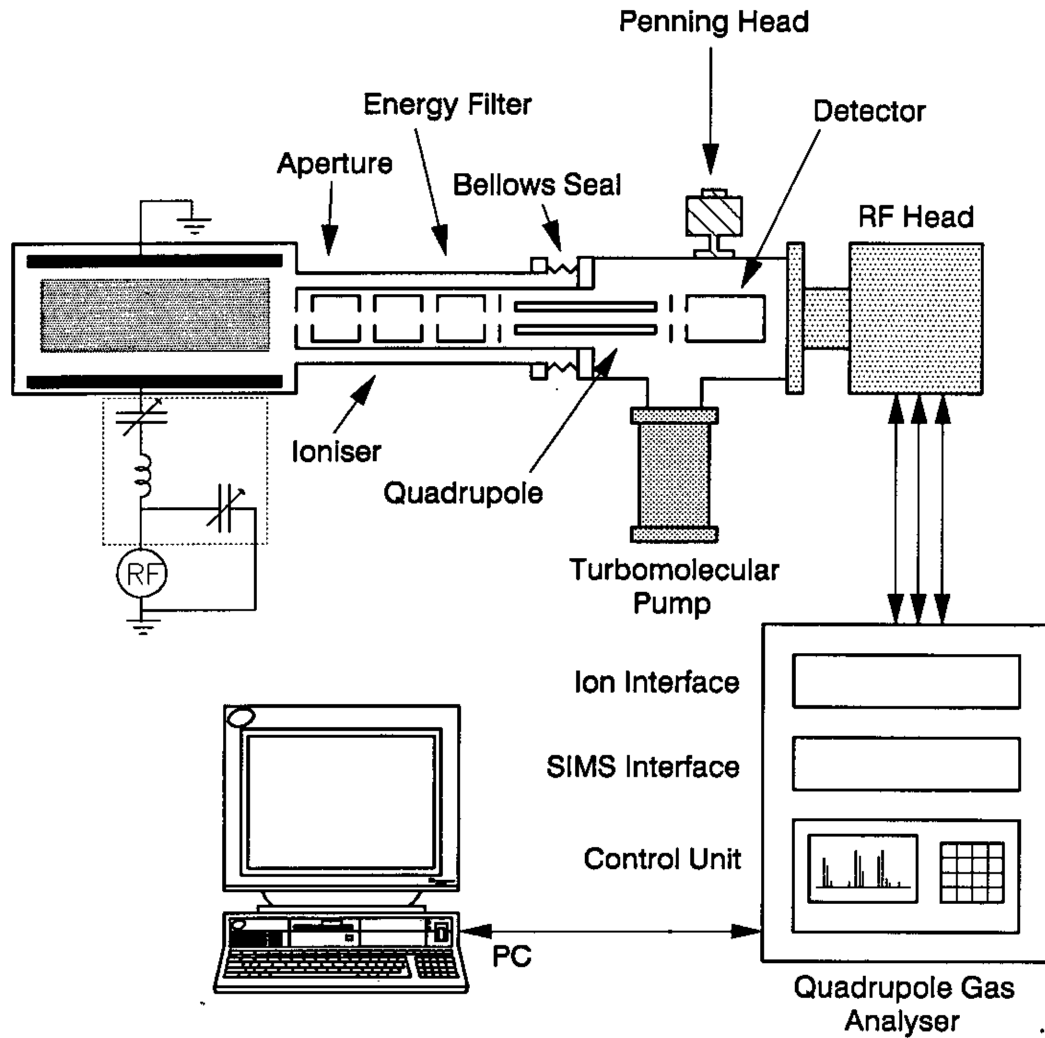

Figure 5–6: Schematic layout of the QMS system attached to the RIE chamber.

over-pressure protection. Off-axis mounting of the Penning head reduced the amount of noise on the signal from the ion detector.

The QMS head is capable of operation in two distinct modes: ion analysis (*SIMS*) or residual gas analysis (*RGA*). Modes of operation of the QMS are shown highlighted in the form *SIMS*. With the QMS operating in ion analysis mode, all the ions sampled were generated within the glow discharge (effectively an in-situ secondary ion mass spectrometer, or in-situ SIMS). For the purposes of this project the QMS was normally operated in an in-situ SIMS mode. Within

the *SIMS* option, data could also be collected from the plasma in four different methods:

1. In *ENERGY PROFILE* mode, the energy distribution of a single mass/charge ratio was displayed from 0 to 50eV.

2. *MASS PROFILE* mode allowed the detector partial pressure profiles to be displayed in a quasi-analogue form for confirmation of spectral quality across a limited range of mass/charge values.

3. With *BAR* mode, the mass outlines observed in *MASS PROFILE* mode were converted into histogram form.

4. *MID* mode allowed the intensities of specific mass channels of interest to be monitored against time.

The quadrupole mass filter consisted of an energy filter; a RGA source; quadrupole rods and an ion collector/detector. The energy filter is a parallel plate design with a 30° acceptance angle. When the system is operating in the ion analysis mode, the energy filter allows the energy spectrum from 0 to 50eV of the incoming ions to be monitored. The next filter section is the RGA source which consists of a tungsten filament, which is coated with thorium to help reduce water absorption. This filament is capable of producing a stream of 70eV electrons when hot, which are able to ionise a neutral gas. The RGA source is followed by the quadrupole mass filter which can be biased with respect to ground in order to select a range of secondary ion energies. Ion detection is carried out by a dual Faraday collector/ continuous dynode electron multiplier detector which is mounted in an off-axis position for improved sensitivity.

The position of the probe relative to the driven electrode in the RIE system could be altered. This was achieved by mounting a variable bellows seal between the access port on the chamber and the QMS head. In this way, the plasma gases could be sampled at any position in a range from directly over the driven electrode to the chamber walls.

Filter voltage settings for the QMS head were sourced from a central control unit. This was a computerised controller which was capable of setting up the probe head and displaying the mass or energy spectrums. Data storage and analysis was achieved by connection of the quadrupole gas analyser to a personal computer which was running a data acquisition and manipulation package called Asyst [2].

Initial investigations using the QMS system focussed on the inter-relations of the probe parameters in order to find a strategy which resulted in the most effective tuning of the probe head. This was followed by some basic research into the effects of varying RIE machine parameters on argon glow discharges.

5.4.1 Tuning

Tuning of the QMS head presented a major problem because of the large number of variables which have to be considered as shown in table 5–1. Despite the large variation in settings which is possible, the task is simplified because some of the parameters are seldom changed (marked with a ‡ in table 5–1).

A schematic representation of the QMS probe head is shown in figure 5–7. Tuning of the QMS head can be very time consuming and is a process that involves many iterative steps. A knowledge of the functional relationship of the various probe parameters can help to reduce this time. For *SIMS* analysis, there are twelve parameters which can be grouped under four headings:

- **Lenses:** extraction voltage (*EXTRACTOR*); lens voltage (*LENS*); focus voltage (*FOCUS*); and suppressor voltage (*SUPPRESSOR*).

- **Energy Analyser:** energy voltage (*ENERGY*); endcap voltage (*END-CAP*); and cylinder voltage.

[2] Asyst Software Technologies, Inc.

energy	25V		Filter
extractor	-90V	‡	
lens	17V		
endcap	-19V		
cylinder	-0.1V	‡	
focus	-20V		
suppressor	-61V	‡	
resolution	0%	‡	Quadrupole
delta m	0%	‡	
discriminator	-30%	‡	Detector
1st dynode	-1200V	‡	
multiplier	1800V		

Table 5–1: QMS variables for ion analysis mode, with some typical values for positive ion extraction

- **Quadrupole Mass Analyser:** resolution; and delta M (*DELTA M*).
- **Ion Detector:** first dynode voltage (*1st DYNODE*); multiplier voltage (*MULTIPLIER*); and discriminator level (*DISCRIMINATOR*).

The *EXTRACTOR* voltage set up the electric field between the plasma and the probe tip. Imaging of the sample onto the input aperture of the energy analyser is achieved using the *LENS*. The *FOCUS* voltage is applied in order to match the output of the energy analyser into the quadrupole entrance analyser. The final lens is the *SUPPRESSOR* which matched the output of the quadrupole mass analyser onto the ion detector. However the major function of the *SUPPRESSOR* is to combine with the detector field to suppress electron generation.

The *ENERGY* voltage set the axial potential of the quadrupole and also defined the energy of the ion which was mass analysed. The *CYLINDER* and *ENDCAP* potentials operated in tandem to influence the transmission and reso-

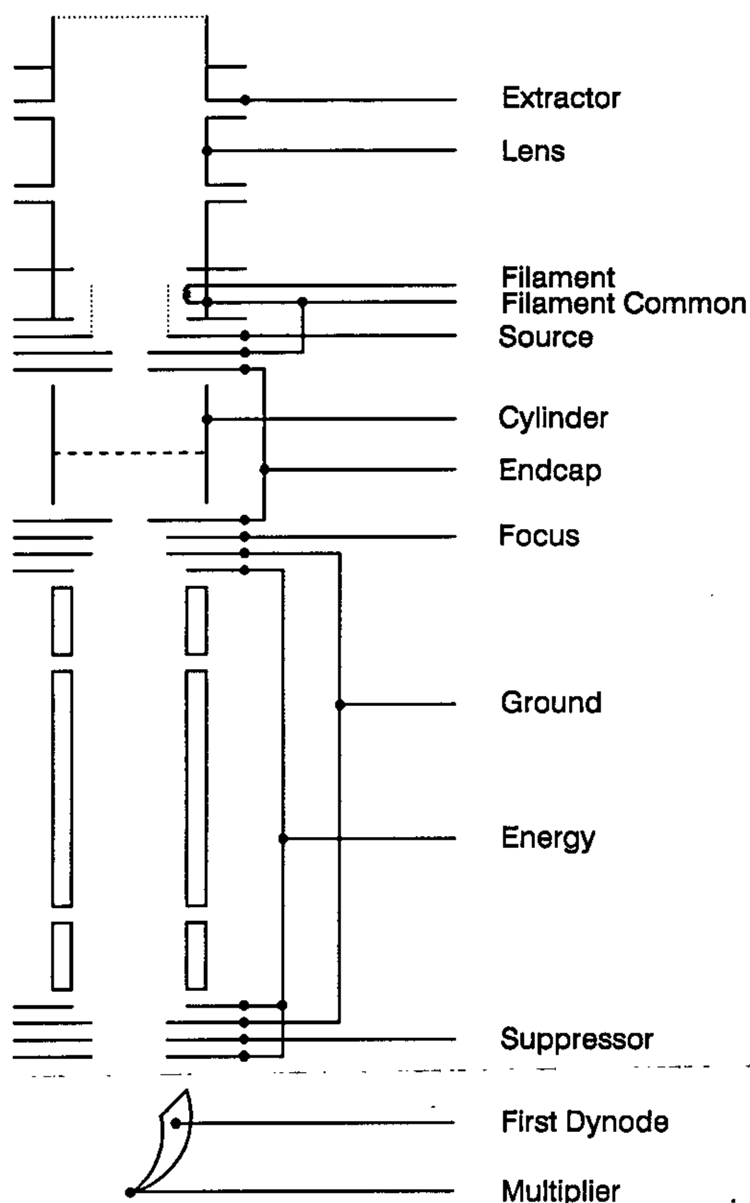

Figure 5–7: Schematic layout of the QMS probe head.

lution of the system. For example, if the difference between the *CYLINDER* and *ENDCAP* parameters is increased, making the *ENDCAP* more negative, then the energy resolution of the system is reduced while the transmission is increased.

In the quadrupole mass analyser, the high mass resolution was set on a +/-100% arbitrary scale. The *DELTA M* parameter was responsible for the low mass resolution and was also variable between +/-100%.

The *1ST DYNODE* voltage in the ion detector defines the voltage on the front end of the electron multiplier with respect to ground. Ion to electron conversion took place at this point. The *MULTIPLIER* voltage set the voltage across the electron multiplier and was therefore directly responsible for the gain of the system. The *DISCRIMINATOR* set a voltage reference level for the detector. If the pulse height of the electron multiplier output was more negative than the *DISCRIMINATOR* level, then the pulse was counted.

In order to tune the QMS in *SIMS* mode a single mass was selected for study and its *PROFILE* energy spectrum analysed. A typical scan could contain several peaks in the energy spectrum. The probe head could then be tuned to filter ions at one of these peaks by setting the *ENERGY* parameter to the same value as the peak energy in eV that was obtained experimentally. Selection of a relevant peak depended on the particular analysis. Once an *ENERGY* value had been selected, the QMS was transferred into mass *PROFILE* mode to check the quality of the tune. Some *ENERGY* peak selections only gave a good sampling profile on a single mass number, whereas other peaks could give good profiles across a range of mass numbers.

Once a suitable peak had been identified and some initial tuning has taken place, the *LENS* and *FOCUS* were used to improve the the profiles of the observed peaks. Both *FOCUS* and *LENS* were used to improve resolution, with the *LENS* parameter proving particularly sensitive. The *ENDCAP* voltage also proved useful at the end of the tuning process to improve mass profiles. The ultimate goal of this series of operations was to achieve distinct, symmetrical and rounded peaks for each sample which was detected in the mass spectrum.

5.4.2 Energy Distributions for Argon

A flow rate of 5sccm of argon was introduced into the RIE chamber at a constant pressure of 10mtorr, and a plasma was struck which had a forward power of 5W. This resulted in a V_{dcb} of -47V. Using *ENERGY PROFILE* mode, the energy spectrum of Ar^{+} at mass 40 was investigated, as shown in figure 5–8. This

contained several peaks on which the system could be tuned and after some initial experimentation tuning based on the high energy peak at 26eV produced the best results. Good profiles were obtained across the entire mass range when the tuning was checked for spectral quality in *MASS PROFILE* mode. However, this QMS setup was found to be inadequate for investigations into the effects of changes in RIE machine parameters. This was because the energy peak was very sensitive to the parameter changes and could not be used across the desired range of values.

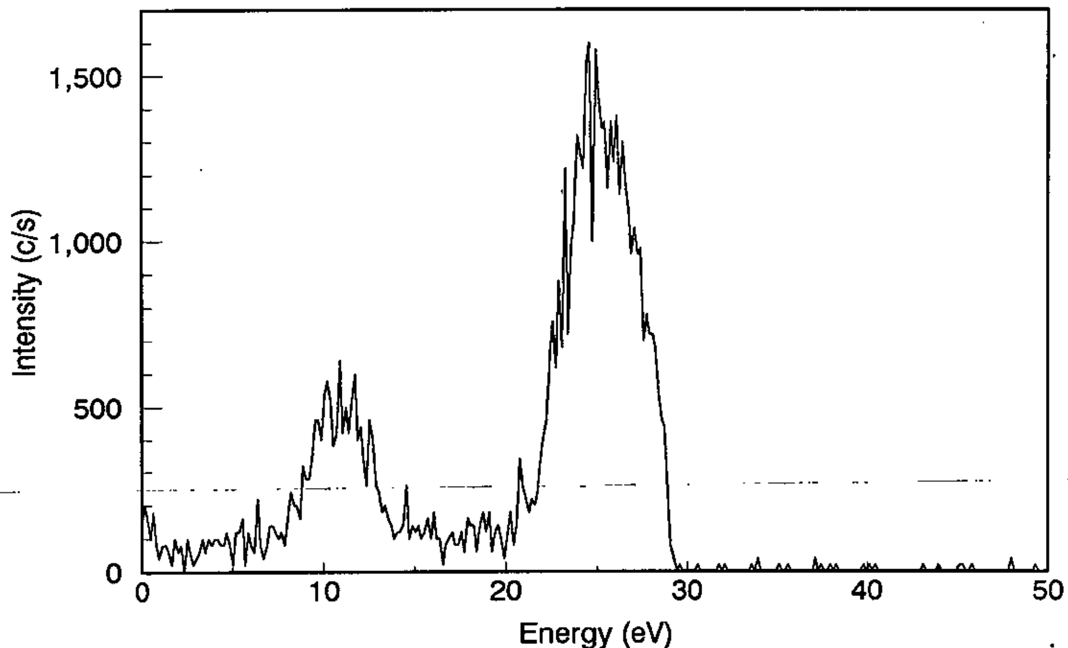

Figure 5–8: The energy spectrum of argon positive ions at mass 40.

The energy spectrum of mass 44 was investigated, and proved to be more stable. This was probably residual CO_2^+ which could have been adsorbed into the chamber walls/electrodes, when the chamber was vented to atmosphere, and then desorbed gradually due to the ion bombardment from the plasma.

5.4.3 Intensity Variations with Machine Parameters

To verify the characteristics of the system, the QMS was operated in the in-situ SIMS mode and used to investigate positive ion concentrations in an Ar glow discharge within the Vacutec RIE. Initially the probe was set-up on the mass 44 energy spectrum using the procedures outlined in section 5.4.1. Ar^+ ion concentrations were investigated by monitoring the average intensities of mass 40 with time. For this investigation, a one dimensional characterisation was performed around the major machine dependent variables of power, pressure and flow rate. It should be noted that RIE/QMS setup had to reach a new equilibrium each time the RIE machine parameters were changed. To ensure that a stable region had been reached, intensity measurements from the QMS were only recorded after a period of 1 minute had elapsed.

For a total argon gas flow rate of 3sccm and a forward power of 5W, the system pressure was varied. The pressure range investigated was 20 to 90 mtorr and the mass 40 ion intensities were noted at each level. The results from this experiment are shown in figures 5–9.

The Ar^+ intensity shown in figure 5–9 decreased exponentially as the chamber pressure was increased. Ionisation occurs due to the electrons at the high energy tail of the electron energy distribution. This exponential decrease in Ar^+ intensity with pressure could be indicative of the sensitivity of these high energy electrons to pressure. As the number of high energy electrons is reduced, the number of ionisation collisions which occur is also reduced. This contrasts with the OES intensities for *atomic* argon shown previously in figure 5–4 which show little pressure dependence.

For a chamber pressure of 20mtorr and a forward power of 5W, the argon flow rate was varied. The flow rate range was 3 to 10sccm and the Ar^+ intensities were recorded at each set-point. The results from this experiment are shown in figure 5–10. It can be seen that across the mass flow range there was only a 20%

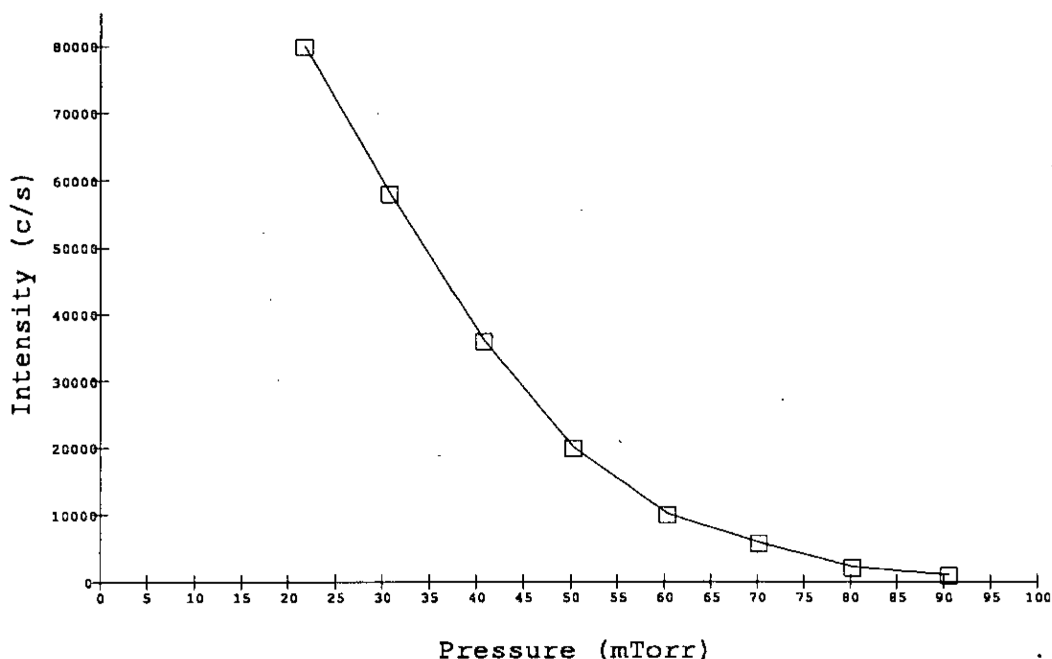

Figure 5–9: Intensity of the Ar^+ trace at mass 40, as the glow discharge pressure is varied at 5W power and 3sccm Ar flow rate.

change in Ar^+ intensity. Therefore it seemed that mass flow rates had only a minimal effect on ion intensities at these RIE machine settings.

For a chamber pressure of 20mtorr and an argon flow rate of 3sccm, the rf power applied to the discharge was varied. The power range investigated was 10 to 60W for a chamber pressure of 20mtorr and an argon flow rate of 3sccm. Because the applied power has a greater influence on the Ar^+ energy distribution than flow rate or pressure, a slightly different analysis technique had to be employed. The tuning peak in the Ar^+ *ENERGY PROFILE* was studied as the power was varied. The value of the *ENERGY* setting was then altered to track the movement of the ion peak caused by the wide range of power settings. This had been unnecessary previously as the tuning peak had exhibited only minimal movement (< 4eV). The results obtained using this method are shown in figure 5–11.

It can be seen from figure 5–11 that the number of Ar^+ ions counted at the detector increased rapidly over the low power range. Ion intensities would be

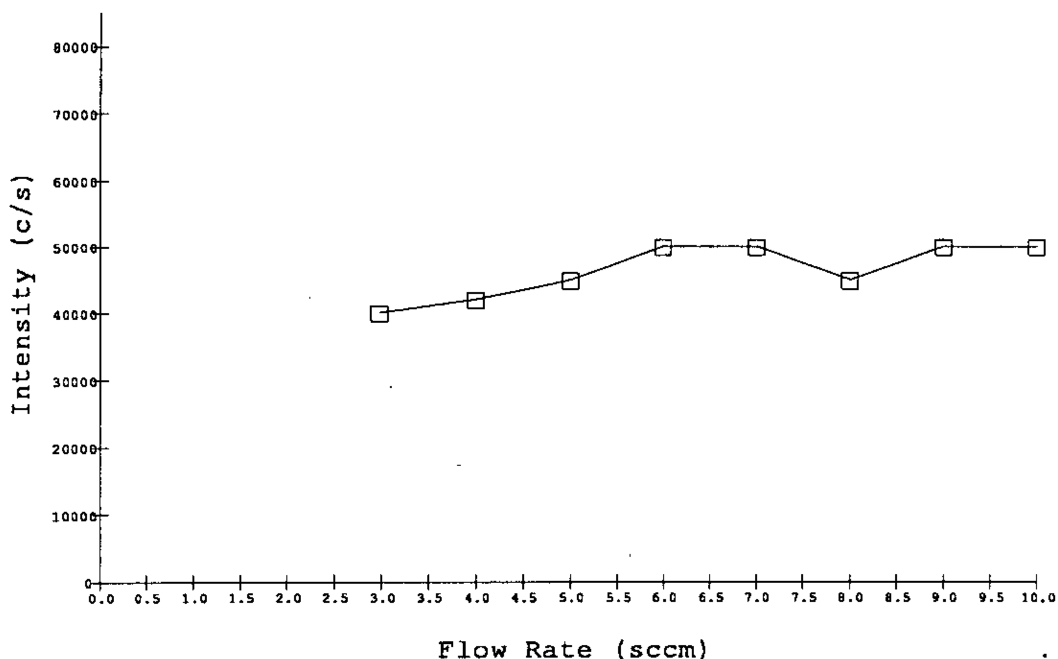

Figure 5–10: Intensity of the Ar^+ trace at mass 40, as the plasma flow rate is varied at a chamber pressure of 20mtorr and a power of 5W.

expected to increase as the electric field strength increased, because the average electron energy would also increase. This is turn would increase the degree of ionisation of the discharge gas. The ion count then saturated and remained stable over the 30 to 60W range, in contrast to the atomic OES information shown in figure 5–3. This saturation of the Ar^+ intensity with power may have been due to a drift in the QMS head tuning which resulted in a lower transmission of Ar^+ ions to the detector.

5.5 Langmuir Probe

Much of the method and associated theory of Langmuir probes has been reviewed in section 4.4. The technique has been employed successfully to obtain key plasma parameters such as V_p and T_e, but this investigation was aimed at determining whether Langmuir probes were able to detect changes in these parameters as

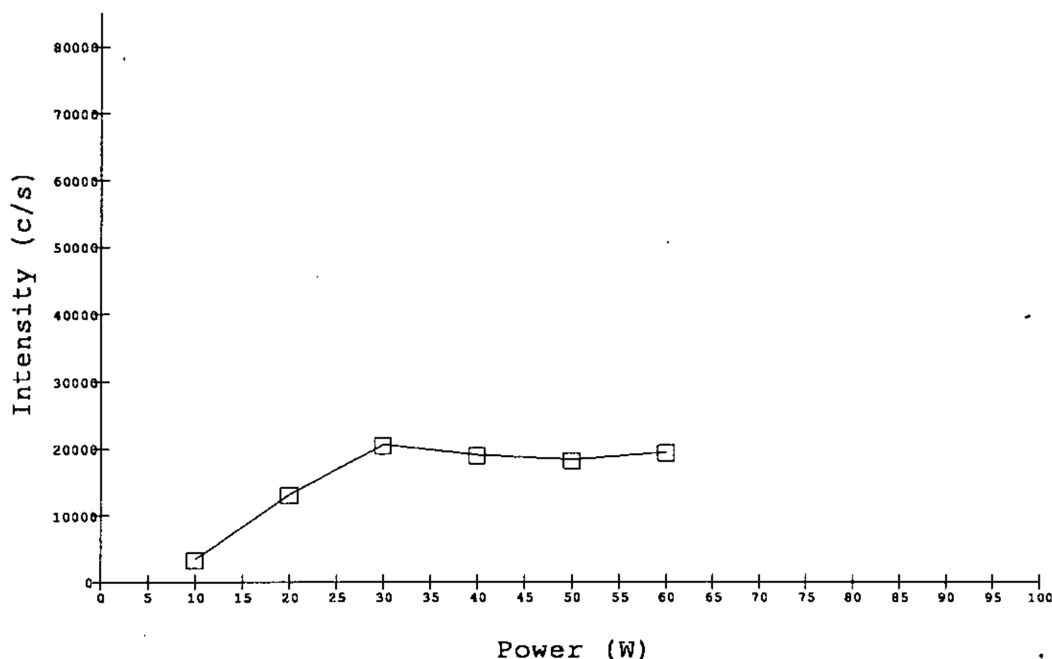

Figure 5–11: Intensity of the Ar^{+} trace at mass 40 as the plasma rf power is varied, at a pressure of 20mtorr and a flow rate of 3sccm.

the operating conditions were changed. To this end, it was important to use a rigorous method for sampling the plasma.

The Langmuir probes used in this investigation were made of 0.25mm diameter wire. The wire was composed of 99.5% pure tungsten. In order to access within the vacuum chamber the wire was mounted within a glass tube as shown in figure 5–12. The glass was melted and re-flowed over the wire to create a glass to metal vacuum seal. The particular construction of the probe tip was designed, similarly to Eser et al [104], to avoid any contact between the wire and the glass tube. This eliminated the possibility of a deposited conducting coating on the glass increasing the effective probe collecting area. The tungsten collecting wire was soldered to a coaxial cable as close to the vacuum seal on the atmospheric side as possible, in order to reduce rf noise from the chamber electric field. Soldering of the copper to the tungsten had to be used when the high temperatures associated with initial welding attempts caused the tungsten to become brittle and break.

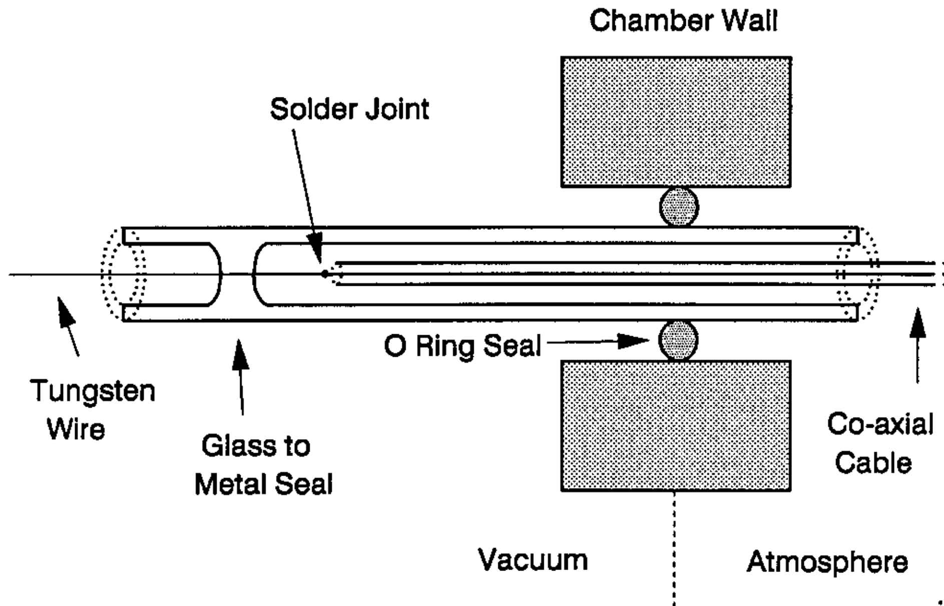

Figure 5–12: Schematic of a Langmuir probe.

Access to the plasma for the probe was achieved by removing one of the quartz viewports and replacing it with a metal flange. This flange contained a $\frac{1}{4}$ inch tube fitting connector which allowed a vacuum seal to be achieved between the glass and the metal, using an 'O' ring seal. This type of arrangement also allowed the probe position to be varied between the gas ring and the central pumping port.

Initial investigations used a variation of the blocking filter technique which was outlined in section 4.4. Two decoupling variable LC chokes were placed close to the probe and tuned to filter out the frequency of the rf signal. The rf signal could be substantially reduced using this technique, although a rf component was still present. In order to obtain an improved IV characteristic a driven rf feedback circuit was employed as shown in figure 5–13. This involved using a second rf signal which was 180° out of phase but with the same amplitude as the rf signal at the probe tip. In this way, the rf component between the plasma and probe could be nullified and an improved IV curve could be obtained.

The circuit employed to achieve the rf feedback was a novel variation on an

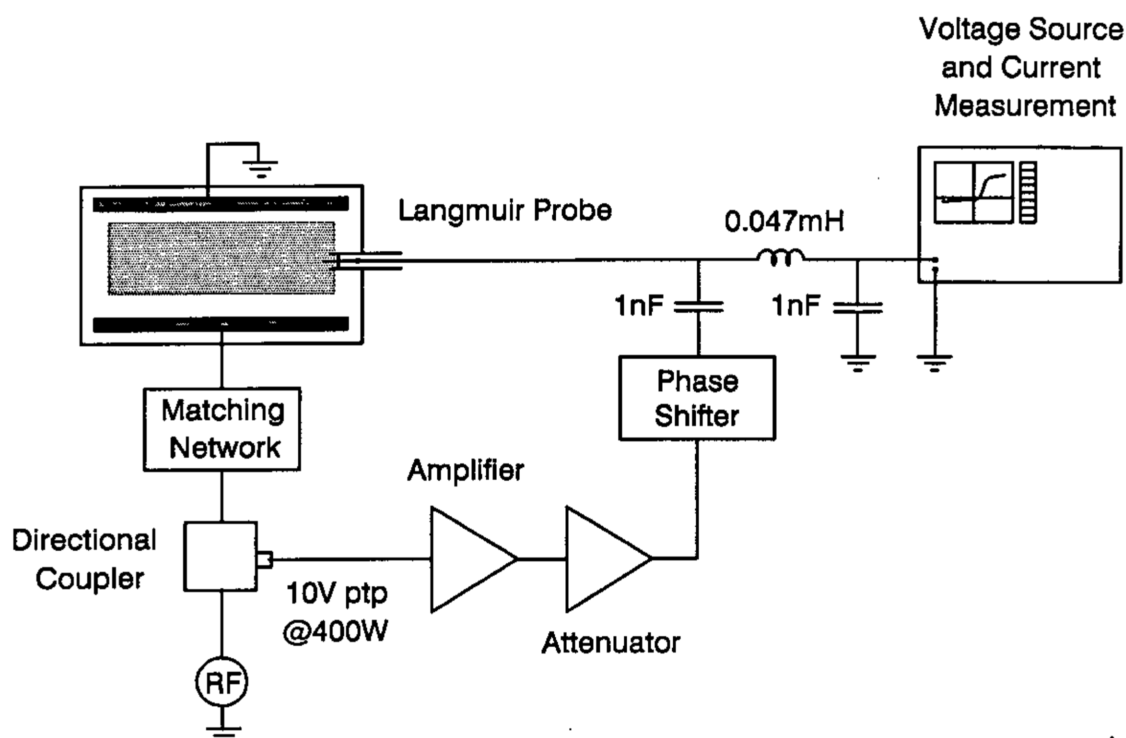

Figure 5–13: The experimental driven rf feedback Langmuir probe measurement system.

arrangement employed by Braithewaite et al [105]. In this configuration, a directional coupler was connected between the rf generator and the matching network of the RIE. This arrangement was advantageous for rf signal sampling when compared to the step down transformer used by Braithewaite et al because of its greater ease of implementation into a standard RIE system. The directional coupler allowed a maximum signal of 10V to be coupled into the feedback circuit, for a generator output of 400W. The amplitude of the signal could then be varied using an rf amplifier/attenuator. The signal was then phase shifted and superimposed on the dc biasing voltage. Phase shifting was achieved by designing and building an LC circuit, shown in figure 5–14, based on a transmission line model. The variable inductors were constructed using insulated copper wire, a coil

former and a ferrite core. The ferrite core could be wound in and out of the coil former to alter the value of the inductor.

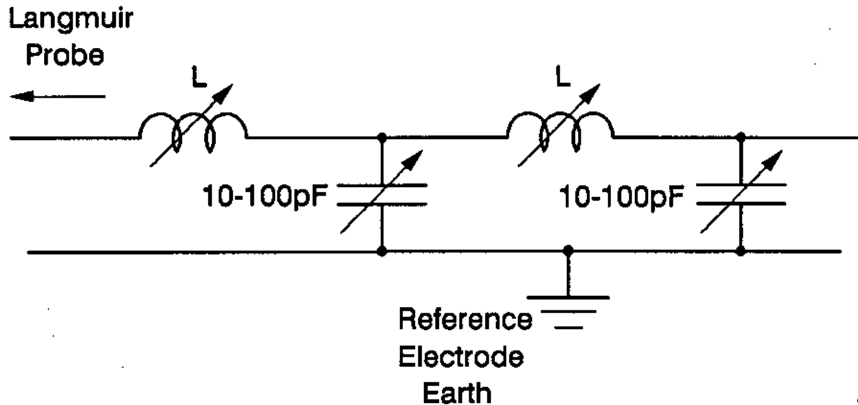

Figure 5–14: The phase shifting circuit used for Langmuir probe rf feedback.

IV characteristics were obtained using either a Hewlett Packard HP4145B parameter analyser or a Tektronix 577 curve tracer. Both sets of equipment could source a dc voltage and monitor the current which flowed between the probe and the reference electrode. Signal ground at all points, except for the rf generator, in the circuit of figure 5–13 was the grounded reference electrode of the RIE system to complete the return current path for the probe. The HP4145B was ideal for the accurate collection and analysis of glow discharge data. However, some machine parameter setups forced the V_p value above +100V, which was outwith the range of the HP4145B, and the Tektronix 577 was employed because it could source voltages up to 1600V. Rf voltages were shielded from the dc voltage source using an LC choke.

Probe contamination is a problem which can affect the IV characteristic of a probe in a plasma. Before recording a characteristic, the probe was cleaned by biasing to a large negative voltage (-100V). This removed surface impurities by positive ion bombardment.

To ensure that the probe-plasma rf noise was minimised, an iterative procedure had to be performed. Probe-plasma rf noise was minimised by maximising the floating potential, V_f. A high impedance voltmeter was connected between

the probe and the reference ground to monitor V_f, and the feedback signal was altered in phase and amplification until a maximum was achieved.

A typical IV characteristic for an argon glow discharge in the RIE is shown in figure 5–15. This IV curve was obtained using the HP4145B from a glow discharge at 52mtorr, 10W rf power and a flow rate of 6sccm argon. The dc voltage range was swept rapidly with a 0.5V step size. It can be seen that in the electron saturation region of the curve, the collected current is approaching 10mA. This is the limiting value of current for the HP4145B and was also the point at which the plasma started to show signs of perturbation. The disturbance in the plasma was marked by a decrease in the magnitude of V_{dcb}, which was displayed on the front panel of the matching network. Visually, this had an obvious effect as it lowered the intensity of the glow discharge, because a significant proportion of the discharge current is now being collected by the probe. The electron current to the electrodes during the positive rf cycle is therefore reduced [12], which forces the magnitude of V_{dcb} to decrease, as outlined in section 2.2.2. During the experimental phase voltage sweeps were therefore constrained from the electron saturation region as much as possible to reduce this perturbation.

In order to find the plasma potential, the gradient of the IV characteristic in figure 5–15 was calculated, and is shown in figure 5–16. The plasma potential, V_p, is the value at the point of maximum gradient of the IV characteristic, which is at 81V. This is a relatively high value of V_p which is characteristic of the particular RIE configuration and machine parameters used in this experiment.

The method for T_e extraction was outlined in section 4.4. Ideally, it involves plotting $\ln(I_e)$ against $(V_p - V_a)$ where V_a is the applied voltage. For practical purposes, I_e can be approximated by the total collected current, as the ion current in the transition region is small in comparison to the electron current. A plot of $\ln(I_e)$ against V_a as shown in figure 5–17 can therefore provide the value for T_e. T_e in electron volts is obtained from the value of $dVa/d\ln(I)$ in the linear region of the curve. From figure 5–17, it can be seen that for this example, there are two linear regions on the curve. These give values for T_e of 13.5eV and 10.7eV

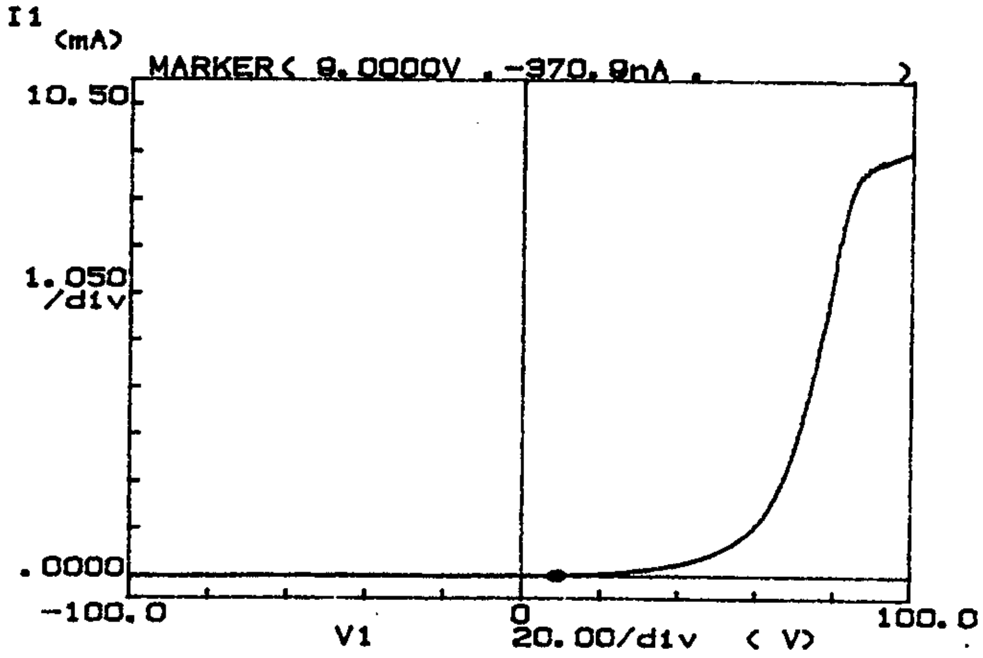

Figure 5–15: Langmuir probe IV characteristics for an argon plasma at 10W power, 52mtorr and 6sccm flow rate.

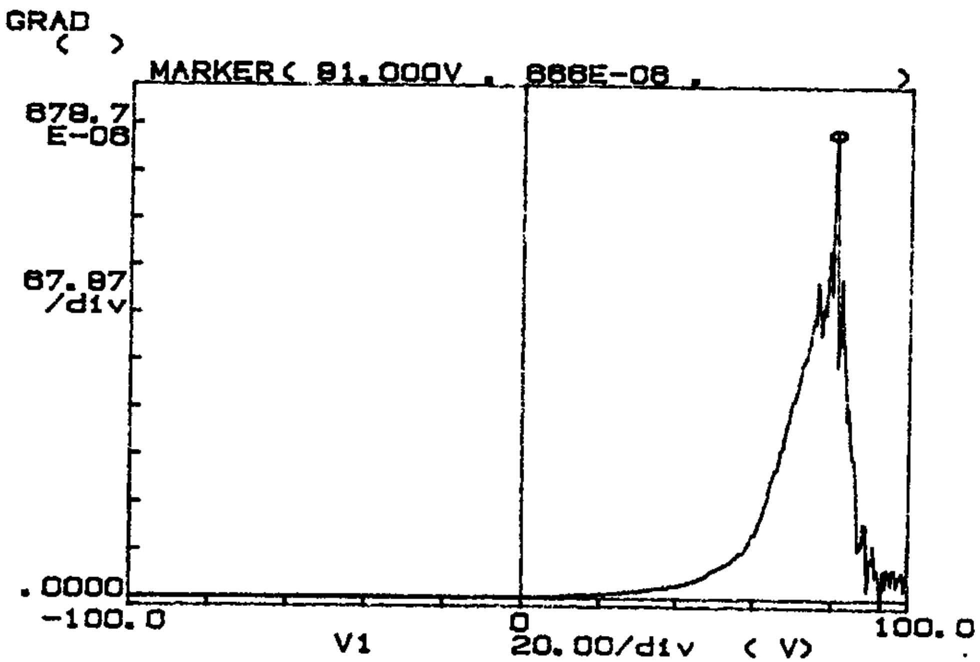

Figure 5–16: Argon plasma potential determined from the gradient of the IV curve.

respectively. This example illustrates the difficulty in interpretation of some IV characteristics.

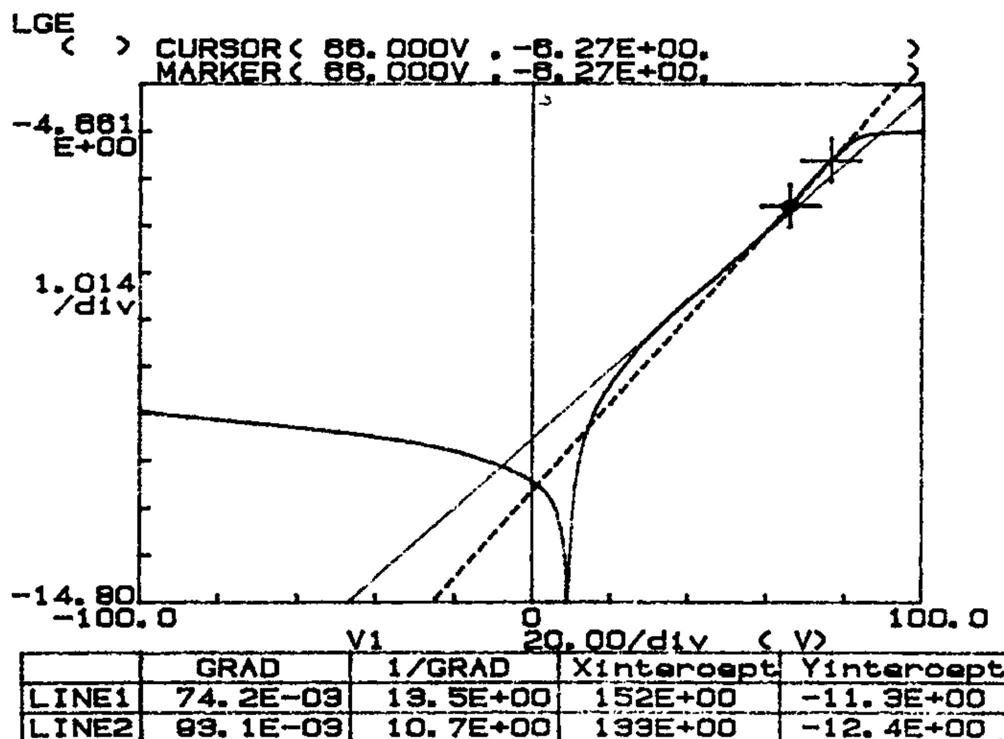

Figure 5–17: Argon plasma electron temperature.

To determine the effect of using the rf driven probe circuit, the HP4145B was directly connected to the Langmuir probe with only the LC choke for isolation. For the same experimental conditions of 10W power, 52mtorr and 6sccm argon flow rate, a second IV characteristic was obtained. This gave a V_p of 72.5V and a T_e of 16eV. This shift in the measured values was due to the extra rf component between probe and plasma.

5.5.1 Plasma Potential Variations with Machine Parameters

To check the validity of the Langmuir probe method for glow discharge characterisation, the driven probe technique was applied to argon plasmas. A one

dimensional machine parameter characterisation was carried out for the major machine variables of power, pressure and flow rate. An initial investigation revealed that V_p would be outwith the range of the HP4145B. The Tektronix 577 was therefore used to obtain these results. However this meant that T_e values could not be obtained. To ensure the plasma reached equilibrium for each machine setting, measurements were only carried out after a period of 1 minute had elapsed.

For a forward power of 10W and a total gas flow rate of 3sccm argon, the system pressure was varied. The results are shown in figure 5–18. A large variation in V_p was measured across the pressure range showing that V_p reduces with increasing pressure. A subsequent set of results using the HP4145B showed the trend in T_e with pressure and are shown in figure 5–19. T_e also reduced with increasing pressure in agreement with the results of Cantin and Gagné [134], Chatterton et al [135] and Eser et al [104]. This reduction in the average value of T_e occurs as a result of the decrease in the electron mean free path as the pressure increases.

For a forward power of 10W and a system pressure of 20mtorr, the argon flow rate was varied. The results from this experiment are shown in figure 5–20. Only a small decrease in V_p was observed across the range of flow rates.

For a system pressure of 20mtorr and a flow rate of 3sccm argon, the power was varied. These experimental results are shown in figure 5–21. It should be noted that although the power has a major influence on the ion bombardment, it has a minimal influence on the plasma potential in this case. The increase in the sheath voltage with power is therefore totally due to the increase in V_{dcb}. For comparison, Chatterton et al [135] found the V_p value to increase slightly for a 40mtorr argon plasma at powers of 10W and 50W.

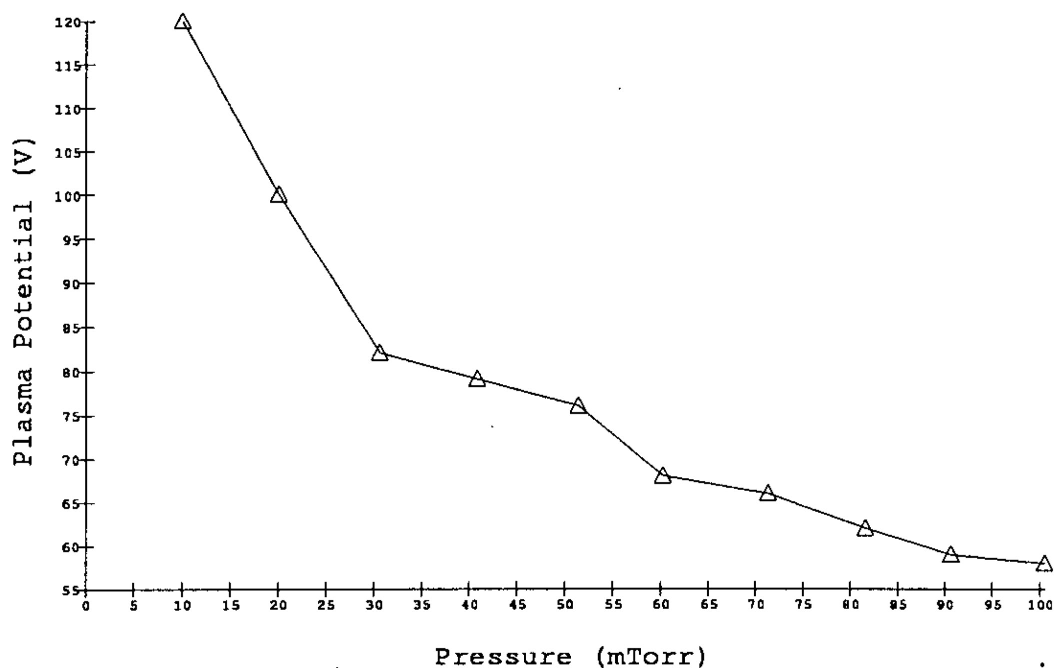

Figure 5–18: Plasma potential variations with pressure at a flow rate of 3sccm argon and a forward power of 10W.

Pressure (mtorr)	T_e (eV)
30	25.1
53	16.9
93	13.4

Figure 5–19: Average electron temperature variations with pressure at a flow rate of 3sccm argon and a forward power of 10W.

5.6 Summary

This chapter described the setup and conversion of a Vacutec RIE machine and the implementation and test of three diagnostic approaches: optical spectroscopy, mass spectrometry and electrostatic Langmuir probes. Together they provided a broad spectrum of plasma information.

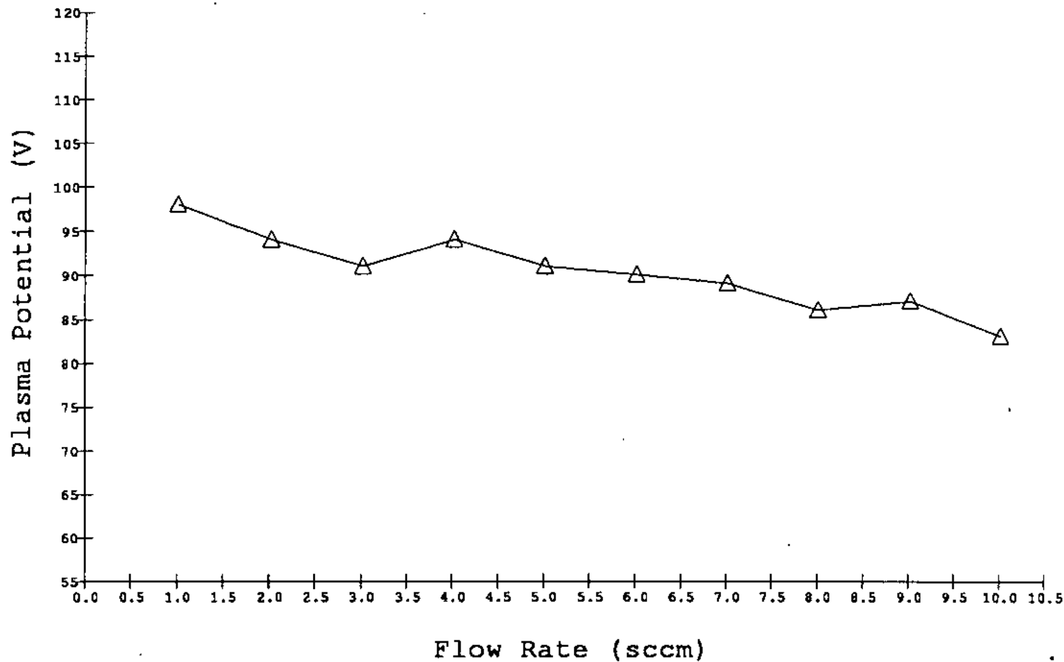

Figure 5–20: Plasma potential variations with argon flow rate at a pressure of 20mtorr and a forward power of 10W.

Using the mass spectrometer in an in-situ SIMS mode allowed plasma positive ion concentrations and energy distributions to be monitored. Optical emission spectroscopy enabled characterisation of the plasma 'glow' from the ultra-violet through the visible spectrum and into the infra-red. Langmuir probe techniques could provide information on the fundamental plasma parameters such as the plasma potential and electron temperature.

This range of diagnostic systems were assembled and interfaced to the modified RIE and preliminary investigations were carried out on a basic glow discharge. Monatomic argon plasmas were used at this stage so that diagnostic equipment evaluations could be performed with a minimum of molecular species interaction. One dimensional RIE machine parameter characterisation was then carried out in order to assess the viability of these techniques for process monitoring. A summary of the major trends which were observed is given below:

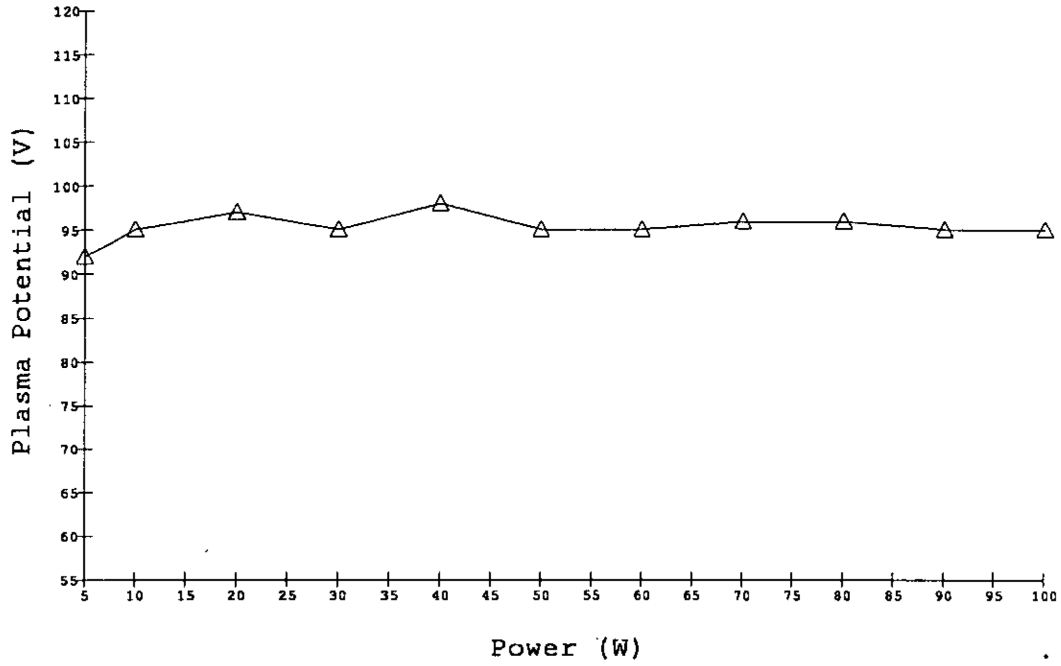

Figure 5–21: Plasma potential variations with power at a flow rate of 3sccm argon and a system pressure of 20mtorr.

		Power ↑	Pressure ↑	FlowRate ↑
OES	Ar^*	↑↑	↔	↔
In-situ SIMS	Ar^+	↑	↓↓	↔
Langmuir Probe	V_p	↔	↓↓	↔
	T_e	-	↓↓	-

Chapter 6

Diagnostic Techniques in a Reactive Gas Chemistry

6.1 Introduction

Having assessed the diagnostic techniques and equipment on simple argon glow discharges in chapter 5, the project now transferred to a complex reactive chemistry. Initially a suitable recipe had to be defined which was capable of etching fine linewidths in aluminium. Once the operating conditions were defined, then OES, in-situ SIMS and Langmuir probes could be applied to the glow discharge in order to perform characterisation work. The objective of this section of the research work was to assess the various diagnostic techniques in a reactive etch environment. From the range of plasma information available, selected diagnostic information could then be used as the process input to the statistical model for the aluminium etch.

6.2 Process Description

It was necessary to develop a process that was capable of etching aluminium based metallisations in the modified Vacutec RIE. This involved a chlorine based chemical recipe and the RIE had been extensively redesigned in order to achieve this, as described previously in section 5.2. It was decided to use a recipe which was composed of BCl_3, Cl_2 and He to etch the metallisation. This is a very complex combination, but is one of the most commonly implemented in commercial microfabrication facilities for fine linewidth aluminium definition (the major alternative was to use $SiCl_4$ instead of BCl_3). Using this chemistry therefore enabled the project to address the current problems faced by the major microfabrication facilities.

BCl_3 fulfilled several process roles: it provided species which are capable of native oxide removal; it dissociates to form Cl radicals which are aluminium etchants; and it is also able to scavenge water vapour and oxygen from the reactor at the start of the process. This last ability was particularly important for the Vacutec RIE system because of the lack of a load-lock chamber, and was one of the major reasons for selecting a BCl_3 chemistry. Cl_2 gas provided a second source of Cl radicals which increased the overall material etch rate. He gas improves the process uniformity by stabilising the gas mixture, as well as providing increased thermal cooling within the glow discharge.

Process operating conditions were a variation on an aluminium etch process used by Olin Hunt [1]. The chosen conditions were as follows:

[1] Olin Hunt Technical Brief No. 10.

Flow Rate (sccm)	BCl_3	21
	Cl_2	11
	He	28
RF Power (W)		200
Pressure (mtorr)		60

The ability of this recipe to etch aluminium was investigated using a batch of test wafers. Silicon wafers which were 75mm in diameter, p-type and 100 orientation were used as the starting material. They had silicon dioxide thermally grown to a thickness of 14000Å, and were then deposited with 1.2μm Al/1%Si, using a Balzers BAS 450PM planar magnetron sputtering system. In the Vacutec RIE with the new chemistry, it was possible to define metal linewidths down to 1μm wide lines with a 1μm spacing. Etch results were examined in an optical microscope and showed that pattern definition to this level was satisfactory for this research work.

6.3 Optical Emission Spectroscopy

OES was used to investigate the characteristics of the BCl_3/Cl_2/He plasma during aluminium etching. The test wafers which were used for this stage were the same batch described in section 6.2.

Initially the EG & G OMA 1460 setup was employed for wide spectrum analysis of the etch, so that the wavelengths that varied most during the reaction could be identified. For comparison purposes, a 'fingerprint' for each gas was obtained by investigating single gas plasmas formed from either BCl_3, Cl_2 or He. The RIE system was then vented up to atmosphere and a single wafer was placed onto the electrode. The optical emission signals from the aluminium etch reactions should be more prominent at this stage because the aluminium layer had no masking layer. This meant that the maximum amount of material was available for reaction. The optical fibre was positioned at a chamber viewport such that the wafer

was between the centre pumping port and the chamber viewport, which allowed an average intensity to be obtained across the plasma section with the highest density of reaction products. A plasma was struck using the process described in section 6.2 and the Al^* atomic emission line at 396.2nm showed by far the greatest variation during the reaction, across the measured spectrum. The BCl_3 and Cl_2 molecules both showed a wide range of peaks in the 400 to 850nm range, but little distinct information could be obtained. He emissions were also very low from the $BCl_3/Cl_2/He$ plasma which was expected because of the greater excitation energies which are necessary to generate He^*.

Having identified a suitable optical emission line for process monitoring, the monochromator system was setup and adjusted to the Al^* line at 396.2nm. A chart recorder was used to record the selected emission intensity with time. A test wafer was placed in the reactor and a $BCl_3/Cl_2/He$ plasma struck. A representation of the Al^* emission intensity which was obtained with time using the chart recorder is shown schematically in figure 6–1. The points at which the plasma is struck and extinguished can be clearly seen. After the plasma is struck, there is an induction period during which the native oxide layer is removed and water vapour and oxygen are scavenged from the reactor chamber. When the bulk aluminium layer is reached, the Al^* emission intensity rapidly increases. The point at which the induction time is completed is open to interpretation as shown in figure 6–1. The gradient of this part of the characteristic is heavily influenced by the uniformity of the process. Greater uniformity results in a higher gradient. The emission intensity is relatively constant throughout the bulk Al etch phase, before it reduces as the Al clears at the process endpoint.

Other OES techniques were considered for their suitability in monitoring Cl based etching. Non-invasive T_e analysis as described by Felts et al [83] was considered for application using the He carrier gas emissions. However the basic He peaks proved too difficult to identify within the complex reactive chemistry. Actinometry was also considered as a means of obtaining an estimate of ground state species concentrations. However Gottscho et al [87] showed that actinom-

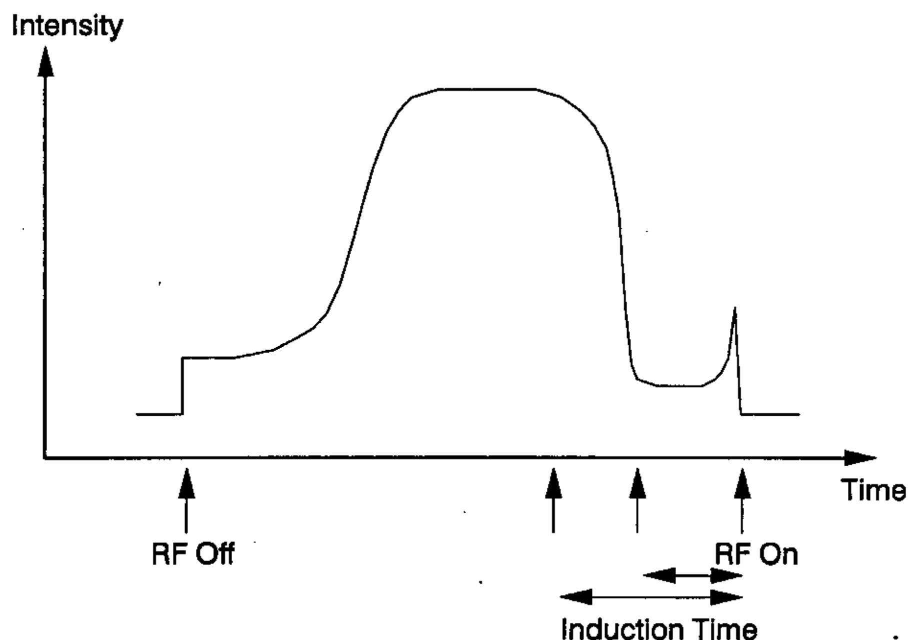

Figure 6–1: A representation of the Al* emission line at 396.2nm during an etch process.

etry may not be applicable to Cl chemistries due to the presence of additional excitation mechanisms.

6.4 Mass Spectrometry: In-Situ SIMS

As described previously in section 5.4, the QMS probe was operated in an in-situ SIMS mode, and used to investigate the characteristics of $BCl_3/Cl_2/He$ plasmas. This allowed the positive ion species which are present in these plasmas to be identified, and then investigated for specific features which could add additional characterisation information and be used as an effective process monitor.

6.4.1 The Detection of Ionic Species

With the QMS probe tuned as previously for argon, a $BCl_3/Cl_2/He$ plasma was struck. Using this setup yielded no information at all regarding the ionic plasma

components. At this stage, the probe had to be re-tuned and the energy profiles of some of the positive ions which were expected to be present in the glow discharge were examined for suitability: $^{35}Cl^+$, $^{37}Cl^+$, $^{35}Cl_2^+$, $^{11}B^{35}Cl^+$, $^{11}B^{35}Cl_2^+$, $^{11}B^{35}Cl_3^+$ and $^{11}B^+$. Of the ions which were investigated, the energy profile of $^{11}B^+$ proved most suitable, due to in part to its high intensity. More importantly, it also allowed the detection of a wide range of other species when checked in *MASS PROFILE* mode.

This setup was used to check the plasma positive ions which were present in the $BCl_3/Cl_2/He$ plasma. Figure 6–2 shows the result of sweeping the the mass/energy range from 1 to 140 in *BAR* mode. The highest peaks from figure 6–2 and the most probable associated ions from the glow discharge are:

m/e Ratio	Ion
4	$^{4}He^+$
10	$^{10}B^+$
11	$^{11}B^+$
27	$^{27}Al^+$
35	$^{35}Cl^+$
46	$^{11}B^{35}Cl^+$
48	$^{11}B^{37}Cl^+$
70	$^{35}Cl_2^+$
81	$^{11}B^{35}Cl_2^+$
83	$^{11}B^{35}Cl^{37}Cl^+$
97	$^{27}Al^{35}Cl_2^+$

The ions which were detected were all in the lower mass/energy range (< 100). This may have been a limitation of the use of a quadrupole mass filter employed which has an inherently higher transmission coefficient for lower mass ratios [92]. Alternatively, it may indicate that the higher mass molecules, present in the discharge such as BCl_3, do not readily ionise. This could be caused by electron impact reactions such as dissociation, dominating their characteristics. The

molecules are then fragmented in preference to either ionisation or excitation reactions occurring.

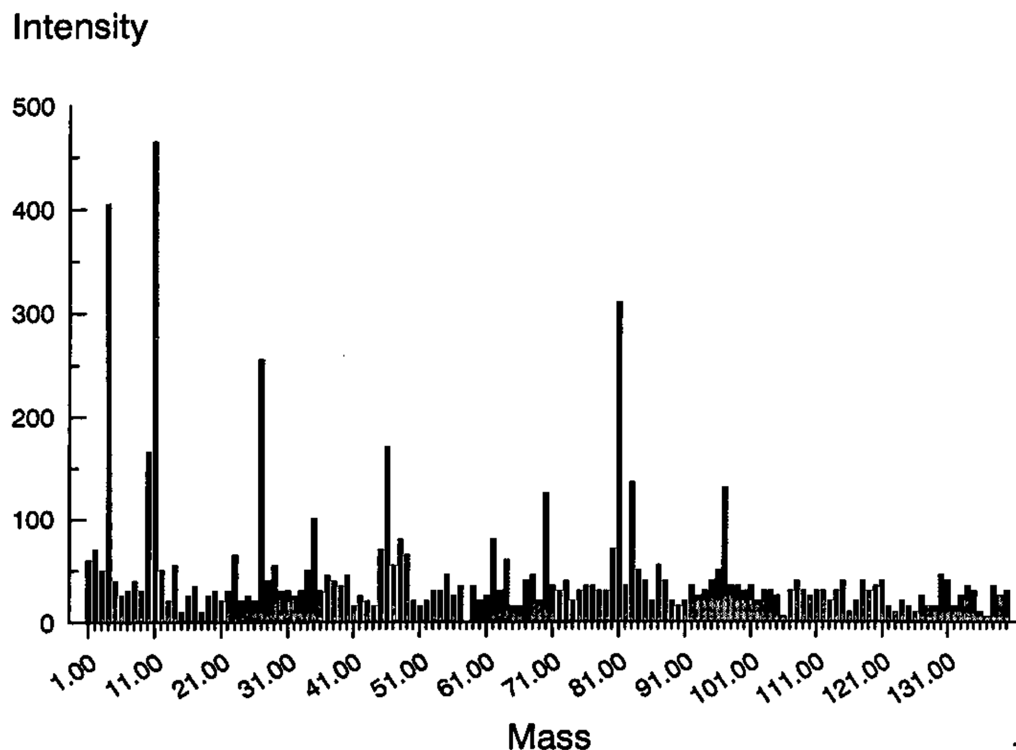

Figure 6–2: Positive ion characteristic of a $BCl_3/Cl_2/He$ plasma.

The $BCl_3/Cl_2/He$ plasma was investigated at this stage for negative ions. The QMS filter settings were all reversed in polarity in order to attempt to attract any negative ions which may have been present. If negative ions were detected then the basis for the calculation of Langmuir probe data may have been invalidated. However, no evidence for the existence of negative ions could be obtained.

6.4.2 Aluminium Etch Monitoring

A test wafer was placed into the RIE chamber and the system pumped down. The QMS probe was configured to scan the 1 to 140 mass range in *BAR* mode, and record the positive ion intensities during the aluminium etch process. The results from this experiment are shown in figures 6–3, 6–4 and 6–5

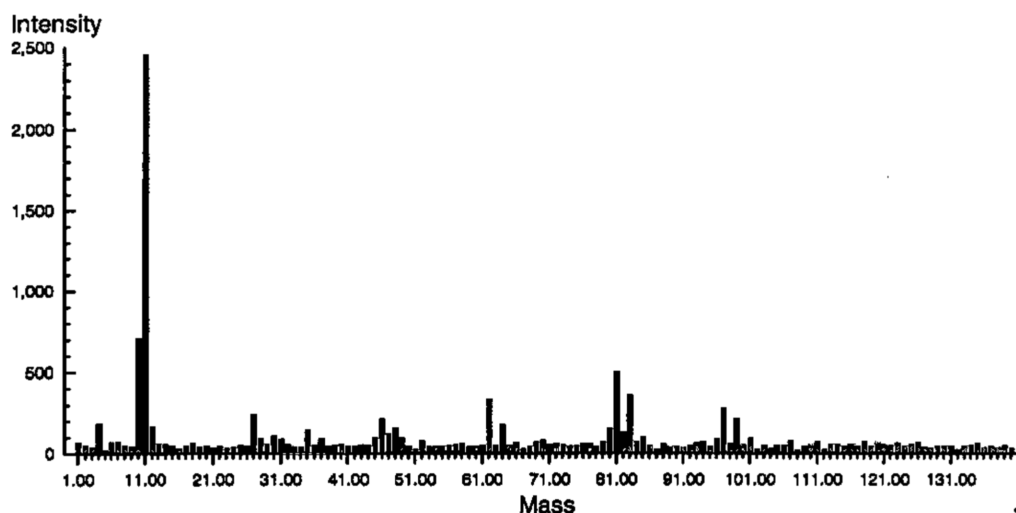

Figure 6–3: In-situ SIMS monitoring of an aluminium etch showing characteristic intensities during the induction period.

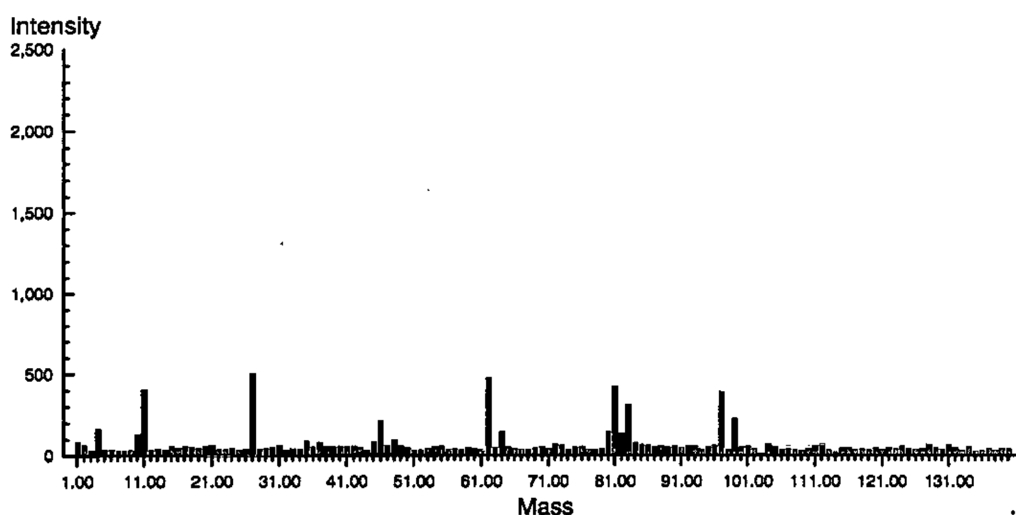

Figure 6–4: In-situ SIMS monitoring of an aluminium etch showing characteristic intensities during bulk aluminium etching.

During the induction period, the dominant positive ions which are being detected are $^{10}B^+$ and $^{11}B^+$. This is due to B atoms being produced as a by-product when BCl_3 based species react with the native aluminium oxide layer to form a-

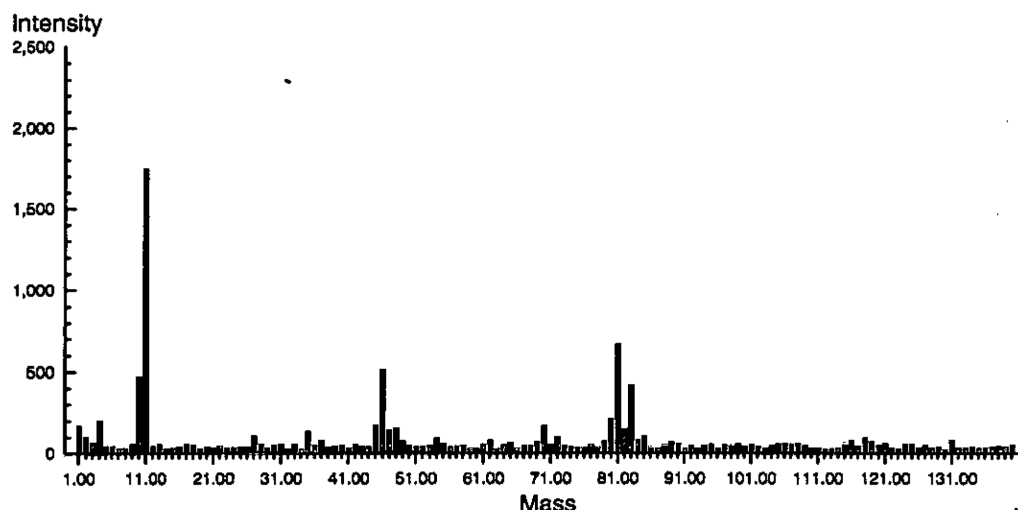

Figure 6–5: In-situ SIMS monitoring of an aluminium etch showing characteristic intensities at the process endpoint (SiO_2 etching).

luminium chlorides. These boron atoms have a relatively low first ionisation potential, shown in table 6–1 of 8.296eV, and are therefore readily ionised.

The in-situ SIMS scan then changed in composition as shown in figures 6–3, 6–4 and 6–5. The B^+ lines decreased dramatically, along with a smaller reduction in the other Cl species which were dissociated from the input gases: 35, 81, 83 m/e. This was accompanied by a marked rise in the intensity of etch product species at 27, 62, 97 and 99 m/e. From the materials involved in the etch reaction, this must have been due to $^{27}Al^+$, $^{27}Al^{35}Cl^+$, $^{27}Al^{35}Cl_2^+$ and $^{27}Al^{35}Cl^{37}Cl_2^+$. This change in the dominant ion distribution is the result of several mechanisms:

- Once the native aluminium oxide has been removed, less B is produced as a reaction by-product. Fewer B^+ reactions therefore take place.

- Bulk aluminium etch product ions have lower 1st ionisation potentials than the etchant gas ions and become preferentially ionised.

- Atomic aluminium appears in the glow discharge during the bulk etch. From table 6–1, Al has a 1st ionisation potential of only 5.984eV, which results in its becoming the dominant ion during the bulk aluminium etch stage.

Species	1st Ionisation Potential (eV)	Reference
Al	5.984	[136]
B	8.296	[136]
Cl	13.01	[136]
He	24.481	[136]
O	13.614	[136]
Si	8.149	[136]
Cl_2	11.48	[136]
N	14.53	[136]
N_2	15.576	[136]
BCl	17.2 → 20.0	[137] [138]
BCl_2	11.8 → 13.01	[137]
BCl_3	10.6 → 12.03	[137]

Table 6–1: 1st ionisation potentials of some plasma species.

The last scan shown in figure 6–5 shows that the B and Cl containing ions have again increased in intensity and the Al based etch product ions have almost disappeared. The B^+ ions are lower in intensity in comparison with the induction period, but the BCl_x^+ ions have increased in intensity. The disappearance of the Al^+ ions shows that the Al layer has been removed and that the silicon dioxide etch stop layer has been reached (SiO_2 has a very low etch rate in a Cl based chemistry). No evidence could be found of Si or O containing positive ions during this overetch period. The high relative reactivity of O along with the low etch rate of SiO_2 is responsible for this. Any oxygen atoms desorbed from the substrate will react quickly with the discharge gases and be removed from the system. Levels of helium ionisation remained constant throughout the etch, as expected for an 'inert' gas. The above characteristics were confirmed for the behaviour of the etch process at an atomic level by monitoring the Al emission line using the OES system.

From figures 6–3 to 6–5 it can be seen that the following mass/energy ratios display the greatest variance: 10, 11, 27, 62, 81, 83, 97, 99. Because these m/e ratios represent ions within the plasma, they are very sensitive to the process conditions. This is because the ions are created by the electrons at the high energy tail of f(ε), which are themselves very dependent on the process conditions. This inherent sensitivity is one of the major reasons for the variations in results from 'identical' process runs, and generally works against the experimenter. However, in the case of in-situ SIMS, this sensitivity allows a greater insight into the process characteristics at an ionic level and allows real time monitoring of the progress of the etch.

A demonstration of the benefits of this technique was given when test wafers from two different batches were etched in the RIE. The test wafers in each batch should have been identical but proved to have very different process etch times. Both sets of wafers were fabricated as described previously in section 6.2 and a single wafer from each batch was etched in the RIE using the operating conditions shown in section 6.2. Each etch process was monitored using in-situ SIMS to track the behaviour of specific ionic species with time (*MID* mode). The results from the first dry etch using batch 1 are shown in figure 6–6 and shows that the total etch time for this wafer is over 13 minutes. However, the majority of this time involved the induction period of the etch with the Al^+ and $AlCl^+$ bulk aluminium etch products only being detected for approximately 4 minutes at the end of the process. This behaviour was initially attributed to a fault either in the RIE system or chemistry, but this could not be found.

A test wafer from the subsequent batch proved to have markedly different characteristics as shown in figure 6–7. This experiment displayed a considerably shorter induction time of approximately 31 seconds and a bulk etch time of 176 seconds. Figure 6–7 clearly shows the interfaces between Al_2O_3/Al and Al/SiO_2. The $^{11}B^+$ is the dominant detected ion during oxide etching of both Al_2O_3 and SiO_2. However, during the bulk etch, aluminium ionic etch products form the majority of the detected species. The variances of some of the other Cl based

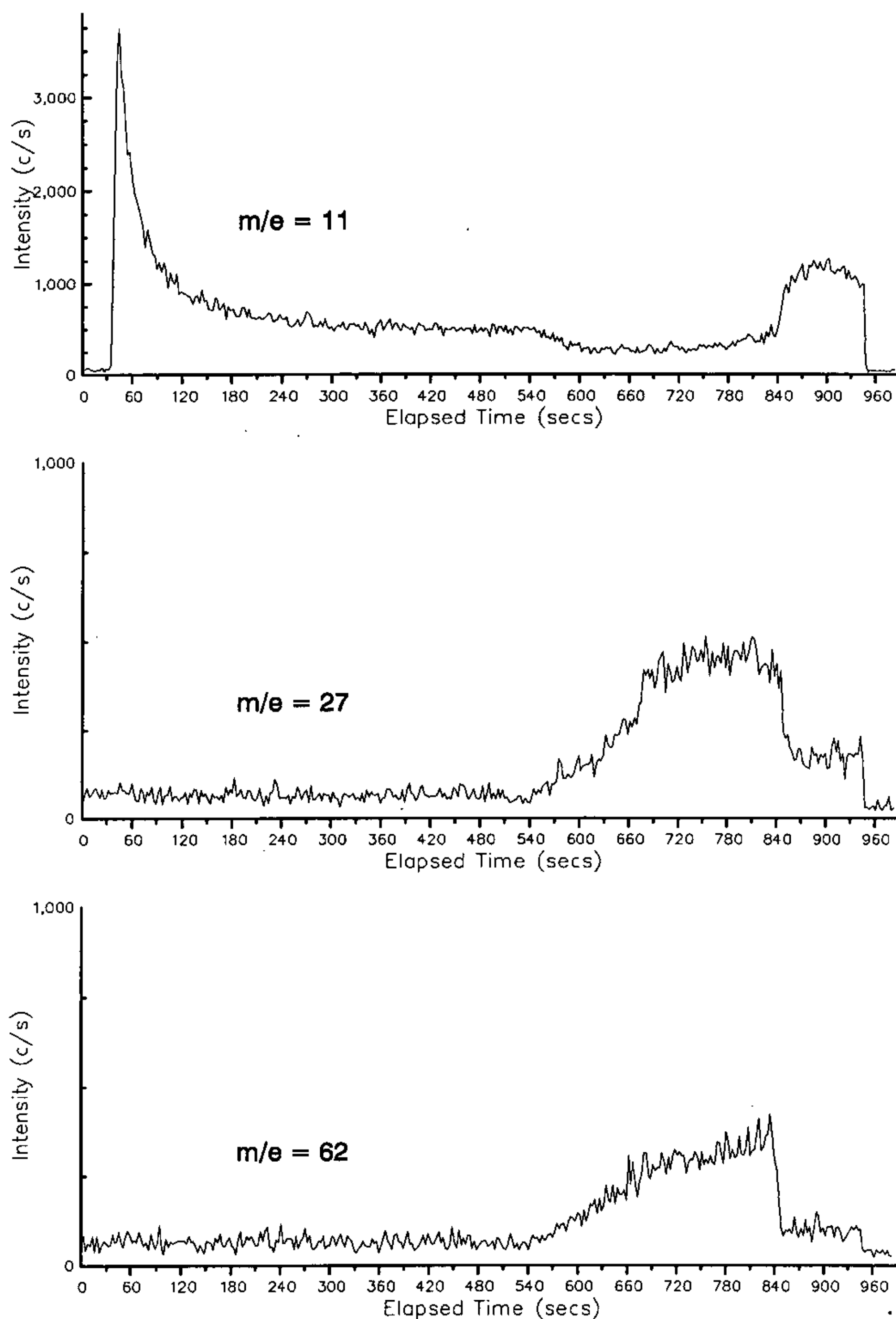

Figure 6–6: In-situ SIMS results for a test wafer from batch 1, which was etched using a $BCl_3/Cl_2/He$ plasma.

ions are shown in figure 6–8. Although the ion concentrations vary with time, their characteristics at the material interfaces are less well-defined.

Test wafers from both batches provided consistent results, which implied that the variation was not due to variations in the dry etch process. Samples from each batch were analysed using a standard SIMS technique to perform material depth profiling [2]. This technique involves using an argon ion beam to sputter the surface of the test sample. Some of the sputtered material is ejected as positive ions which can be analysed using a mass spectrometer. The results from the batch 1 test wafer are shown in figure 6–9 and from the batch 2 test wafer in figure 6–10. If the oxygen trace (mass 16) is compared for the two samples, then it can be seen that the batch 1 wafer shows oxygen present to a far greater depth. Effectively, this meant that the batch 1 wafers consisted of a far thicker aluminium oxide layer, which was resistant to dry etching and therefore provided the characteristic shown in figure 6–6. It is worth noting that the mass 16 profile in figure 6–9 and the mass 11 profile in figure 6–6 are very similar in shape. This might indicate that the oxygen content of the film to be etched has a direct influence on the B^+ intensity. With this information, it was possible prove that the plasma etch process was not the source of this observed variation. Further investigation revealed that the Balzers sputtering system had developed a small leak through one of its 'O' ring seals. This leak was small enough not to register as a marked rise in system pressure due to the large chamber volume, but was large enough to cause a radical change in the deposited film properties.

Using in-situ SIMS, this positive ion sensitivity in reactive plasmas has also been successfully used to precision track the progress of a $BCl_3/Cl_2/He$ plasma etch through an ion implanted silicon wafer and also through SiGe/Si heterostructures [139].

In addition to the in-situ SIMS work, some *RGA* work was also undertaken. RGA scans of the process gas mixture were carried out both before and after

[2]Work carried out by Edinburgh University Geology Dept.

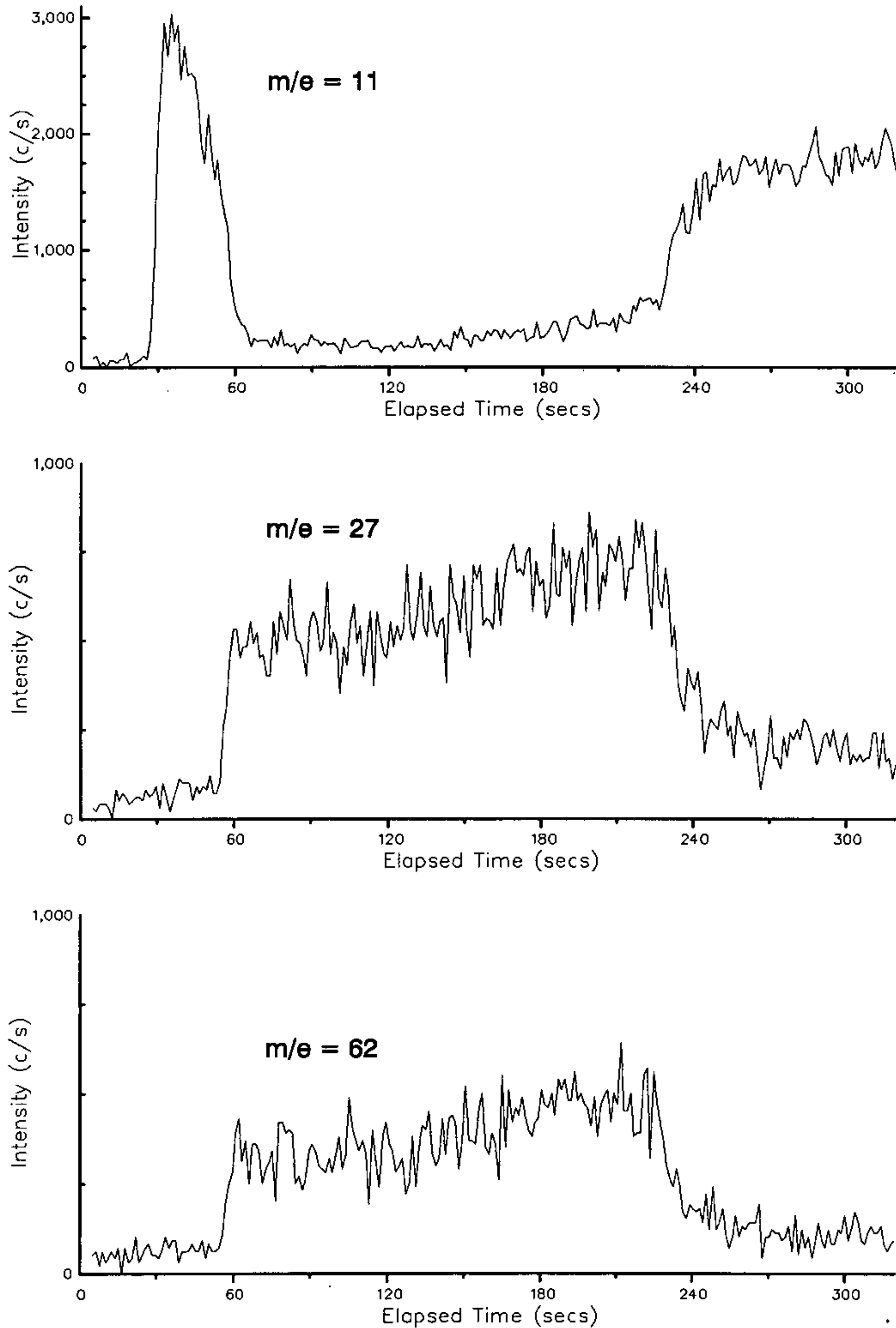

Figure 6–7: In-situ SIMS results for a test wafer from batch 2, which was etched using a $BCl_3/Cl_2/He$ plasma.

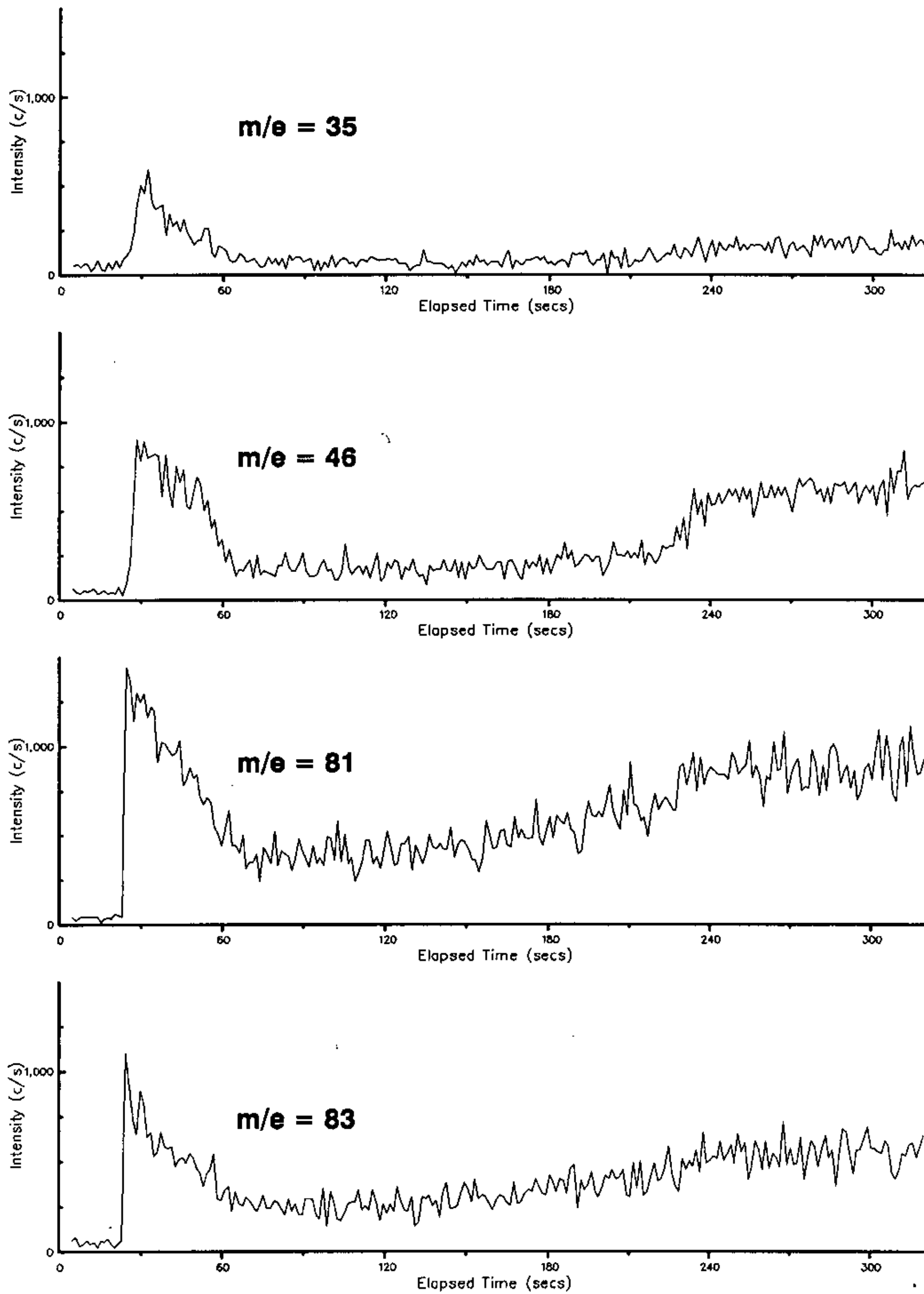

Figure 6–8: In-situ SIMS results for a test wafer from batch 2, which was etched using a $BCl_3/Cl_2/He$ plasma.

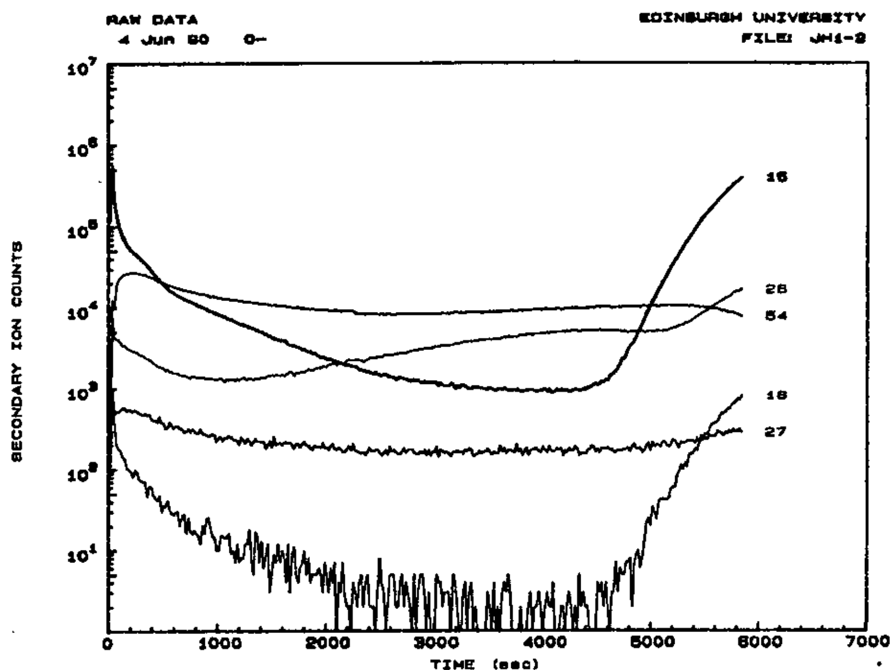

Figure 6–9: Depth profiling results of a batch 1 test wafer, using standard SIMS.

striking the plasma. They revealed that nitrogen was initially present as the process gases switched on. This nitrogen was present in the system due to small vacuum leaks in the system, which allowed air to seep in when the RIE was under long term vacuum. In order to achieve the desired process gas mix, it was necessary to allow time for the process gas to purge out more of the nitrogen using the recipe mixture. All etch experiments allowed a 1 minute period for the gas mixture to reach equilibrium.

With a test wafer on the electrode, the QMS probe was further extended into the chamber so that its sampling port was directly above the centre of the wafer. During a plasma etch, the neutral discharge products were monitored using *RGA MASS BAR* mode. Despite the close proximity of the QMS to the wafer surface, no trace of Al containing reaction products could be detected and a spectrum characteristic solely of the input gases was obtained.

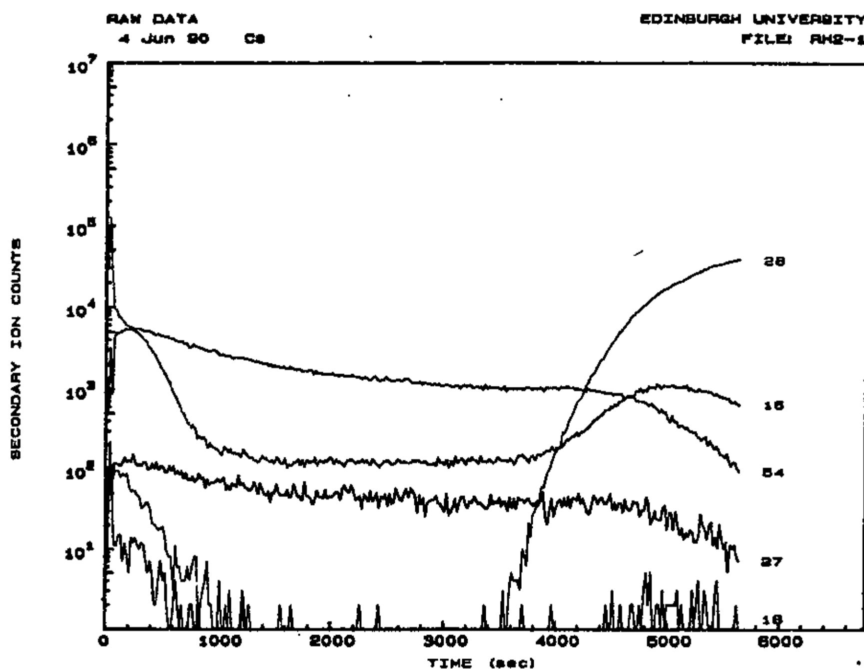

Figure 6–10: Depth profiling results of a batch 2 test wafer, using standard SIMS.

6.4.3 Energy Distributions During Etching

Using the in-situ SIMS setup it was also possible to investigate the energy distributions of ions present in the plasma. A specific mass/charge ratio was selected and then swept across the 0 to 50eV range. The objective of this work was to attempt to identify peak values in the ion energy distribution which could be used to characterise the glow discharge because these detected ions are influenced by the potential drop across the sheath (V_p, as the chamber walls are at vacuum ground) as well as the discharge parameters.

Initial investigations were carried out on the dominant detected ions in the $BCl_3/Cl_2/He$ plasma. The results of monitoring $^{11}B^+$ during an aluminium etch are shown in figure 6–11. During the induction period, there are four peaks in the energy distribution between 14 and 21eV and the distribution is well-defined. During the bulk Al etch B^+ ions are greatly reduced as observed previously, and the distribution becomes less well-defined. When oxide etching takes place B^+ concentrations increase but the peaks in the distribution are now in the range

11 to 20eV, indicating that the discharge conditions have changed as different material layers are etched. The $^{27}Al^{+}$ energy distribution during the bulk Al etch stage is shown in figure 6–12. This distribution does not display any distinctive peak values and showed little variance between etch runs with different process conditions.

The energy profiles for positive ions from the plasma could have been 's-moothed' by using a longer integration period for each energy value of the scan. This would have given a better average value of the number of counts at the detector. However, aluminium etching is a dynamic process which is continually changing the form of the glow discharge, as seen in figures 6–6, 6–7 and 6–8. As the total etch process lasts only $\approx$ 3 minutes, there is a trade-off between profile 'smoothness' and accuracy.

Because it proved difficult to uniquely define peak characteristics within the positive ion energy distributions, evaluations of these characteristics were not the subject of further research at this stage.

6.5 Langmuir Probe

Using the driven Langmuir probe circuit described in section 5–13, investigations of $BCl_3/Cl_2/He$ plasmas were carried out. These reactive plasmas displayed characteristics which departed from the smooth IV characteristics obtained previously in argon discharges.

The probe was sputter cleaned before all the experimental runs by biasing the tip to $-100V$ in the $BCl_3/Cl_2/He$ plasma to remove contamination. Using the RIE with the standard etch recipe shown in figure 6.2, the dc voltage on the probe tip was then swept rapidly from $-100V$ to 100V using the HP4145 and the current monitored. The results of this sweep are shown in figure 6–13. Compared to the scan in figure 5–15, the current collected in the reactive plasma transition region displays a discontinuity at 45V followed by a comparatively

'noisy' region. This abrupt transition was also present on all the other IV traces which were obtained in $BCl_3/Cl_2/He$ plasmas, but varied in position. This was not a function of the driven probe circuit as the same discontinuity was apparent using an undriven circuit. Therefore this feature must have been characteristic of the highly complex physical and chemical interactions which were present within this type of glow discharge.

The consequences of this 'noisy' transition region can be observed on the dI/dV_a as shown in figure 6–14. Obtaining an accurate value for the plasma potential is now very difficult. The maximum gradient point may now be due to a small discontinuity on the IV characteristic which is unrepresentative of the actual plasma potential. This problem is also evident when attempting to ascertain the value of the electron temperature, as shown in figure 6–15. The linear region of of the $\ln(I_e)$ curve also features discontinuities which make T_e assessment difficult.

6.5.1 Plasma Potential Variations with Machine Parameters

With care, it was possible to use the driven Langmuir probe technique to monitor changes in V_p as the major machine parameters were altered. It was found that the IV characteristics changed if a second sweep was carried out for the same discharge conditions. Further investigation showed that the IV characteristic reached a steady state value after two complete IV sweeps. Therefore, for each individual set of operating conditions, three IV sweeps were performed after the probe had been sputter cleaned and the rf feedback optimised:

1. The first sweep was used to check the required range for a specific set of operating conditions.

2. The second sweep was used to stabilise the characteristic and reduce the swept range to within the current compliance.

3. The third sweep was analysed to yield the V_p value.

The effect of a one-dimensional change in power on V_p is shown in figure 6–16. There are two different sets of results displayed on this graph: V_{p2} was obtained under identical setup conditions four days after V_{p1}. Both sets of results show that as rf power is increased, the V_p value is reduced. This means that the increase in ion bombardment potential with increasing rf power is due to an increase in V_{dcb} and not an increase in V_p. It should be noted that although the trends for different experimental days are the same, there is an offset in the results with the V_{p2} values approximately 4.5V lower in value.

The variation in V_p with pressure is shown in figure 6–17, and shows a slight reduction as pressure rises. Experiments were also carried out to examine the change in V_p with rises in BCl_3 flow rate shown in figure 6–18; with Cl_2 flow rate shown in figure 6–19; and with He flow rate shown in figure 6–20. These experiments showed that as both He and BCl_3 flow rates increased, the magnitude of V_p reduced slightly. Cl flow rate had little effect on the value of V_p. All these characteristics showed a marked offset in the results between V_{p2} and V_{p1}. This behaviour may be attributable to a combination of probe and chamber contamination, but demonstrates the repeatability problems which are prevalent with electrostatic probes.

On comparison of the Langmuir probe results for reactive plasmas with the results for argon plasmas obtained in section 5.5.1, there are some obvious differences. The greatest changes in the V_p value for argon plasmas were obtained as a result of pressure variation, whereas power variation produced the greatest variation of the V_p value in reactive plasmas. As expected, variation of the gas flow rates were found to have little effect on V_p in either case.

Because the HP4145B was being employed to obtain the IV characteristic, the effects of signal averaging could be assessed. The above IV trace was obtained by recording the current at each step value of dc voltage. Two other modes exist: one finds the average value of 16 current readings at each voltage, and the other finds the average of 256 current readings at each dc voltage. Averaging

over 16 samples did not provide a significant improvement in the IV trace and also had the disadvantage of collecting more current, leading to greater plasma perturbation. Averaging over 256 readings collected a much larger current and caused a greater disturbance to the glow discharge.

A serious problem which was encountered with reactive $BCl_3/Cl_2/He$ plasmas was the amount of current collected during the IV run. Figure 6–13 shows that the current collection limit of the HP4145 has almost been reached. This also resulted in an obvious disturbance of the glow discharge which lowered the magnitude of the dc bias at the driven electrode. This effect has been discussed previously in section 5.5 and would have to be reduced for the technique to be successfully employed to monitor reactive plasmas. With reference to equations 3.1 and 3.2 in section 3.4 it can be seen that the current to the probe could be reduced by reducing the collecting area of the Langmuir probe. Various different approaches to this problem were attempted:

- The probe tip length was reduced from 1cm to 0.5cm.
- The tungsten wire diameter was reduced from 0.25mm to 0.125mm.
- The orientation of the probe relative to the driven electrode was altered from parallel to perpendicular.

These alterations had no significant effect on the amount of current being collected by the Langmuir probe. This is because the effective collecting area of the probe is the outside area of the insulating sheath which is formed between the plasma and the probe. The sheath area is related to the Debye length λ_D, which was defined previously in equation 2.5. The overall probe collecting area is therefore dependent on T_e and n_e which are a function of the discharge operating conditions.

Although Langmuir probes allow access to some of the physical parameters of the glow discharge, the problems associated with the practical implementation make them unsuitable for this particular application. This is predominantly due to the discontinuities and noise which were observed in the transition region

of the IV characteristic, and also the large amount of current which was being collected by the probe. These features hindered the simple, accurate parameter extraction from the IV transition region characteristics. Electrostatic probes do allow trends within the glow discharge to be evaluated, but the reactive nature of the $BCl_3/Cl_2/He$ plasma alters the probe properties with time. Probe cleaning can reduce but not eliminate this problem. The use of a 'cleaner' probe wire such as platinum, instead of tungsten, may have provided a longer term solution. Reduction of the total collected current may prove to be more difficult to remedy, due to its dependence on the glow discharge parameters as well as the physical collecting area of the probe.

6.6 Summary

During this phase of the research work a process recipe was developed which proved capable of defining linewidths down to $1\mu m$ in $1.2\mu m$ thick Al/1%Si alloy. This process was developed from a typical commercial process so that the project could address many of the same problems which are encountered in commercial wafer fabrication facilities.

Optical emission spectroscopy techniques were applied to the reactive glow discharge. Although the majority of the molecular information was indistinguishable, the atomic aluminium emission line at 396.2nm was identified as a suitable real-time process monitor. This could be successfully used to identify material interfaces during the etch process.

Positive ion monitoring in the $BCl_3/Cl_2/He$ plasma was also carried out using the novel method of in-situ SIMS. This technique used the inherent sensitivity of the positive ion distributions within the plasma to characterise the progress of the etch through an aluminium layer. In-situ SIMS was also used to investigate the positive ion distributions of the major ionic species within the plasma during the etch process. The value of this technique as a process monitor was demonstrated when oxygen contaminated layers of aluminium were etched in the standard

process. Material impurities proved to have a major effect on the behaviour and intensity of certain ionic components within the plasma. This technique has been extended to precision etch monitoring through ion implanted profiles in silicon and also the progress through Si/SiGe heterostructures. The sensitivity of this mass spectrometer configuration contrasts sharply with the results of Lehmann et al [94] who detected no Al based products using the RGA approach.

This project also performed the first attempts at Langmuir probe analysis of $BCl_3/Cl_2/He$ plasmas. The driven technique was employed to investigate trends in the V_p value for one-dimensional changes in the major machine operating parameters: power, pressure and flow rates. Several major problems became evident at this stage: transition region perturbation; high extracted currents which led to plasma perturbation; and contamination problems which led to offsets between experimental results. Some of these problems could be individually addressed and solved to provide a more accurate solution, but the combination of these errors proved that Langmuir probes in their present form cannot be used for routine process characterisation with any degree of confidence. Therefore Langmuir probes were not used further in this research work.

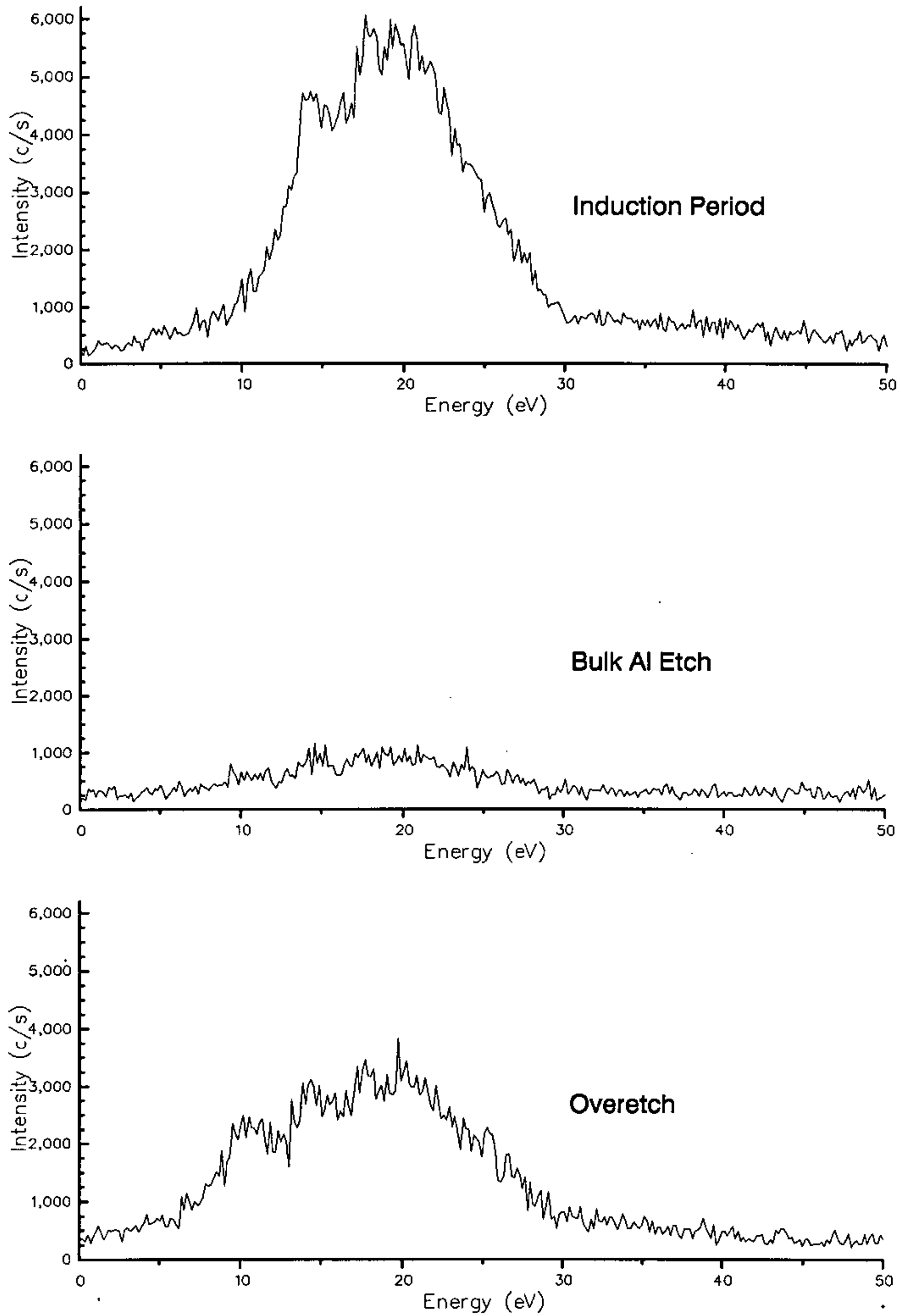

Figure 6–11: Energy profiles of $^{11}B^{+}$ ions during Al etching.

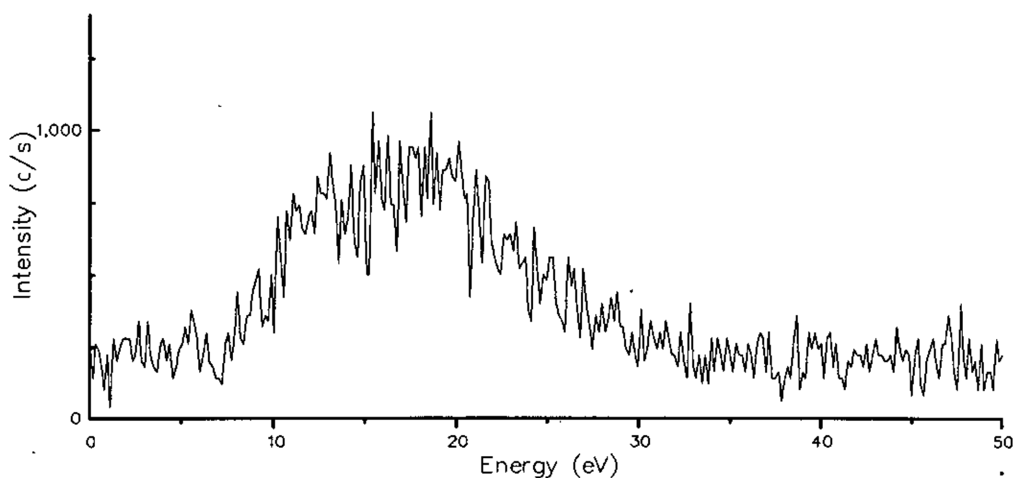

Figure 6–12: Energy profile of $^{27}Al^{+}$ ions during the bulk Al etch.

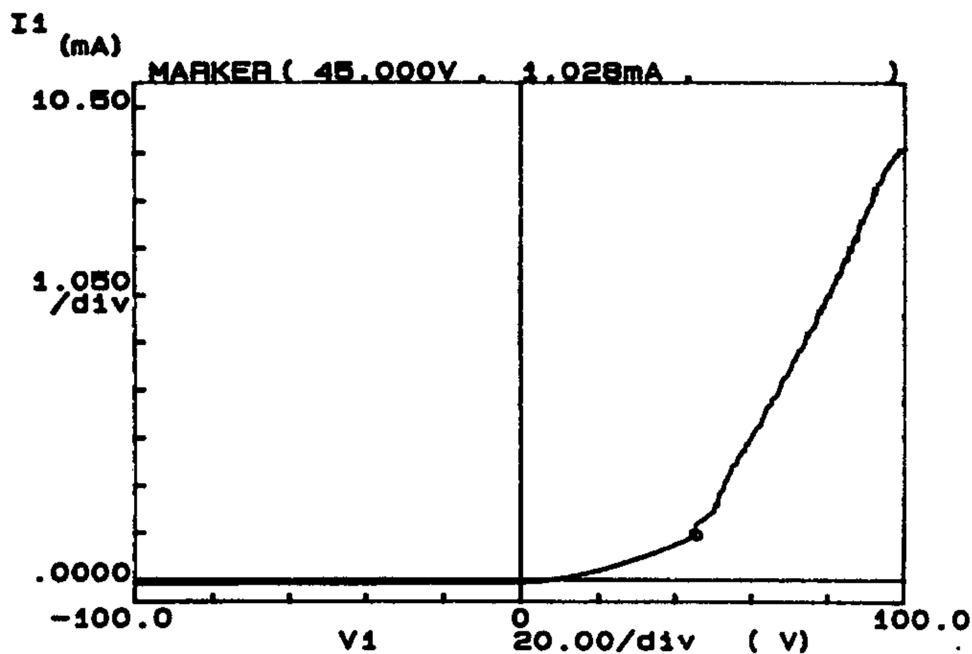

Figure 6–13: Driven Langmuir probe IV characteristic from a 200W, 60mtorr, $BCl_3/Cl_2/He$ plasma.

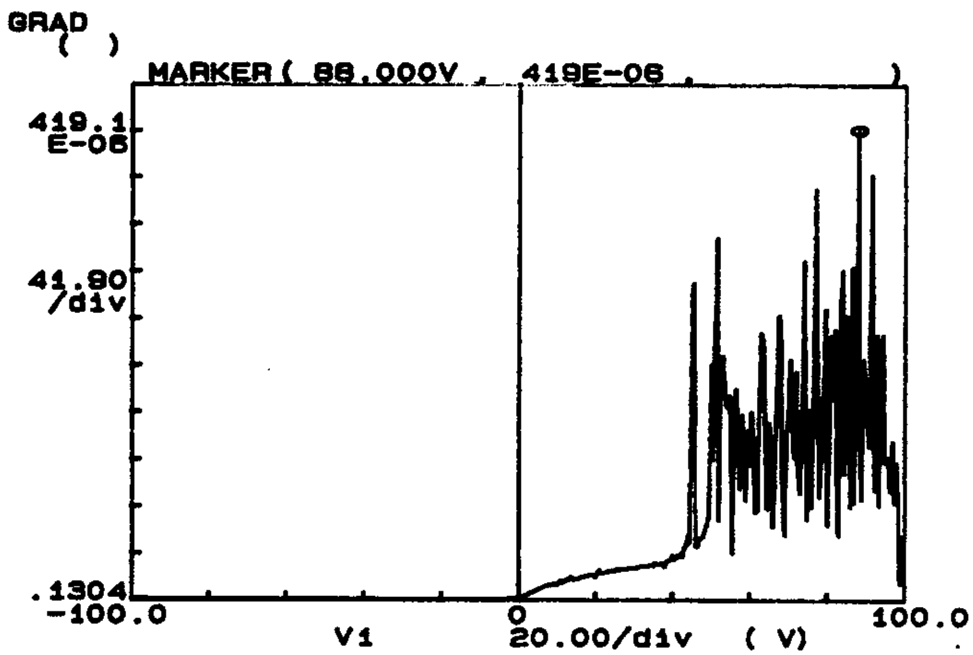

Figure 6–14: Gradient of the Langmuir probe IV characteristic for a 200W, 60m-torr $BCl_3/Cl_2/He$ plasma.

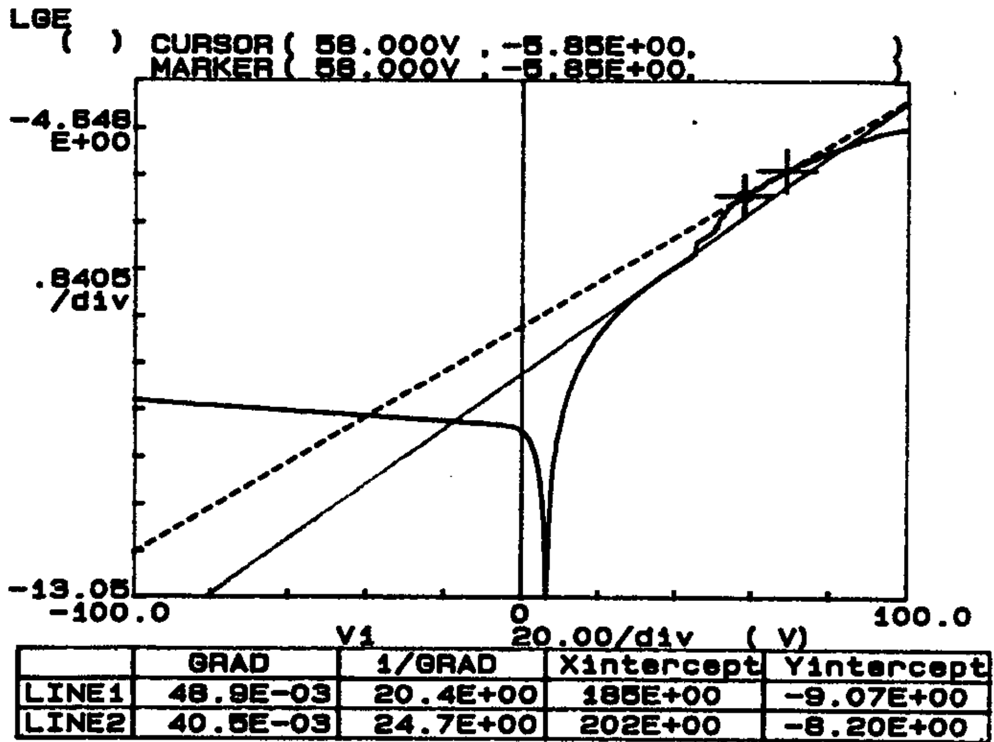

	GRAD	1/GRAD	Xintercept	Yintercept
LINE1	48.9E-03	20.4E+00	185E+00	-9.07E+00
LINE2	40.5E-03	24.7E+00	202E+00	-8.20E+00

Figure 6–15: Electron temperature of a 200W, 60mtorr $BCl_3/Cl_2/He$ plasma.

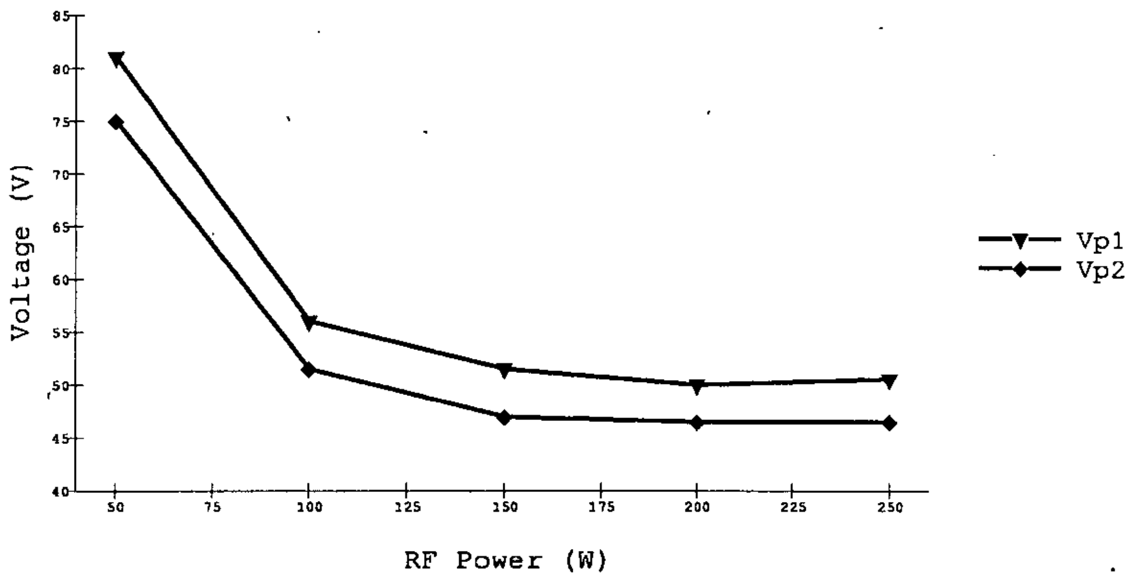

Figure 6–16: Plasma potential variation with power in a 60mtorr, 21sccm BCl_3, 11sccm Cl_2, 28sccm He plasma.

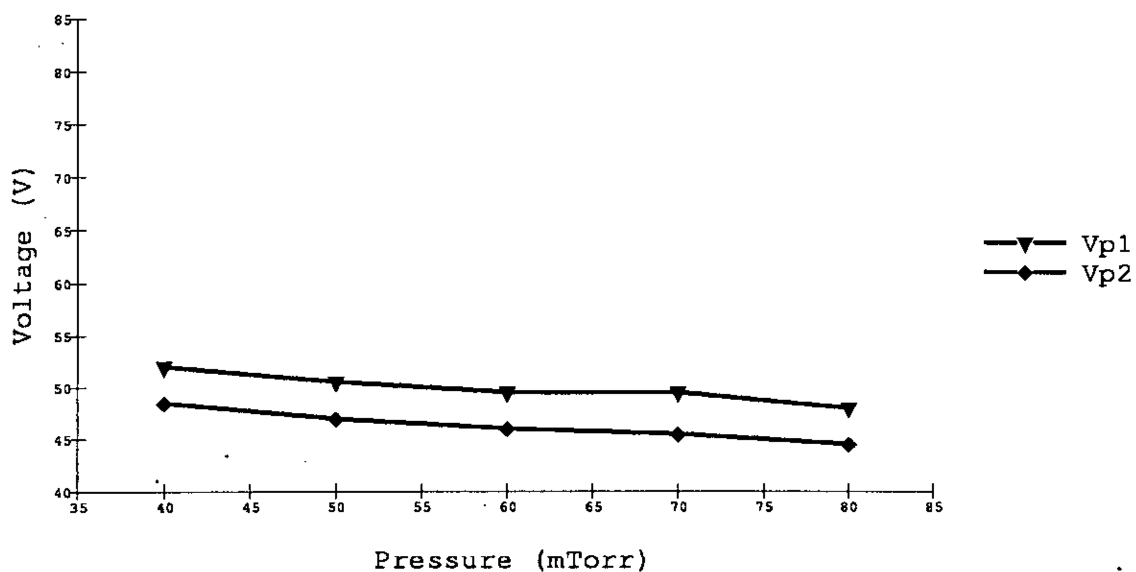

Figure 6–17: Plasma potential variation with pressure in a 200W, 21sccm BCl_3, 11sccm Cl_2, 28sccm He plasma.

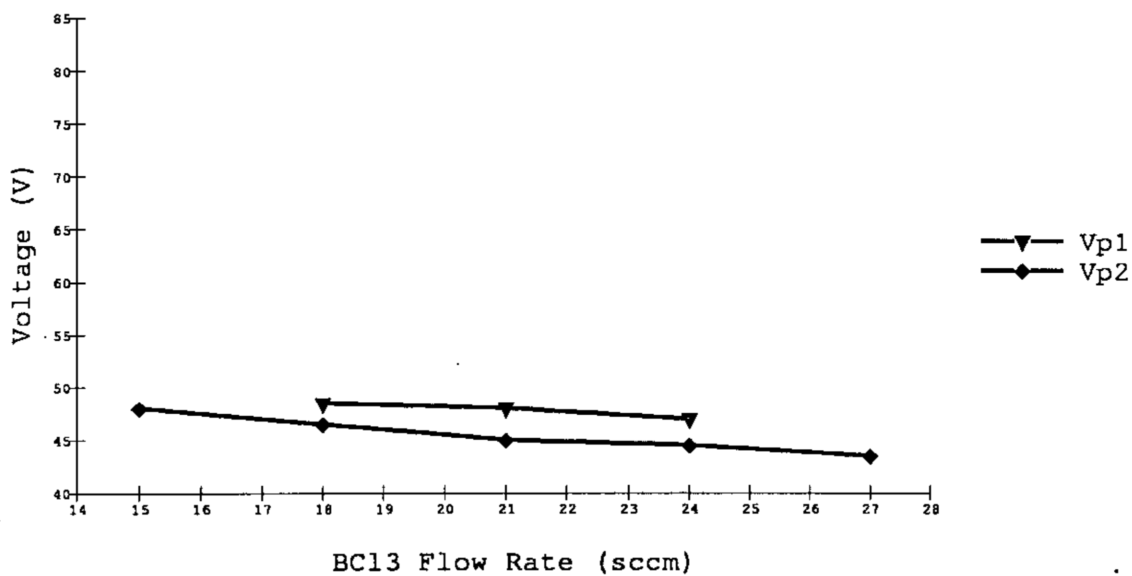

Figure 6–18: Plasma potential variation with BCl_3 flow rate in a 200W, 60mtorr, 11sccm Cl_2, 28sccm He plasma.

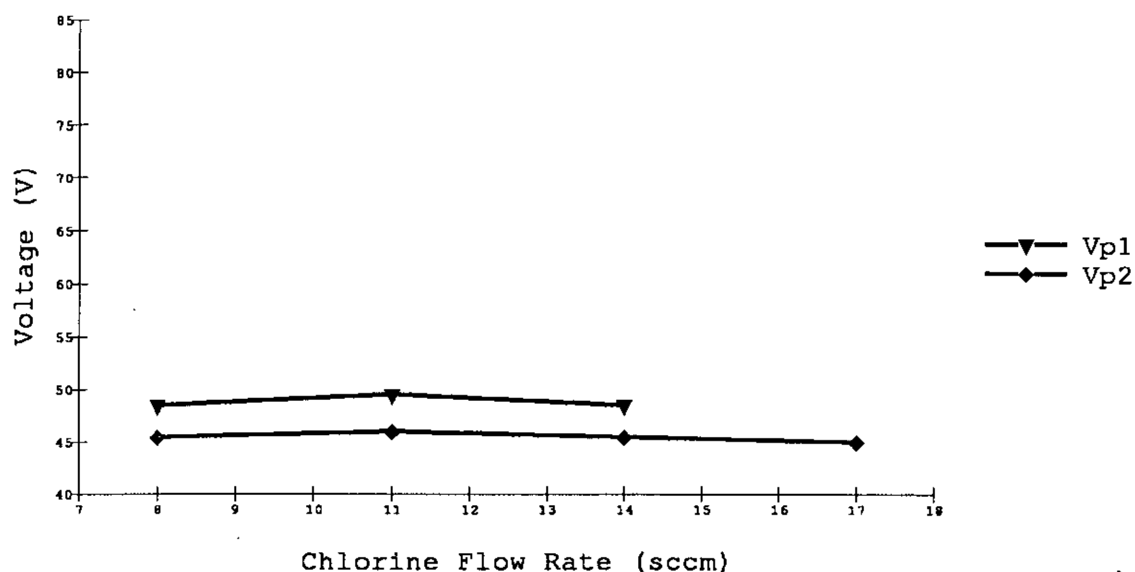

Figure 6–19: Plasma potential variation with Cl_2 flow rate in a 200W, 60mtorr, 21sccm BCl_3, 28sccm He plasma.

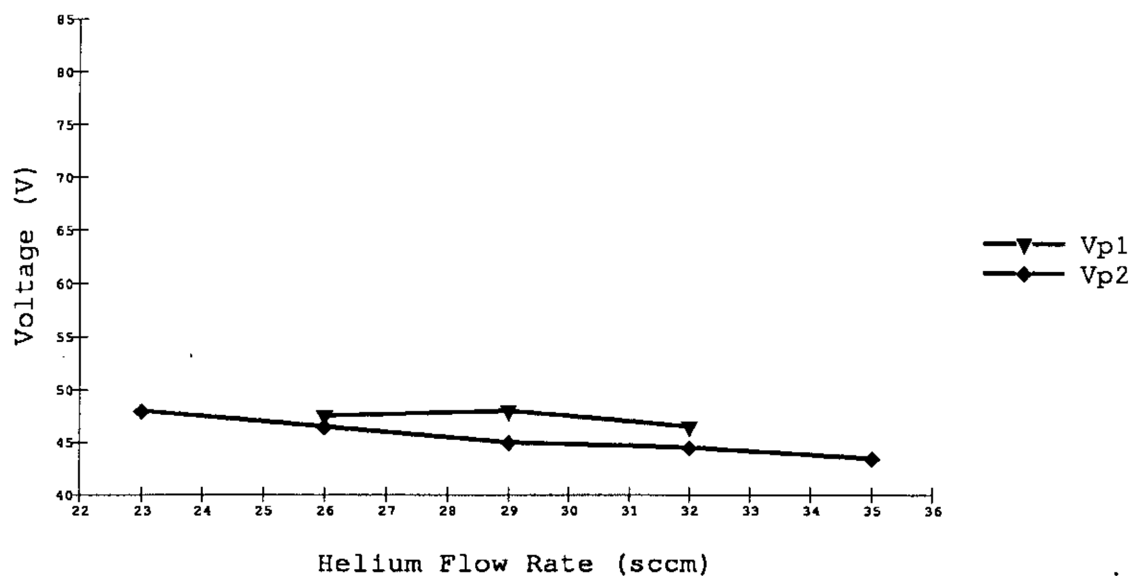

Figure 6–20: Plasma potential variation with He flow rate in a 200W, 60mtorr, 11sccm Cl_2, 21sccm BCl_3 plasma.

Chapter 7

Statistical Process Model

7.1 Introduction

Statistical models have been used previously to allow complex process characterisation to be performed as described in section 4.3.1. This type of approach has most commonly addressed the problems of fluorine based dry etching using one or two process input gases. However, one of the most problematic process steps in silicon wafer fabrication is aluminium alloy dry etching using three or more gases due to a multitude of reasons which were outlined previously in section 2.3.6.

This project addressed the problems associated with statistical modelling of an aluminium dry etch. The overall objective was to create a statistical process model for this complex process which would act as a benchmark for process improvement and provide the first step to implementation of an automatic process feedback and control system. As well as attempting to model the major performance etch parameters of etch rate, selectivity and directionality, the novel approach of modelling some of the process characteristics during the etch was undertaken. This established a link between the final performance variables which are measured post-process and off-line and the actual plasma conditions. In particular, this allowed process assessment of the important ion bombardment component and induction period to take place.

This chapter describes the statistical model choice, experimental procedure and diagnostic monitoring which were carried out for the aluminium etch. The results and a measure of the accuracy of specific models are described.

7.2 Statistical Design for Aluminium Etching

Many software packages are presently available to assist the non-statistician involved in complex process characterisation. In the course of the present work the RS/1 [1] suite of programs was employed. These programs provide a complete environment for experimental design, graphical data exploration, statistical analysis and process visualisation.

At this stage of the project a model had to be chosen along with the most influential RIE machine parameter inputs. The chosen design was a quadratic centre cubic faced (CCF) design which was a symmetrical, rotatable arrangement which featured three process inputs on three different levels. The CCF design is a fractional factorial design with additional 'star' points. Quadratic models have been shown to give a good degree of accuracy and have been extensively applied to the field of dry etching [119,140,126,127,129] although some researchers have opted for a more complex cubic model [125]. The quadratic model was selected because of the finite process window that exists for aluminium etching in a $BCl_3/Cl_2/He$ chemistry. Polymer deposition problems can lead to problems with process replication after many etch runs and it was felt that the reduced number of experiments associated with the quadratic model would be advantageous compared to the cubic model.

Rf power, system pressure and the etchant composition (% Cl_2/BCl_3) were selected as the process inputs for the model. The total process gas flow rate was not used as an input parameter as it had not demonstrated any major effects on the plasma when monitored using diagnostic techniques previously in chapters 5 and 6. The final experimental design is shown in figure 7–1 and the data was

[1]RS/1 is a trademark of BBN Software Products Corporation.

fitted to a quadratic model of the form:

$$\eta = \beta_0 + \sum_{i=1}^{n} \beta_i \xi_i + \sum_{i=1}^{n} \beta_{ii} \xi_i^2 + \sum_{i=1}^{n} \sum_{j=i+1}^{n} \beta_{ij} \xi_i \xi_j \tag{7.1}$$

where ξ_i represents the set of input variables and β_i is the set of weighting coefficients.

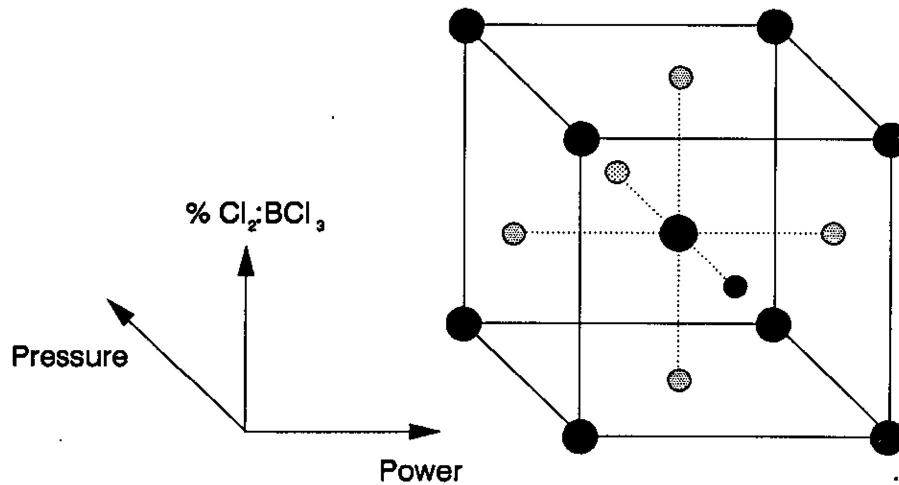

Figure 7–1: CCF design for the experimental characterisation of an aluminium etch process.

7.2.1 Experimental Process Range

Having chosen the model, the range of process conditions which would be characterised had to be decided. The experimental centre point was defined as previously in section 6.2, and from this point, the operating conditions were defined as follows:

Fixed Operating Conditions	
He Flow Rate	28sccm
Total BCl_3/Cl_2 Flow Rate	32sccm
Reactor Geometry	Fixed
Rf Frequency	13.56MHz
Electrode Cooling	ON

Variable Operating Conditions	
RF Power	160 → 240W
Pressure	50 → 70mtorr
Cl_2/BCl_3 Ratio	28 → 41%

The central point for this design was repeated five times to allow some assessment of the degree of process repeatability. This gave a total of 20 experimental runs for the CCF model, compared to a full factorial investigation which would have needed a minimum of 27 runs. To help minimise the effect of other external effects, the runsheet was randomised and is shown in figure 7–2.

0	1 POWER (Watts)	2 PRESSURE (mtorr)	3 CL2_RATIO (%)
1	160	60.0	34.5
2	200	60.0	41.0
3	200	60.0	34.5
4	160	50.0	28.0
5	240	70.0	28.0
6	240	50.0	41.0
7	200	60.0	28.0
8	200	60.0	34.5
9	240	60.0	34.5
10	200	60.0	34.5
11	160	70.0	28.0
12	240	50.0	28.0
13	160	70.0	41.0
14	160	50.0	41.0
15	240	70.0	41.0
16	200	60.0	34.5
17	200	60.0	34.5
18	200	70.0	34.5
19	200	60.0	34.5
20	200	50.0	34.5

Figure 7–2: Aluminium etch experimental worksheet.

7.3 Experimental Procedure

A set of test wafers was fabricated for use in this experiment. Silicon wafers which were 75mm in diameter, p-type and 100 orientation were used as the starting material. They had silicon dioxide thermally grown to a thickness of 14000Å, and were then deposited with 1.13μm Al/1%Si, using a Balzers BAS 450PM planar magnetron sputtering system. The wafers were then dipped in a solution of aluminium etch such that the aluminium was removed from $\frac{1}{5}$ of the wafer surface. The wafers were then coated in 1.3μm of positive photoresist and a test pattern defined by an Optimetrix 10X reduction wafer stepper. The reticle used in this work was a test reticle which featured a square pattern of parallel lines in various mark/space ratios from 6μm $\rightarrow$ 0.7μm. This arrangement allowed for the possibility of scanning electron micrograph analysis of cleaved wafers. The wafers were then hard baked prior to experimental dry etching.

Each experimental run in the design in figure 7–2 is succeeded by a different set of operating conditions, which feature different plasma characteristics within the chamber. To attempt to increase the probability of stabilising these conditions at the correct level a 'conditioning' run was performed before each experimental run. A $\frac{1}{4}$ wafer sample coated with unpatterned aluminium was placed in the chamber and etched. This also allowed the machine variables to be set up accurately.

After the 'conditioning' run a $\frac{1}{2}$ test wafer was etched. Test wafers were halved down the crystal lattice such that the exposed, patterned SiO_2 and Al covered areas were equally divided. An experimental $\frac{1}{2}$ wafer sample was then placed in the chamber at the same position for each run. A period of one minute was allowed at the start of each run for gas and pressure stabilisation. The power was then switched on and the process monitored using OES to assess the endpoint. Although some overetch was necessary to ensure the Al had achieved endpoint, interface times for the Al_2O_3/Al and Al/SiO_2 barriers were obtained by studying the recorded OES Al* intensity.

In order to create as little plasma disturbance as possible, only non-invasive monitoring was employed to obtain the process characteristics. OES was used to analyse the induction time and bulk Al etch time by monitoring the Al* emission line at 396.2nm. The self bias, V_{dcb}, was also measured during the induction period and the bulk Al etch to infer the average ion energy which was present during the process.

After etching, a Sloan Dektak surface profilometer was used to make multiple step height measurements at the wafer centre above the Al tracks and the SiO_2. This allowed the combined average height of the Al track and photoresist mask to be measured. The wafers were then photoresist stripped using an oxygen plasma in a Tegal barrel asher and also wet etched in fuming nitric acid. The Dektak surface profile measurements were then repeated to give the stripped surface profile. When allied with the OES measurements of induction and bulk Al etch time and processed film thickness data, these measurements allowed the evaluation of photoresist etch rate, SiO_2 etch rate, bulk Al etch rate and their relative selectivities.

7.4 Process Models

Once the experiments had been completed, statistical models were created by performing a least squares regression analysis on the process data. The models were then analysed using the ANOVA and model fit techniques outlined in Appendix A. The sections below describe the results of these analyses for the process variable correlations. Values of the coefficients, R^2_{adj} and $\frac{S^2_L}{S^2_e}$ are given in table 7–1 for all models. If a transform has been used to improve the model fit, then that is also indicated in the table. The criterion for a model with good fit and predictive ability was that it should have a R^2_{adj} value of > 0.8 and ideally ≈ 1 with $\frac{S^2_L}{S^2_e}$ value of < 6. To visualise the process interactions, 3D plots are presented in the following sections. For the most accurate models, these are accompanied by contourplots in order that absolute values can be evaluated.

Term	V_{dcb1}	V_{dcb2}	t_{ind}
1	-340.309	-321.300	0.03826
Pwr	-37.200	-41.100	0.00669
Pres	12.500	16.800	-0.00214
Cl	-3.700	-0.300	-0.00555
Pwr^2	2.273	0	0
Pwr.Pres	-1.375	-1.375	0
Pwr.Cl	-3.875	-4.625	-0.00961
$Pres^2$	1.773	2.500	0.00781
Pres.Cl	-1.125	-1.125	-0.00266
Cl^2	2.773	3.000	-0.01330
Goodness of Fit	1.42	2.63	0.36
R^2_{adj}	0.924	0.941	0.660
transform	η	η	$\frac{1}{\eta}$

Table 7–1: Coefficients of process response variables where V_{dcb1} is the self bias during the induction period; V_{dcb2} is the self bias during the bulk Al etch; t_{ind} is the induction time; Pwr is the rf power; Pres is the system pressure and Cl is the $\%Cl_2/BCl_3$ ratio.

7.4.1 DC Self Bias

During an aluminium plasma etch at constant power, the value of V_{dcb} exhibits a greater value of magnitude during the induction period than during the bulk Al etch. For this reason, the process was modelled during both stages of the etch.

From table 7–1 it can be seen that both models for V_{dcb} exhibited good values for Fit and R^2_{adj}. For the induction period, the 3D plots of the V_{dcb} are shown in figure 7–3 and the contourplots are shown in figure 7–4. For the bulk Al etch period, the 3D plots of V_{dcb} are shown in figure 7–5 and the contourplots are shown in figure 7–6.

As expected, it can be seen that power and pressure were the major influences on the magnitude of V_{dcb}. V_{dcb} decreased in magnitude with increasing pressure due to a reduction in the electron mean free path; and with decreasing power due to a decrease in electric field strength. The resultant changes $f(\varepsilon)$ leads to a lowering of the magnitude of V_{dcb}. Both effects are manifested in a nearly

linear fashion. The ratio of Cl_2/BCl_3 exerted a minimal influence on the V_{dcb} characteristic.

7.4.2 Interface Times

Using the OES system an estimate of the interface times for the Al_2O_3/Al boundary was obtained. The induction time t_{ind}, has provided particular problems with repeatability for the process engineer as discussed in section 2.3.6 and could provide a useful benchmark for the etch progress in comparison to the predicted behaviour for a feedback control system. From table 7–1 it can be seen that the model for t_{ind} has a lower Fit value than the V_{dcb} model which may indicate that variation due to pure error is greater. The R^2_{adj} values of 0.660 for t_{ind} shows that this is a relatively poor model. However, it does show trends which appear consistent with expected phenomena, especially at low Cl_2 flow rates.

The 3D response surfaces for the variation of the induction period are shown in figure 7–7. It can be seen that for low flow rates of Cl_2 and high BCl_3 flow rates in the process gas mix, that the rf power had a major influence on the induction time. This is consistent with the hypothesis that the native Al_2O_3 removal can only be achieved by ion bombardment in the presence of an effective reducing agent such as BCl_x. As the BCl_3 flow rate decreases, this effect becomes less obvious and the induction time rises.

The results from this model should be treated with caution due to poor statistical fit of the model, especially at high Cl_2 flow rates. The reason for this low level of model confidence can be attributed to both random process variation (see section 7.6) and problems with interface identification using the OES. As the process has not been optimised for uniformity, the rise and fall times for the Al^* signal are longer than optimum, leading to problems with interface identification.

Term	ER_{metal}	ER_{Al}	ER_{pr}	Dir	$S_{Al/pr}$	S_{Al/SiO_2}
1	4801.100	6862.082	1480.281	0.93102	4.628	0.01735
Pwr	201.586	-265.700	320.500	0.28001	-1.260	0.00774
Pres	-41.485	33.800	-0.500	-0.01700	0.180	-0.00235
Cl	13.921	404.200	88.900	-0.04084	0.060	-0.00464
Pwr^2	199.822	142.545	23.545	0.22064	0.305	0.00253
Pwr.Pres	66.941	44.500	115.875	-0.27676	-0.375	0.00128
Pwr.Cl	-193.217	-201.000	26.875	-0.20957	-0.125	-0.00271
$Pres^2$	-17.689	-520.955	51.545	0.08622	-0.495	0.00432
Pres.Cl	-33.845	23.500	56.375	0.09044	-0.075	-0.00104
Cl^2	-450.744	-129.955	-139.455	-0.06504	0.405	-0.00434
Goodness of Fit	0.90	0.45	3.44	1.43	0.41	0.23
R^2_{adj}	-0.062	0.007	0.941	0.838	0.783	0.538
transform	η	η	η	$\log \eta$	η	$\frac{1}{\eta}$

Table 7–2: Coefficients of performance response variables where ER_{metal} is the overall metal etch rate; ER_{Al} is the bulk Al etch rate; ER_{pr} is the photoresist etch rate; Dir is the directionality; $S_{Al/pr}$ is the bulk Al to photoresist selectivity; S_{Al/SiO_2} is the bulk Al to SiO_2 selectivity; Pwr is the rf power; Pres is the system pressure and Cl is the $\%Cl_2/BCl_3$ ratio.

7.5 Performance Models

Performance models were created by analysing the data extracted from the processed wafers. Specific variables studied were overall metal etch rate; bulk Al etch rate; photoresist etch rate; directionality; bulk Al to photoresist selectivity; and bulk Al to SiO_2 selectivity. The analysis techniques were identical to those described for process models. The model coefficients and statistical data are presented in table 7–2.

7.5.1 Etch Rate

The etch rates of the various materials in contact with the reactive plasma were calculated as follows:

$$\mathrm{ER_{metal}} = \frac{\mathrm{T_{Al}}}{\mathrm{t_{Al/SiO_2}}} \tag{7.2}$$

$$\mathrm{ER_{Al}} = \frac{\mathrm{T_{Al}}}{\mathrm{t_{Al_2O_3/Al}} - \mathrm{t_{Al/SiO_2}}} \tag{7.3}$$

$$\mathrm{ER_{pr}} = \frac{\mathrm{T_{pr}}}{\mathrm{t_{total}}} \tag{7.4}$$

$$\mathrm{ER_{SiO_2}} = \frac{\mathrm{T_{SiO_2}}}{\mathrm{t_{total}}} \tag{7.5}$$

where ER is the etch rate; T is the thickness and t is the time. The data for $\mathrm{ER_{SiO_2}}$ was not modelled directly but was used for selectivity characterisation in section 7.5.3. It should also be noted that the thickness of the native oxide layer was not accounted for in the assessment of $\mathrm{ER_{metal}}$ as it forms $\leq 0.3\%$ of the layer thickness and is not readily measurable.

From table 7–2 it can be seen that all the etch rate models pass the Fit test. However the near-zero results for the R^2_{adj} test show that the models for $\mathrm{ER_{metal}}$ and $\mathrm{ER_{Al}}$ exhibit poor model fit characteristics. Although inadequate for the purposes of feedback and control, the models display some interesting features that are worthy of further comment and are displayed in figures 7–8 and 7–9.

The $\mathrm{ER_{metal}}$ encompasses the two differing etch processes of native oxide removal and bulk Al etching. Native oxide is removal is an ion-induced reaction as shown for low Cl_2 flow rates in figure 7–7 whereas bulk Al etching in figure 7–8 features an ion-enhanced mechanism with a large chemical component. The attempt to model these conflicting processes as a single response allied with the problems of $\mathrm{t_{Al/SiO_2}}$ identification has resulted in the poorest model quality for the entire range of parameters investigated. The model indicates that the overall etch rate is heavily influenced by the $\mathrm{t_{ind}}$ characteristics showing high power dependence at low rates but little power dependence at high Cl_2 flow rates.

The bulk Al etch characteristics given in figure 7–9 seem to indicate that increasing power resulted in a decreasing etch rate at higher Cl_2 flow rates in contrast to t_{ind}. This exemplifies the hypothesis that bulk Al etching features a high chemical etch component. High ion energies at the material surface may lower the etch rate by reducing the rate of reactant adsorption, product formation or product desorption at the surface.

Photoresist thickness was measured using the Dektak prior to etching, post-etch and after resist stripping to obtain data on the reactive plasma etched resist thickness. The etch time in this case was the total time that the rf power was on which could be accurately determined. In contrast to the poor statistical characteristics of ER_{metal} and ER_{Al}, the ER_{pr} model has a high R^2_{adj} coefficient of 0.941. This demonstrates the relative ease with which single layer films such as photoresist can be characterised compared to the difficulties associated with films such as aluminium which effectively comprise multiple films. Three dimensional models of this response are shown in figure 7–10 and the associated contourplots are shown in figure 7–11.

ER_{pr} is strongly dependent on the power density with the etch rate increasing in a pseudo-linear with increasing power. Higher pressures and higher Cl_2 flow rates also caused increased etch rates which could be attributed to greater etchant concentrations.

7.5.2 Directionality

To gain an insight into the directionality of the etch process, samples had to be prepared which were suitable for cross-sectional viewing in a SEM. Etched samples were stripped of resist and then low temperature pyrolytic SiO_2 was deposited onto the wafer surfaces. Each sample was then cleaved about its centre and dipped into an aluminium wet etch solution. This left the oxide layer intact but removed the exposed aluminium track. The samples were then given a thin gold coating to reduce SEM charging effects. Samples were mounted at 90° to the SEM chuck and, on investigation, displayed a range of sidewall angles from

the highly directional profile of figure 7–12 to the isotropic profile shown in figure 7–13.

The range of observed profiles presented a problem in assessment of the wall angle as some curvature was present in many of the profiles. One solution is shown in figure 7–14 with the measurements which were performed to estimate the directionality, $\tan\theta$, as follows:

$$\tan\theta = \frac{h}{\frac{d_b - d_t}{2}} = \frac{2h}{d_b - d_t} \tag{7.6}$$

It should be noted that this method provides no information on consequences of mask erosion and only provides a measure of the final wall angle.

The directionality model displayed a good degree of fit with a R^2_{adj} of 0.838 and a Fit coefficient of 1.43. The 3D models of this response are shown in figure 7–15 and the associated contourplots in figure 7–16. As expected, the directionality coefficient, $\tan\theta$, increased as the power increased and the pressure decreased, resulting in more vertical sidewalls. These factors both give greater sheath voltages at the driven electrode and hence increase the average ion energy at the wafer surface. As the BCl_3 flow rate is increased, the directionality also increased which may be indicative of BCl_x based polymer formation on the sidewall acting as a lateral etch rate limiter.

7.5.3 Selectivity

Using the data for the etch rate of bulk Al, selectivity for the process with respect to the photoresist and underlying SiO_2 etch rates were calculated as follows:

$$S_{Al/pr} = \frac{ER_{Al}}{ER_{pr}} \tag{7.7}$$

$$S_{Al/SiO_2} = \frac{ER_{Al}}{ER_{SiO_2}} \tag{7.8}$$

Because these calculations incorporated the data for ER_{Al} which has already been shown to be statistically poor, the selectivity models also failed the R^2_{adj} test with values of 0.783 and 0.538 for $S_{Al/pr}$ and $S_{Al/pr}$ are shown in figure 7–17 and the

models for S_{Al/SiO_2} are shown in figure 7–18. Again, although the models have a poor quality of fit, they effectively demonstrate the lowering of selectivity that occurred for higher powers. This transpired because of an increase in the ion bombardment energy which resulted in a greater, non-selective, physical element to the etch.

7.6 Induction Time Variations

One of the most probable sources of pure error which led to a poor statistical fit for the induction period model could be due to water in the chamber. To check on the extent of the water influence, the QMS was set up in *RGA* mode and the water content of the chamber monitored for an 'inert' He plasma and a reactive BCl_3/Cl_2/He plasma at the same operating pressure, total flow rate and power density. Before each plasma was struck, the chamber was vented to atmosphere and the lid opened to simulate wafer loading. The results of monitoring the peak at mass 18 are shown in figures 7–19 and 7–20.

As the He plasma is struck, there is a large rise in the intensity of mass 18 as water is forcibly desorbed from the chamber electrodes by ion bombardment. In this case it takes $\approx$ 60 seconds to return to level of pre-plasma water detection. As the reactive BCl_3/Cl_2/He plasma is struck there is also a rise in the detected intensity at mass 18 but this rise is markedly less. This is most probably due to the reaction of BCl_3 based species with H_2O, and this time $\approx$ 40 seconds pass before the intensity returns to the pre-plasma level.

The range of experimentally observed induction times ranged from 15 seconds to just under 1 minute. The RGA results show that although the BCl_3 species reduced the effect, there remained a large water presence for much of the time which was not accounted for in the model and could therefore have been a major source of pure error. One possible solution to this problem would be to employ a load lock so that the main reaction chamber continually remained at low pressure.

This would dramatically reduce the amount of water vapour which was available for adsorption by the electrodes.

7.7 Summary

In this chapter, a CCF design for a statistical model of an aluminium etch process was described. The model was constructed from the major RIE machine variables of power, pressure and $\%Cl_2/BCl_3$. Statistical modelling was carried out for both process variables and performance variables. This work uses a quadratic model which covers 3 manipulated machine variables, 3 process variables and 6 performance variables. This is the first time that rigorous statistical modelling techniques have been applied to a $BCl_3/Cl_2/He$ based chemistry or an Al dry etch process in order to systematically analyse both the plasma process and post-process etch performance, although McLaughlin et al [129] have recently used a similar technique for the characterisation of CF_4/O_2 and CF_4/H_2 etching of Si and SiO_2 films. Results from this section of the research have already been presented [141]. This type of work is a necessary step towards the goal of automated feedback and control which will be crucial to achieving the fine linewidth definition needed for the next generation of etching machines.

Non-invasive process monitoring was carried out using OES and V_{dcb} analyses. The models for V_{dcb} showed a high quality of statistical fit, but t_{ind} modelling gave a poor model fit. This was attributed to inaccuracies in interface identification with the OES and also variations due to water desorption during etching which were not accounted for in the model.

Performance monitoring provided good quality models for directionality and also for the important erosion rate of photoresist. However, models for ER_{metal}, ER_{Al}, $S_{Al/pr}$ and S_{Al/SiO_2} did not achieve satisfactory levels of statistical significance. This was due to problems with absolute identification of the bulk Al endpoint using the OES system. As the process was not optimised in terms of uniformity across the wafer, there was a 'blurring' of the endpoint as the wafer

cleared. This gave a large error component in the data which prevented accurate process characterisation. A reduction of these problems may be achieved by employing in-situ SIMS as a secondary diagnostic monitor and altering the process centre point so that a more uniform etch occurs. Although many of the models did not achieve the statistical significance required for process feedback and control, they did provide a useful insight into the aluminium process characteristics.

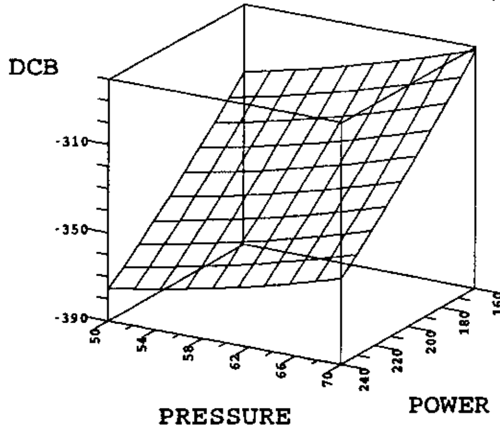

28% Cl2/BCl3

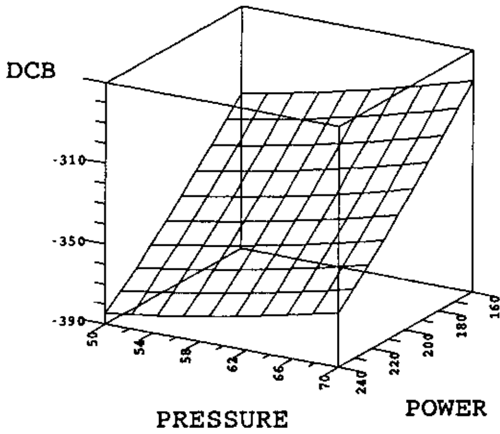

34.5% Cl2/BCl3

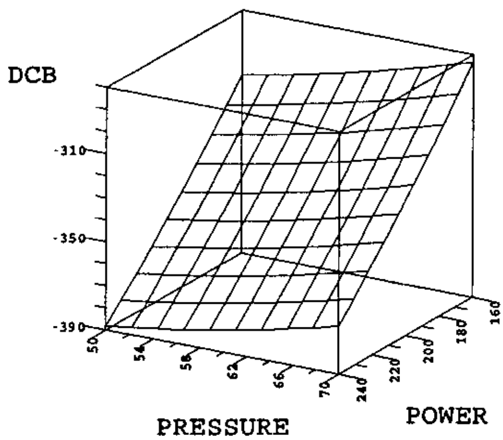

41% Cl2/BCl3

Figure 7–3: 3D statistical model for V_{dcb} during the induction period.

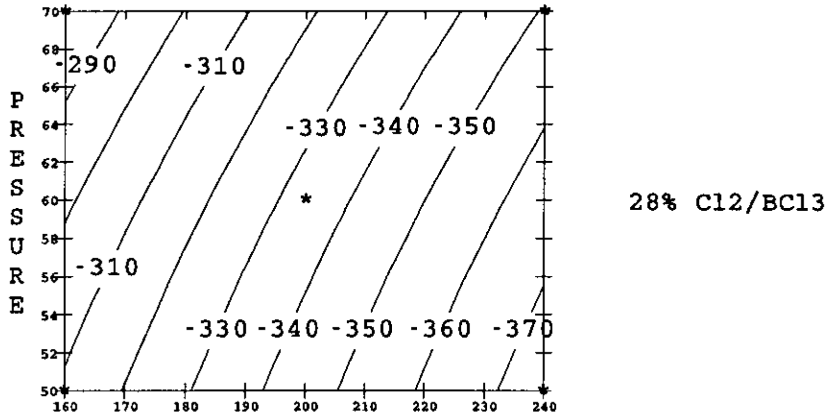

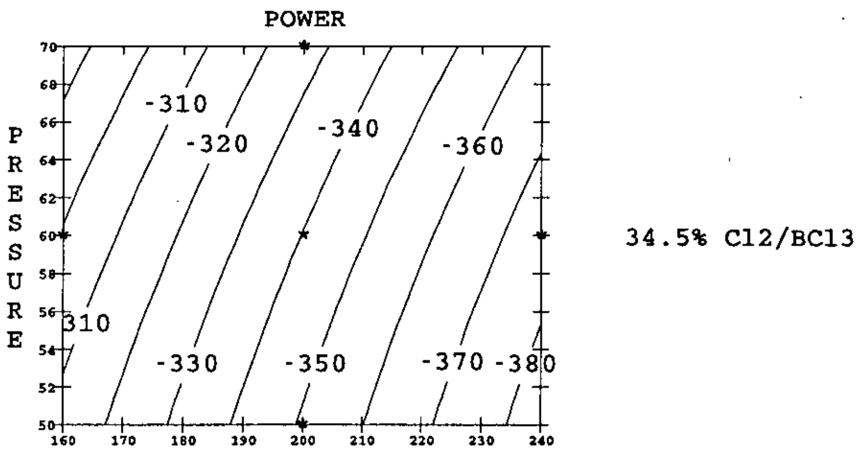

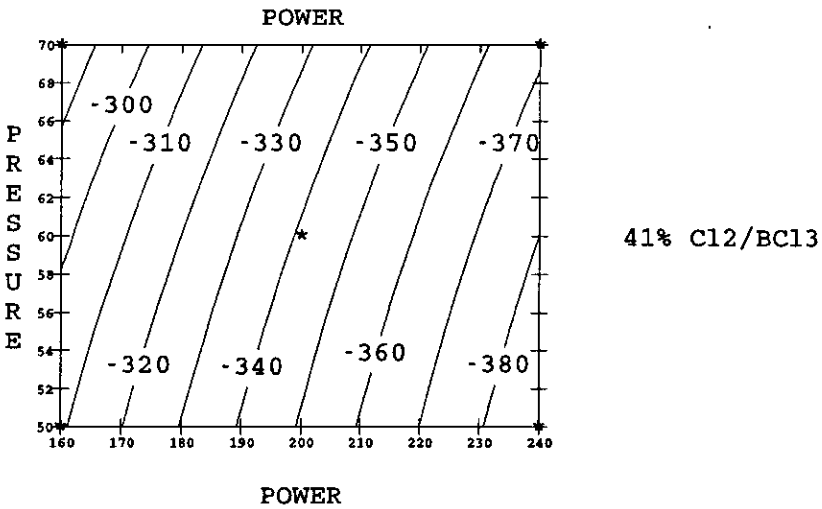

Figure 7–4: Statistical model contourplots for V_{dcb} during the induction period.

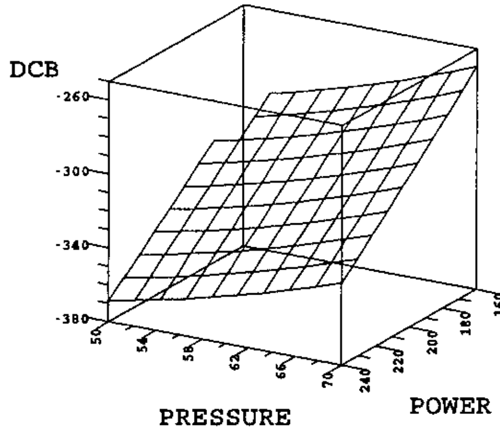

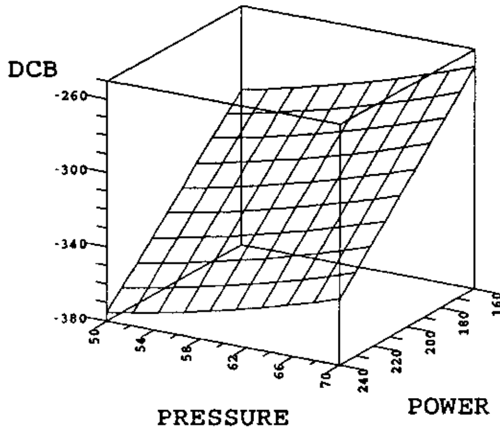

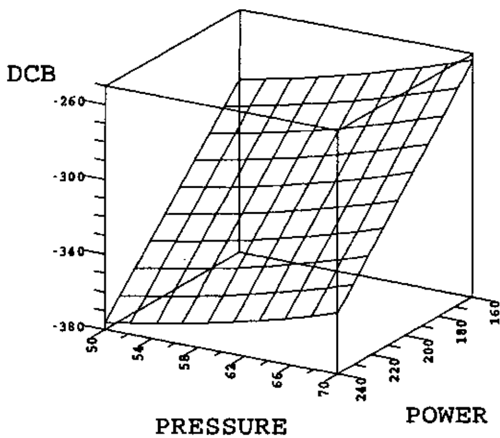

Figure 7–5: 3D statistical model for V_{dcb} during the bulk Al etch.

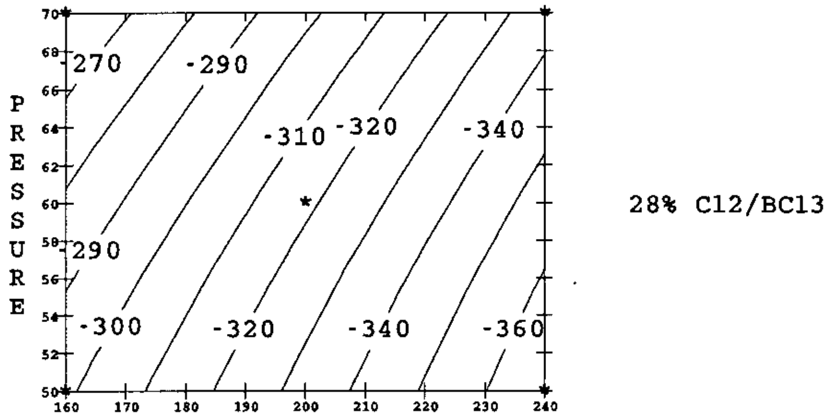

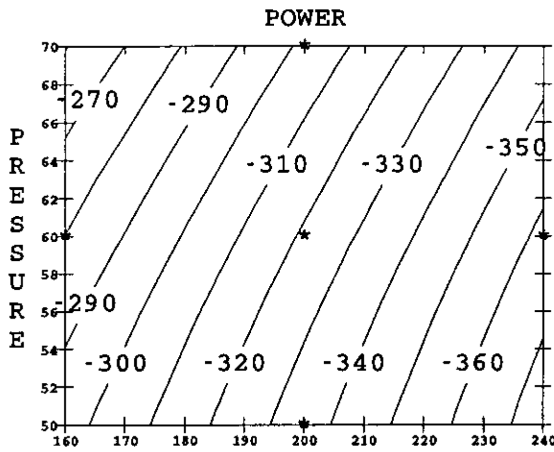

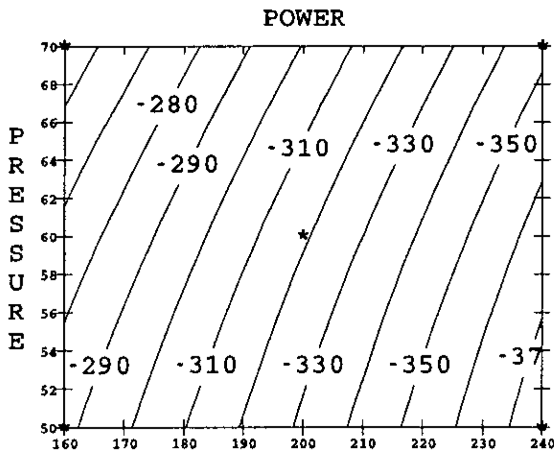

Figure 7–6: Statistical model contourplots for V_{dcb} during the bulk Al etch.

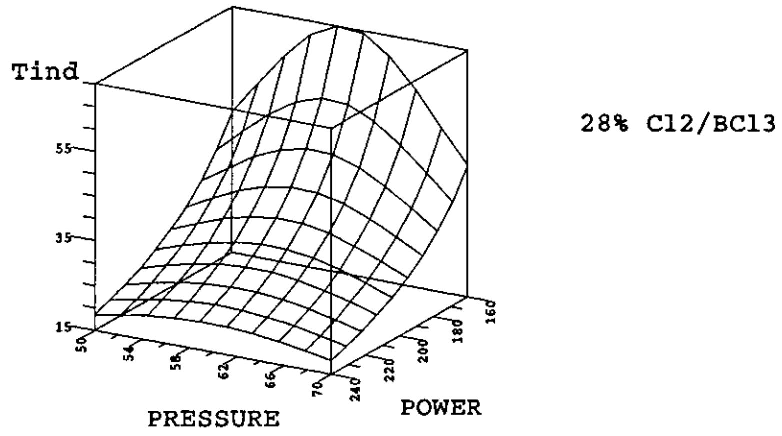

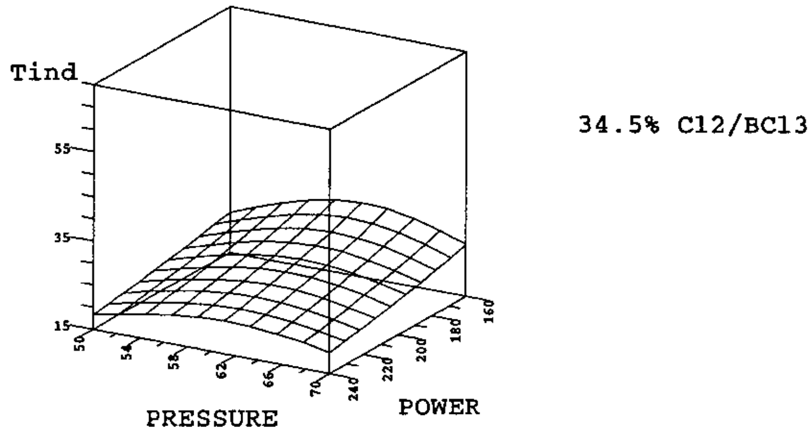

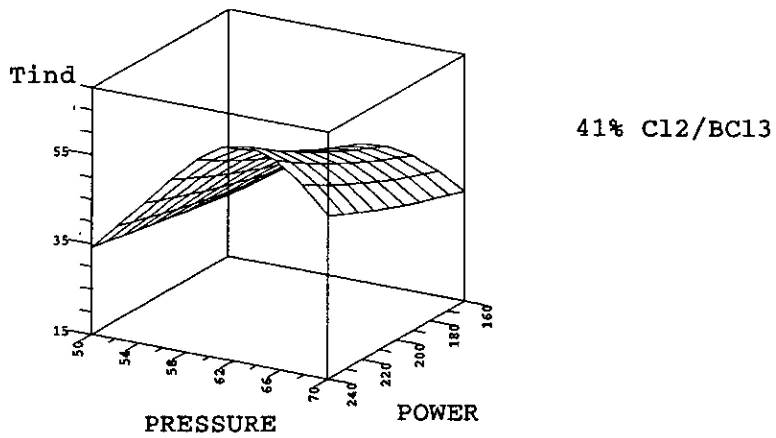

Figure 7–7: 3D statistical model for the induction time.

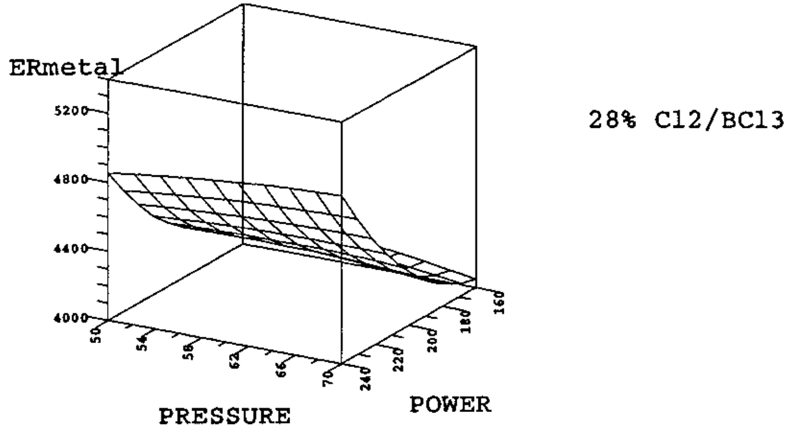

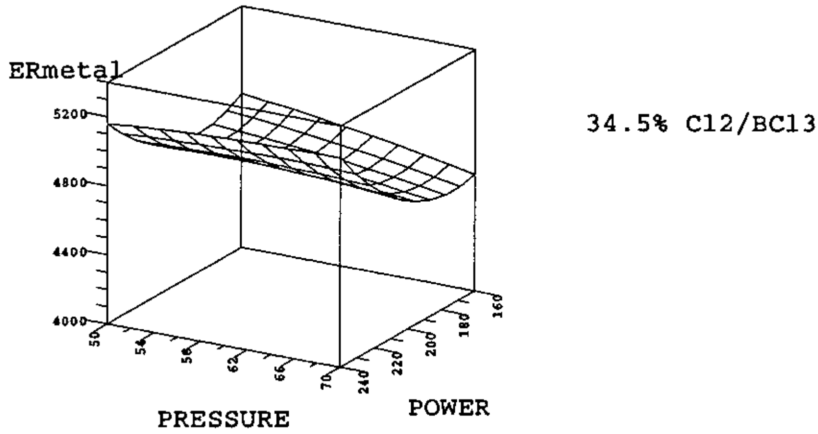

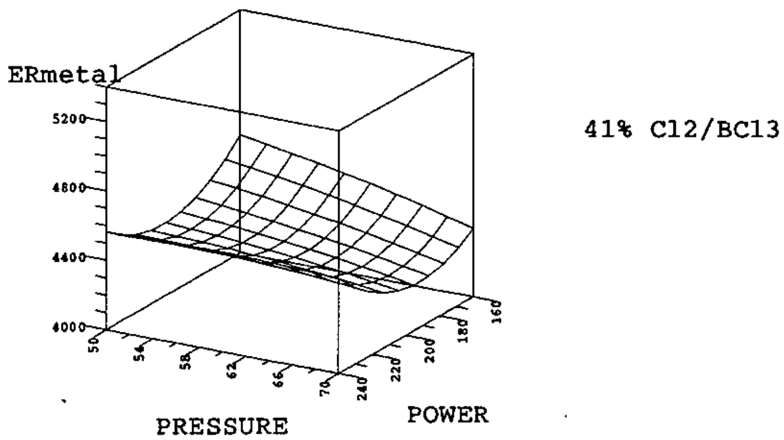

Figure 7–8: 3D statistical model for the overall metal etch rate.

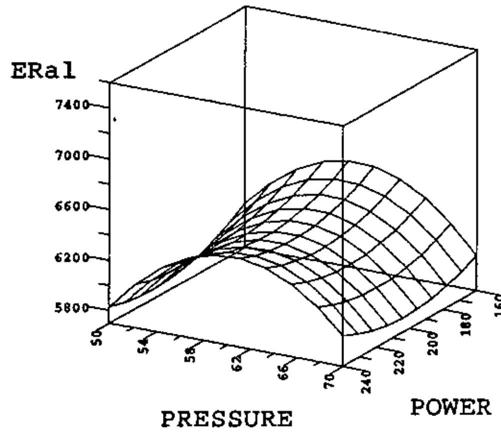

28% Cl2/BCl3

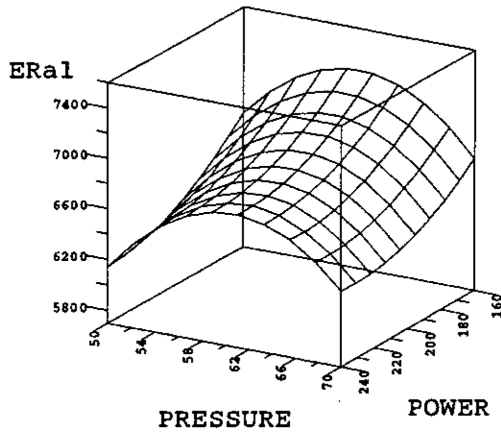

34.5% Cl2/BCl3

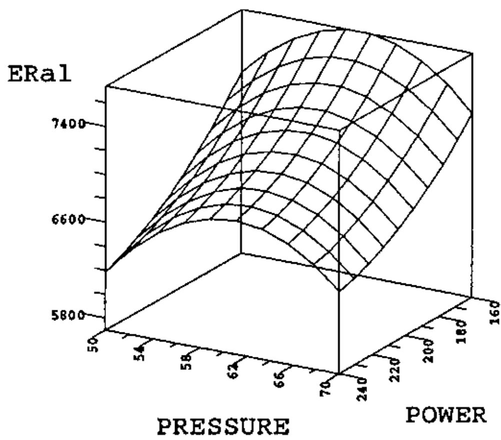

41% Cl2/BCl3

Figure 7–9: 3D statistical model for the bulk Al etch rate.

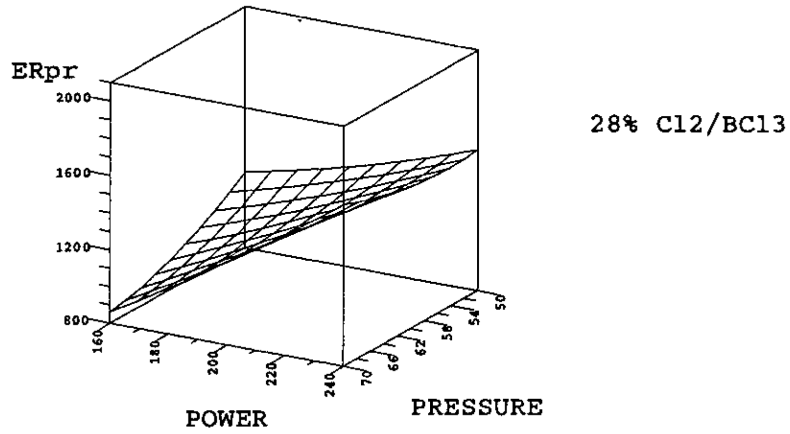

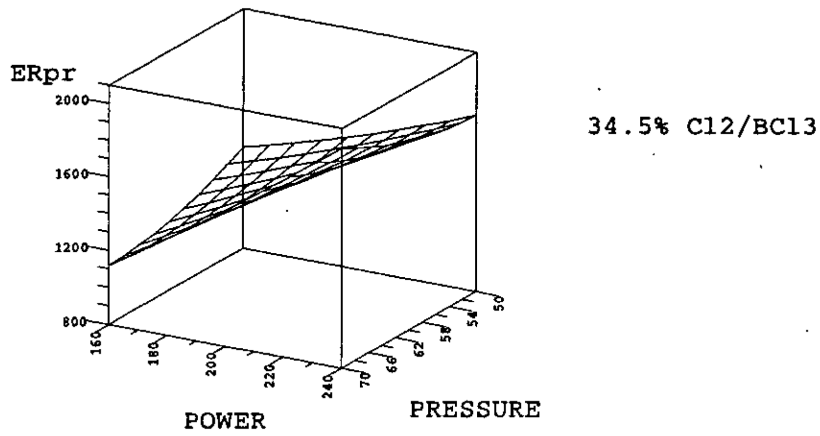

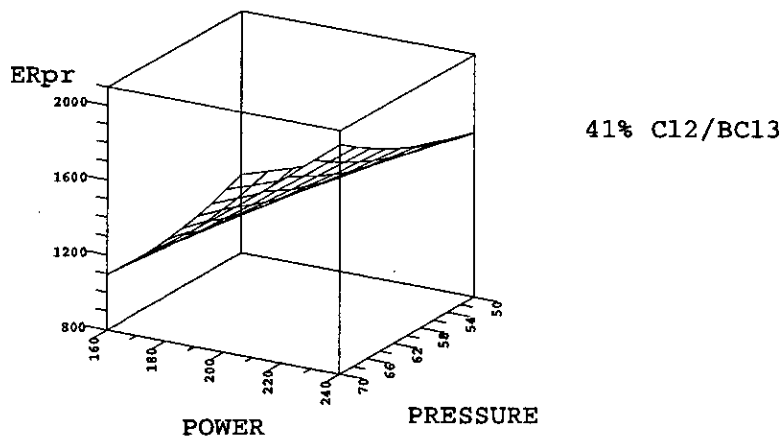

Figure 7–10: 3D statistical model for the photoresist etch rate.

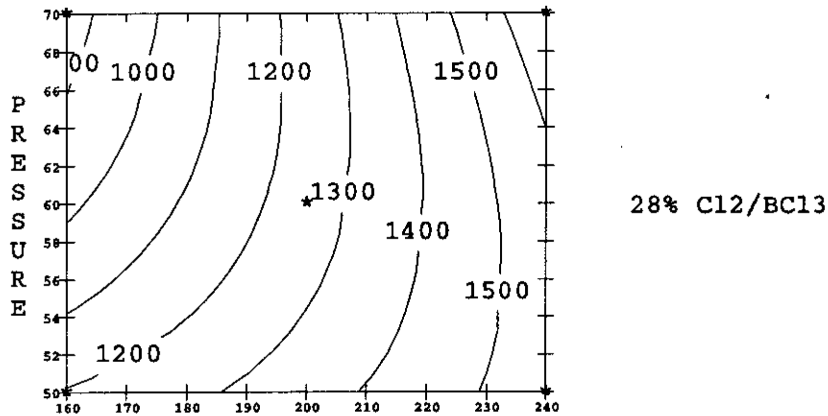

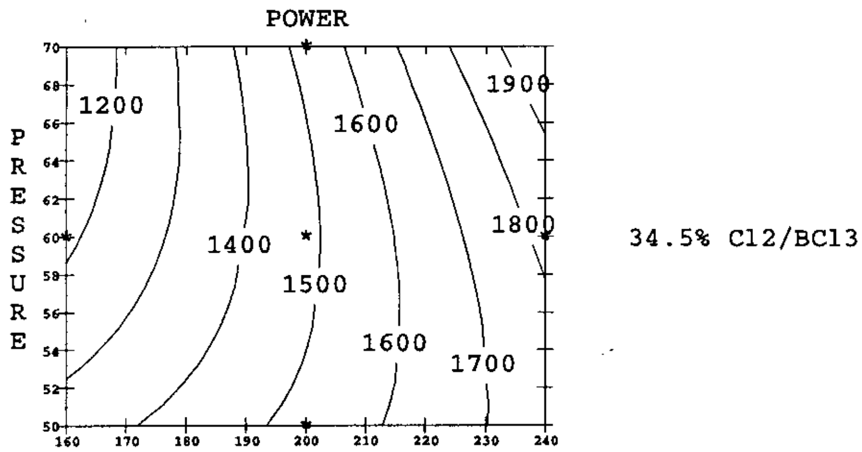

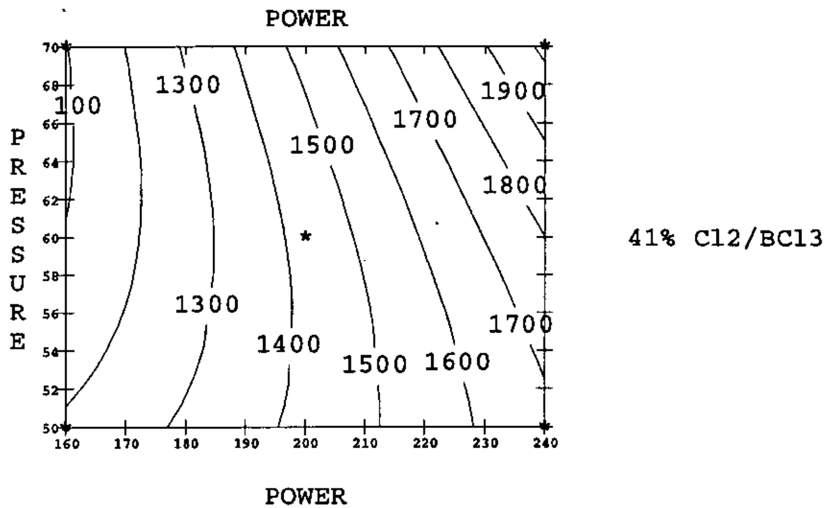

Figure 7–11: Statistical model contourplots for the photoresist etch rate.

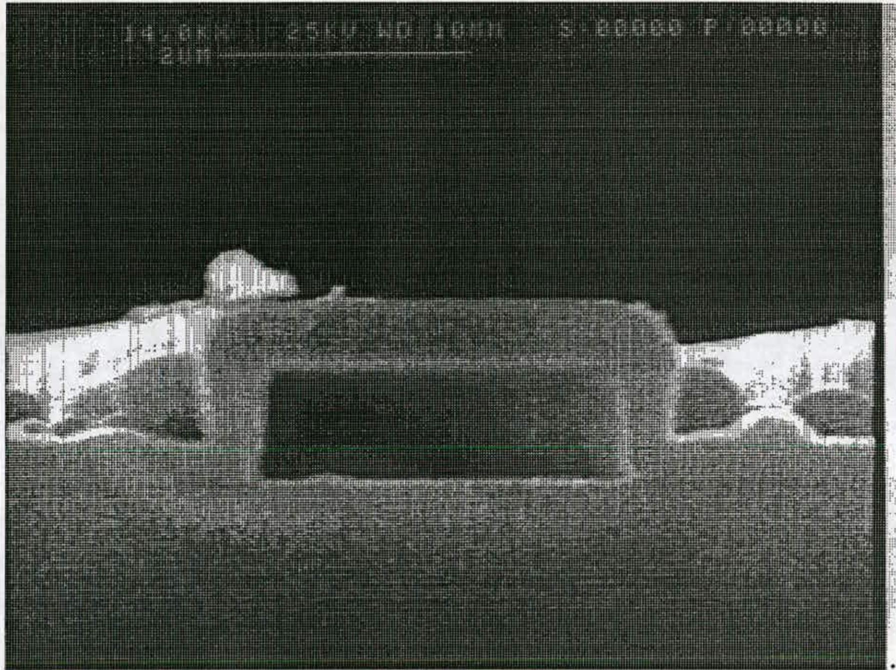

Figure 7–12: SEM etch profile of a highly anisotropic aluminium track.

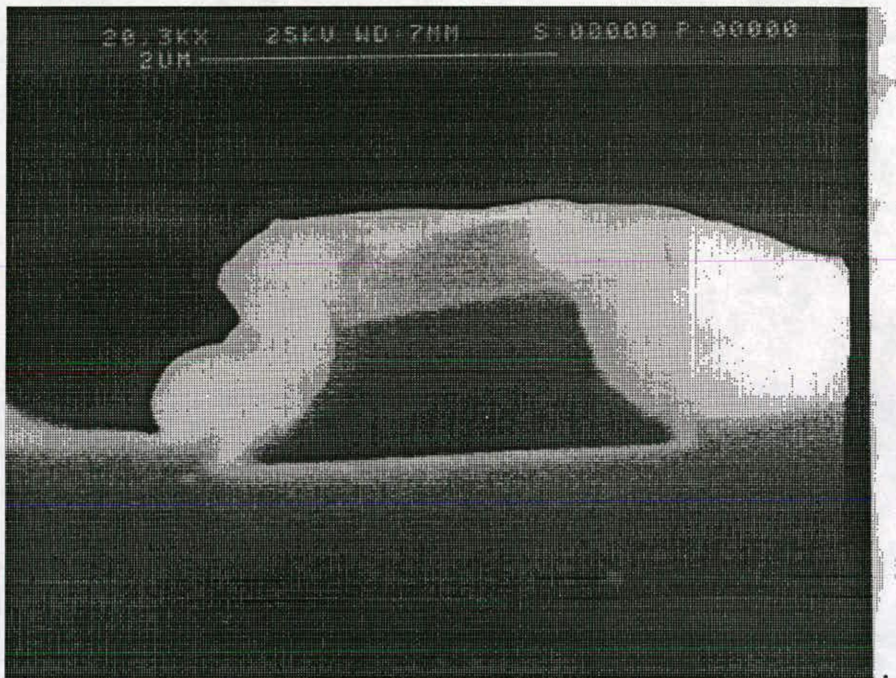

Figure 7–13: SEM etch profile of a less anisotropic aluminium track.

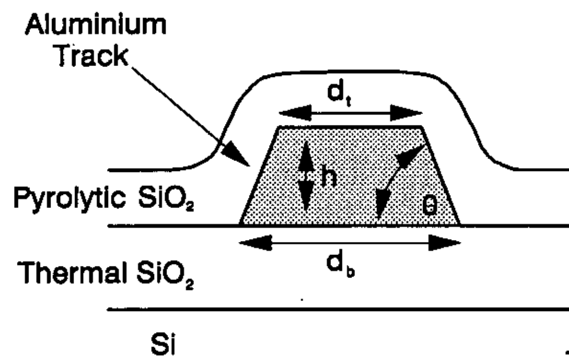

Figure 7–14: Measurements taken on SEM Al track cross-section to estimate the process directionality.

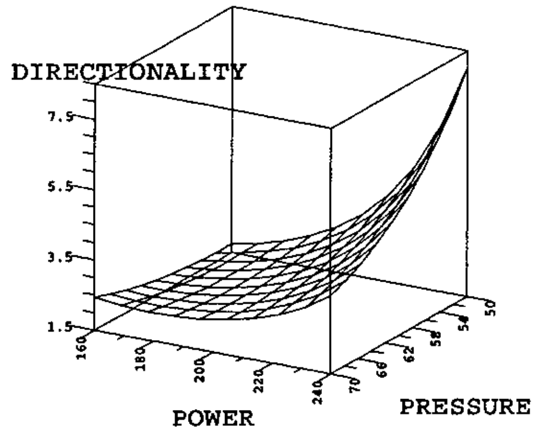

28% Cl2/BCl3

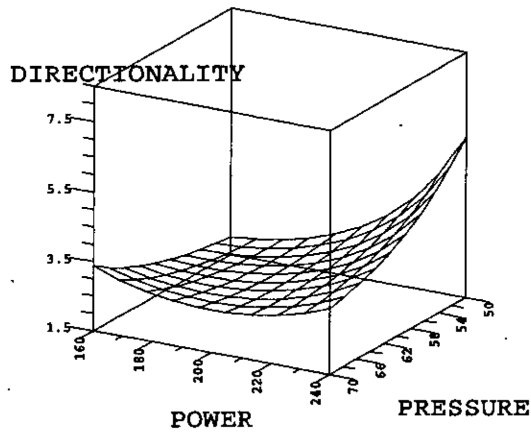

34.5% Cl2/BCl3

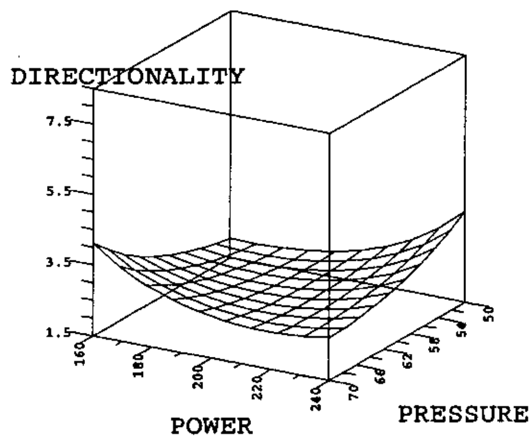

41% Cl2/BCl3

Figure 7–15: 3D statistical model for the etch directionality.

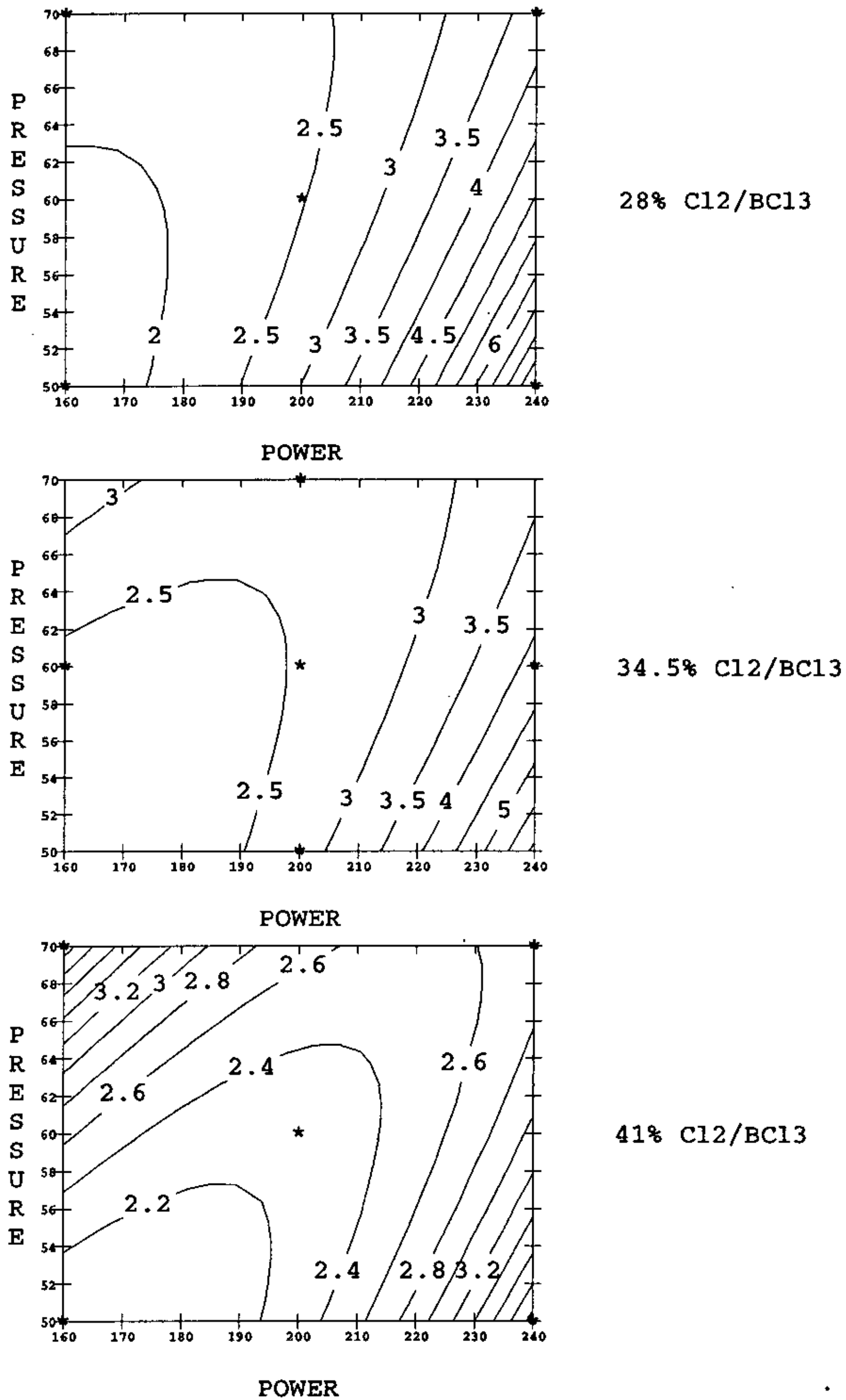

Figure 7–16: Statistical model contourplots for the etch directionality.

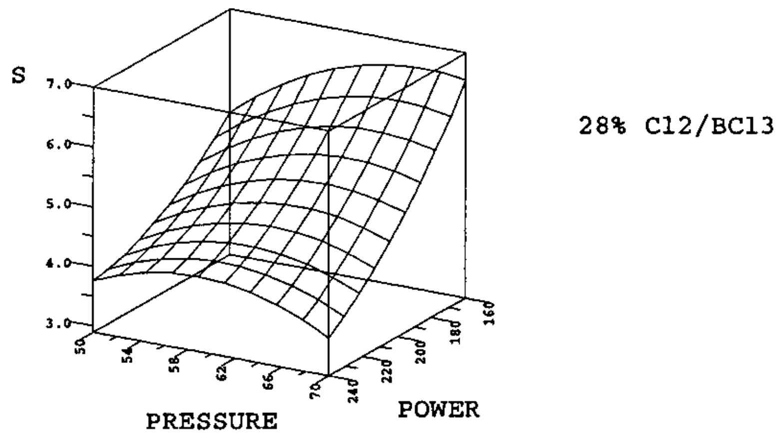

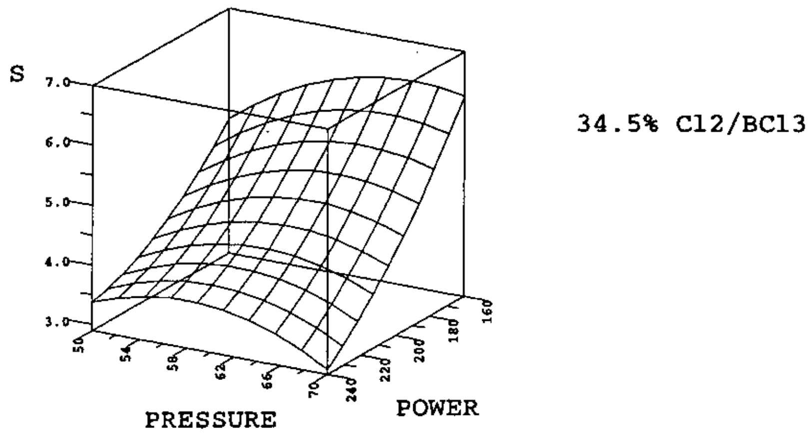

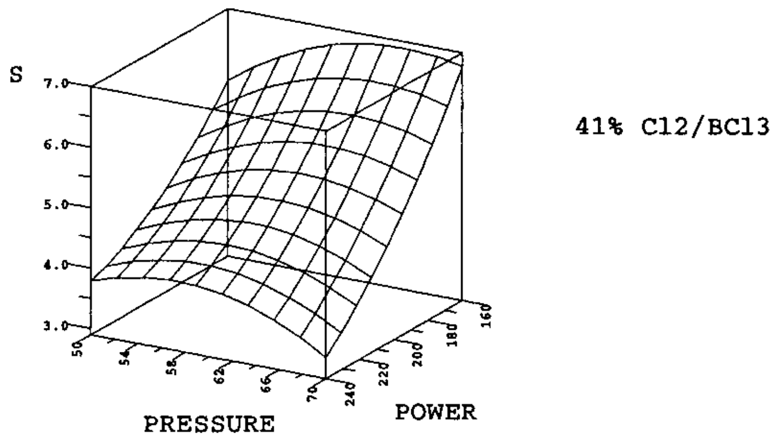

Figure 7–17: 3D statistical model for the etch rate selectivity of bulk Al to photoresist.

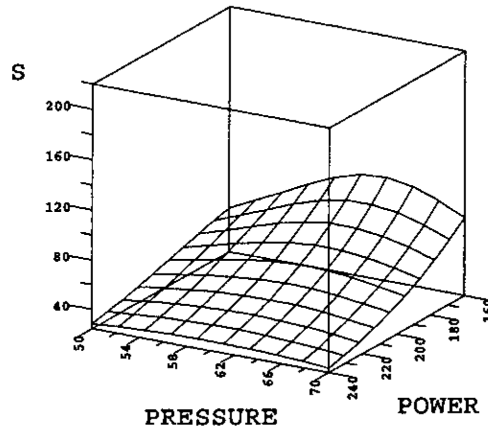

28% Cl2/BCl3

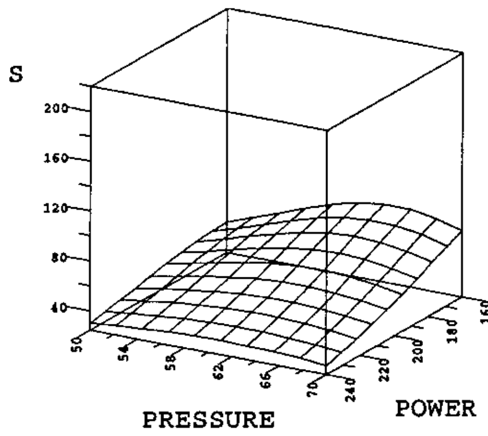

34.5% Cl2/BCl3

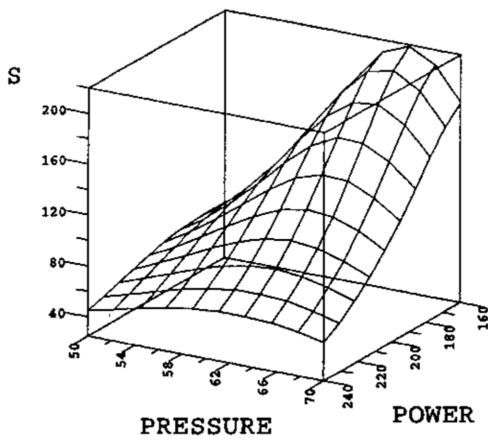

41% Cl2/BCl3

Figure 7–18: 3D statistical model for the etch rate selectivity of bulk Al to SiO_2.

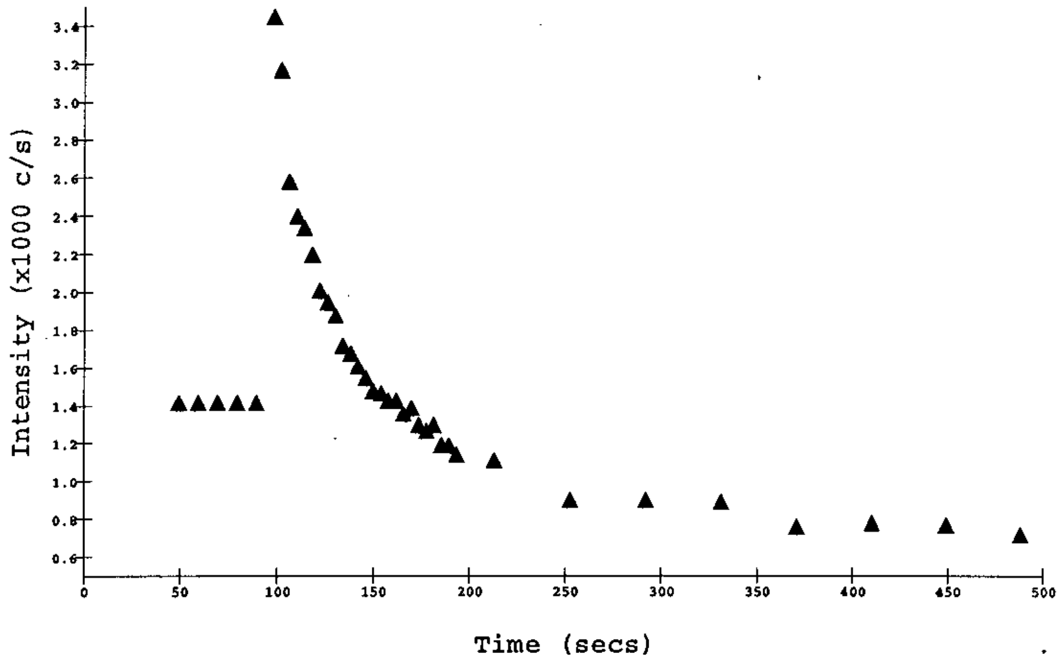

Figure 7–19: RGA monitoring of the H_2O peak at mass 18 during a He plasma.

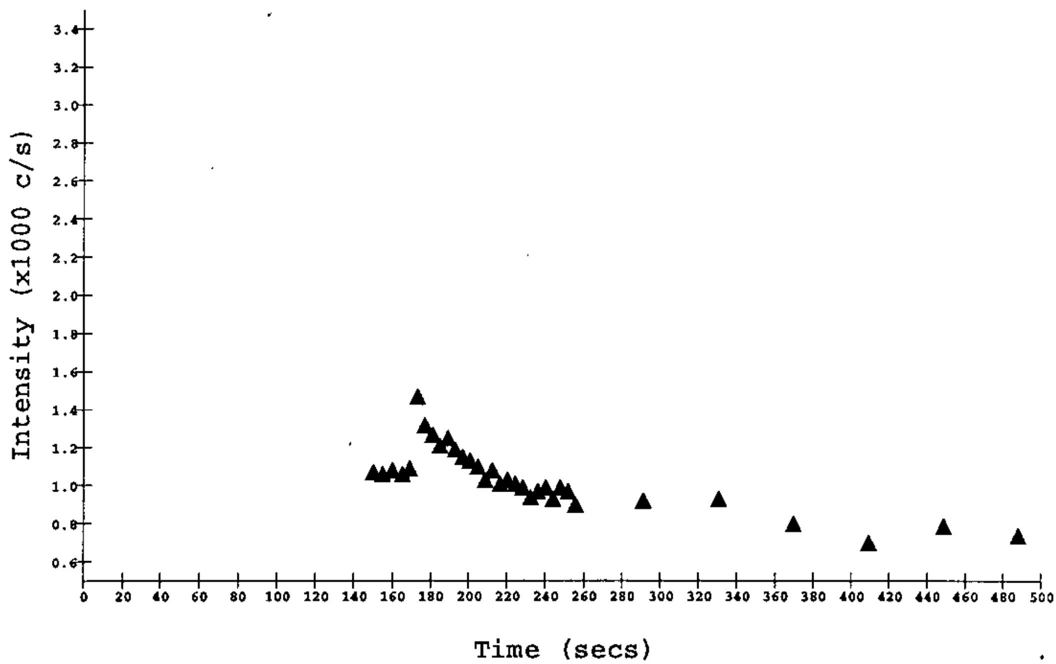

Figure 7–20: RGA monitoring of the H_2O peak at mass 18 during a $BCl_3/Cl_2/He$ plasma.

Chapter 8

Conclusions

There is no doubt that dry etching processes are crucial to the fabrication of VLSI and ULSI circuits and are likely to remain so for the foreseeable future. However, the technique remains difficult to implement and the inherent complications are epitomised by the problems encountered when patterning aluminium and its alloys. This is arguably one of the most difficult steps in the fabrication sequence. Many of these problems have occurred due to the implementation of novel machine configurations and chemistries far in advance of any real understanding of the interactions occurring within the process chamber. The underlying problem with the dry etch process is the large parameter space of inter-related fundamental chemical and physical parameters, most of which are not easily accessible or alterable due to the self insulating nature of the plasma. Historically, process development in this field has proceeded as a result of improvements in vacuum technology and design coupled to one dimensional, empirical trend analyses. Reproducible automatic processing has relied on a stable, 'well-characterised' process for repeatable automatic operation which few dry etch operations possessed.

These traditional approaches to process development have become severely limited with the advent of ULSI. This is evidenced by the gap which has opened up between leading-edge photoresist pattern definition and etched material pattern definition as shown previously in figure 1–4. In order to reduce this gap, traditional process development methodologies must now be supplemented with new techniques which result in a more rigorous characterisation of the parameter

space. Improved characterisation leads to increased process control and opens the way for equipment manufacturers to develop automated feedback and control systems for dry etch machines.

Within the field of dry etching, the patterning of aluminium and its alloys are among those that have presented the greatest challenges to the process engineer. This project aimed to address the problems of characterisation of a leading-edge dry etch process: the $BCl_3/Cl_2/He$ etching of an aluminium alloy. As stated previously, this was approached by investigating two major areas of interest:

- Assessment of diagnostic techniques.
- Improved characterisation through rigorous empirical modelling.

At the outset of the project the ultimate aim was to attempt to link the two approaches together by feeding some diagnostic process outputs into the model. This would result in a comprehensive approach with both process and performance variables being modelled.

To accomplish the above aims involved investigating several different areas of interest. Chapter 2 reviewed the concepts and terminology which are necessary for a basic understanding of reactive plasma etching. Diagnostic methodologies for plasma etch characterisation were outlined in chapter 3. Modelling strategies and techniques for dry etch processing were described in chapter 4.

To achieve these goals, a Vacutec RIE machine, previously used to etch SiO_2, was extensively redesigned and converted into a purpose-built aluminium etcher. Modifications centred around the need to operate a chlorine based chemistry and allow access to the plasma for the selected diagnostic equipment: optical emission spectroscopy, mass spectrometry and Langmuir probes. This range of diagnostic equipment allowed access to a large range of process parameters. Chapter 5 described the assembly and test of the equipment used in this research.

Preliminary investigations carried out on basic glow discharges within the RIE were also described in chapter 5. Monatomic argon plasmas provided an

environment with a minimum of molecular species interaction in which to test the equipment. The mass spectrometer was operated in an innovative in-situ SIMS mode which entailed the detection of positive ions generated solely by the RIE plasma. This allowed ion intensity monitoring which is closely linked to the spread of the hot electron 'tail' of the electron energy distribution function within the glow discharge. Electrostatic Langmuir probe studies were realised using a driven rf feedback circuit in order to minimise the probe-plasma rf component which allowed a more accurate dc characteristic to be obtained. The arrangement involved an original variation on the circuit used by Braithewaite et al [105]. Greater flexibility and ease of implementation to a standard RIE was achieved using this technique. Atomic argon emissions were investigated using OES.

One dimensional RIE machine parameter characterisation using the diagnostic information disclosed that rf power and system pressure had the greatest influences on monitored parameters. Total flow rate effected only a minimal influence on the monitored outputs of the argon glow discharges.

In chapter 6 a $BCl_3/Cl_2/He$ process recipe suitable for dry etching aluminium alloys was developed. The diagnostic techniques were then applied in order to investigate suitable inputs for process modelling. In-situ SIMS provided the most innovative data of the three implemented techniques. Plasma monitoring revealed the major ionic components of the etching plasma as shown in section 6.4.1. Characteristic ion intensity distributions were obtained for the three stages of an Al etch: induction period, bulk Al etch and overetch (SiO_2 etching). By identifying the most sensitive ions ($^{11}B^+$, $^{27}Al^+$ and $^{27}Al^{35}Cl^+$) and monitoring with time, the interface points could be estimated. Although the plasma was only $\approx 0.1\%$ ionised, the inherent sensitivity of the ion distributions allowed real time etch progress monitoring. The value of this technique as an innovative process monitor was evidenced when when attempting to etch oxygen contaminated aluminium alloy. Incorporated material impurities proved to have a dramatic effect on the behaviour and intensity of certain ionic components within the glow discharge which was reflected in the in-situ SIMS results and later confirmed by

depth profiling using full SIMS. Preliminary ion energy profiling results were also described.

OES techniques were also applied to the reactive glow discharge. Although the majority of the molecular information was indistinguishable, the atomic Al emission line at 396.2nm was identified as a suitable process monitor. This could be used as a non-invasive etch process monitor.

This project performed the first attempts at Langmuir probe analysis of $BCl_3/Cl_2/He$ plasmas. Driven electrostatic probes were employed to investigate trends in V_p for one-dimensional changes in the major machine parameters. Data extraction from the IV curve in these reactive chemistries was impeded by problems with transition region perturbation; high extracted currents and contamination problems. Although some of these problems were addressed, the combination of these errors proved that Langmuir probes in their present form could not be used for routine process characterisation in $BCl_3/Cl_2/He$ plasmas with any degree of confidence.

This research also targeted the problems associated with statistical modelling of an aluminium dry etch in chapter 7. As well as modelling the major performance variables of etch rate, directionality and selectivity, the novel method of modelling some of the process characteristics during the etch was undertaken. This established a link between the final performance variables which are measured post-process and off-line and the actual plasma conditions.

A CCF experimental design was constructed from the major machine parameters of rf power, system pressure and $\%Cl_2/BCl_3$. The final quadratic model covered 3 manipulated machine variables, 3 process variables and 6 performance variables. This is the first time that rigorous empirical modelling techniques have been applied to a $BCl_3/Cl_2/He$ based chemistry or an Al dry etch process in order to systematically analyse both the plasma process and post-process etch performance.

Non-invasive process monitoring was employed at this stage, using OES and V_{dcb} analyses. Models were obtained for V_{dcb} during the induction period and

the bulk etch which showed a high quality of statistical fit. The final process variable, which was the induction interface time, gave a poor model fit. This was attributed to inaccuracies in interface identification from the OES trace and also variations due to water desorption in the chamber which were not accounted for in the model.

Performance variable monitoring provided good quality models for directionality and also the important erosion rate of photoresist. However, models for ER_{metal}, ER_{AL}, $S_{Al/pr}$ and S_{Al/SiO_2} did not achieve satisfactory levels. Again this was due to problems in absolute identification of the bulk Al endpoint using the OES system. Although many of these models did not achieve acceptable levels of statistical significance, they did provide a useful insight into the process characteristics. In particular, the major influence of the removal of $\approx$ 30Å native oxide on the overall Al dry etch was apparent.

In retrospect, the single major factor which could have improved the process reproducibility and hence the quality of the empirical models would have been the installation of a load-lock. There was a water vapour variable present in the process which was evidenced by the RGA results in section 7.6. As this variable was not accounted for in the model, it inevitably acted as a source of variation. More accurate interface detection could also have improved the model characteristics. Extending the research project to model the process using invasive techniques such as in-situ SIMS may also have provided an improvement in model quality.

An unquestioned need for dry etch process improvement exists and this project has shown that statistical techniques can provide rigorous process characterisation for even the most difficult of plasma etch operations. With the advent of more complex etching technologies such as ECR; increased device sophistication; and the continuing trend to smaller linewidths, the dual approaches of rigorous empirical modelling and innovative diagnostics will be necessary to achieve adequate process control.

Bibliography

[1] The business of semiconductor technology. SERC school on microfabrication, EMF, University of Edinburgh, June, 1990.

[2] CAM, yield and information management. SERC school on microfabrication, EMF, University of Edinburgh, June, 1990.

[3] G Burns, J Grenier, R McGeary, M Reagan, and P M Wood. Wafer fabrication equipment five-year forecast. *Solid State Technology*, 32(1):35–38, Jan, 1989.

[4] A J Anderson. In *Multiple Processing: A Systems Overview*. Prentice-Hall, London, 1989.

[5] R J Kopp. What's ahead in wafer processing and materials. *Semiconductor International*, 12(1):54–58, Jan, 1989.

[6] J T M Stevenson and A M Gundlach. The application of photolithography to the fabrication of microcircicuits. *J. Phys. E: Sci Instrum.*, 19:654, 1986.

[7] W Kern and G L Schnable. Wet etching. In S J Moss and A Ledwith, editors, *The Chemistry of the Semiconductor Industry*. Blackie & Son Ltd, Glasgow, 1987.

[8] R J Holwill. Private communication.

[9] P K Vasudev. Advanced process integration trends for megagate ULSI. In *Tegal 16th Annual Plasma Seminar Proceedings*, page 1, 1990.

[10] R J Kopp. Navigating to advanced wafer processing. *Semiconductor International*, 15(1):34, Jan, 1992.

[11] *SPC: The Motorola Guide to Statistical Process Control for Continuous Improvement Towards Six Sigma Quality.* Motorola Inc., USA.

[12] B. Chapman. *Glow Discharge Processes.* John Wiley & Sons, New York, 1980.

[13] C J Mogab. Dry etching. In S M Sze, editor, *VLSI Technology*, page 303. McGraw-Hill, 1983.

[14] E. Nasser. *Fundamentals of Gaseous Ionisation and Plasma Electronics.* Wiley Interscience, London, 1971.

[15] J L Vossen. Glow discharge phenomena in plasma etching and plasma deposition. *J. Electrochem. Soc.:Solid State Science and Technology*, 126:319, Feb, 1979.

[16] L M Ephrath. Etching needs for VLSI. *Solid State Technology*, 5:87, July, 1982.

[17] J W Coburn. Plasma-assisted etching. *Plasma Chemistry and Plasma Processing*, 2:1, 1982.

[18] H S Butler and G S Kino. Plasma sheath formation by radio-frequency fields. *The Physics of Fluids*, 6(9):1346, Sept, 1963.

[19] A T Bell. An introduction to plasma processing. *Solid State Technology*, 20(4):89, April, 1978.

[20] H H Sawin. A review of plasma processing fundamentals. *Solid State Technology*, 28(4):211, April, 1985.

[21] A T Bell. Abstract: Fundamentals of plasma chemistry. *J. Vac. Sci. Technol.*, 16(2):118, Mar/Apr, 1979.

[22] J I G Cadogan. *Principles of free radical chemistry.* The Chemical Society, London, 1973.

[23] D L Flamm and J A Mucha. Plasma etching. In S J Moss and A Ledwith, editors, *The Chemistry of the Semiconductor Industry.* Blackie & Son Ltd, Glasgow, 1987.

[24] J W Coburn. Plasma-assisted etching in VLSI: Equipment-related considerations. In A P Mammana, editor, *Fourth Brazilian Workshop on Microelectronics*, page 41. Companhia de Promocao de Pesquisa Cientifica e Tecnologica do Estado de Sao Paulo, Sao Paulo, 21st Feb to 4th March, 1983.

[25] D L Flamm, V M Donnelly, and D E Ibbotson. Basic principles of plasma etching for silicon devices. In *VLSI Electronics: Microstructure Science*, volume 8, page 189. Academic Press, 1984.

[26] S M Irving. A plasma oxidation process for removing photoresist films. *Solid State Technology*, 14(6):47, June, 1971.

[27] A R Reinberg. Plasma processing with a planar reactor. In *Circuits Manufacturing*, page 25, April, 1979.

[28] V G I Deshmukh and T I Cox. Physical characterisation of dry etching plasmas used in semiconductor fabrication. *Plasma Physics and Controlled Fusion*, 30(1):21, 1988.

[29] S J Fonash. Advances in dry etching processes: A review. *Solid State Technology*, 28(1):150, Jan, 1985.

[30] H Okano, T Yamazaki, and Y Horiike. High rate reactive ion etching using a magnetron discharge. *Solid State Technology*, 25:166, April, 1982.

[31] R A H Heinecke. Plasma etching of films at high rates. *Solid State Technology*, 21, April, 1978.

[32] P B Johnson and P A McNally. RIE of multilayer metal interconnects for VLSI. *Semiconductor International*, 10:256, May, 1987.

[33] R N Carlile, V C Liang, and M M Smadi. High quality trench etches in silicon. *Solid State Technology*, 32:119, April, 1989.

[34] R W Light. Reactive ion etching of aluminium/silicon. *J. Electrochem. Soc.: Solid State Science and Technology*, 130:2225, November 1983.

[35] J M Eldridge, G Olive, B J Luther, and J O Moore. Effects of oxygen on the RIE characteristics of aluminium films. *J. Electrochem. Soc.: Solid State Science and Technology*, 134:1025, April, 1987.

[36] R A H Heinecke. Control of relative etch rates of SiO_2 and Si in plasma etching. *Solid-State Electronics*, 18:1146–1147, 1975.

[37] V M Donnelly, D L Flamm, W C Dautremont-Smith, and D J Werder. Anisotropic etching of SiO_2 in low-frequency CF_4/O_2 and NF_3/Ar plasmas. *J. Appl. Phys.*, 55:242, Jan, 1984.

[38] L Giffen, J Wu, R Lachenbruch, and G Fior. Silicon dioxide profile control for contacts and vias. *Solid State Technology*, 32:55, April, 1989.

[39] R N Castellano. Profile control in plasma etching of SiO_2. *Solid State Technology*, 27:203, May, 1984.

[40] A G Nagy. Sidewall tapering in reactive ion etching. *J. Electrochem. Soc.: Solid State Science and Technology*, 132:689, March, 1985.

[41] J S Chang. Selective reactive ion etching of silicon dioxide. *Solid State Technology*, 27:214, April, 1984.

[42] J A Bondur. CF_4 Etching in a Diode System. *J. Electrochem. Soc.: Electrochemical Science and Technology*, 126:226, Feb, 1979.

[43] G C Schwartz, L B Rothman, and T J Schopen. Competitive Mechanisms in Reactive Ion Etching in a CF_4 Plasma. *J. Electrochem. Soc.: Solid State Science and Technology*, 126:464, March, 1979.

[44] P H Singer. Today's plasma etch chemistries. *Semiconductor International*, 11:68, March, 1988.

[45] D Bollinger, S Iida, and O Matsumoto. Reactive Ion Etching: Its Basis and Future (part 2). *Solid State Technology*, 27:167, June, 1984.

[46] D L Flamm. Mechanisms of radical production in CF_3Cl, CF_3Br, and related plasma etching gases: The role of added oxidants. *Plasma Chemistry and Plasma Processing*, 1(1):37, 1981.

[47] J W Coburn and E Kay. Some chemical aspects of the fluorocarbon plasma etching of silicon and its compounds. *IBM Journal of Research and Development*, 23:33, Jan, 1979.

[48] C J Mogab, A C Adams, and D L Flamm. Plasma etching of Si and SiO_2: The effect of oxygen additions to CF_4 plasmas. *J. Appl. Phys.*, 49:3796, July, 1978.

[49] D W Hess. Plasma etching of aluminium. *Solid State Technology*, 24:189, April, 1981.

[50] S P Murarka. Metallization. In S M Sze, editor, *VLSI Technology (2nd Edition)*, page 375. McGraw-Hill, London, 1988.

[51] C M Horwitz. New dry etch for Al and Al-Cu-Si alloy: Reactively masked sputter etching with SiF_4. *Appl. Phys. Lett.*, 42(10):898, 15 May 1983.

[52] P M Schaible, W C Metzger, and J P Anderson. Reactive ion etching of aluminium and aluminium alloys in an RF plasma containing halogen species. *J. Vac. Sci. Technol.*, 15(2):334, March/April 1978.

[53] R H Bruce. Anisotropy control in dry etching. *Solid State Technology*, 24:64, Oct, 1981.

[54] H F Winters. Etch products from the reaction on Cl_2 with Al(100) and Cu(100) and XeF_2 with W(111) and Nb. *J. Vac. Sc. Technol. B*, 3(1):9, Jan/Feb 1985.

[55] W-Y Lee and J M Eldridge. Reactive ion etching induced corrosion of Al and Al-Cu films. *J. Appl. Phys.*, 52(4):2994, April, 1981.

[56] J E Spencer. Management of $AlCl_3$ in plasma etching aluminium and its alloys. *Solid State Technology*, 27:203, April, 1984.

[57] D L Flamm, V M Donnelly, and D E Ibbotson. Basic chemistry and mechanisms of plasma etching. *Semiconductor International*, 6(3):136, April, 1983.

[58] W B Pennebaker. Influence of scattering and ionisation on RF impedance in glow discharge sheaths. *IBM Journal of Research and Development*, 23:16, Jan, 1979.

[59] E A Truesdale, G Smolinsky, and T M Mayer. The effect of added acetylene on the RF discharge chemistry of C_2F_6: A mechanistic model for fluorocarbon plasmas. *J. Appl. Phys.*, 51:2909, May, 1980.

[60] B N Chapman and V J Minkiewicz. Flow rate effects in plasma etching. *J. Vac. Sci. Technol.*, 15:329, March/April, 1978.

[61] W C Dautremont-Smith, R A Gottscho, and Schutz. Plasma processing mechanisms and applications. In G E McGuire, editor, *Semiconductor Materials and Process Technology Handbook*. Noyes Publications, Park Ridge, New Jersey, USA, 1988.

[62] R H Bruce. Frequency dependence of CCl_4 etching. In R G Frieser and C J Mogab, editors, *Plasma Processing: Symposium on Plasma Etching*

and Deposition, May 1980,, volume 81, page 243. Electrochemical Society, 1981.

[63] B Gorowitz and R J Saia. Reactive ion etching. In *VLSI Electronics: Microstructure Science*, volume 8, page 297. Academic Press, 1984.

[64] J W Coburn and E Kay. Positive-ion bombardment of substrates in RF diode glow discharge sputtering. *J. Appl. Phys.*, 43:4965, Dec, 1972.

[65] H R Koenig and L I Maissel. Application of RF discharges to sputtering. In *IBM Journal of Research and Development*, page 168, March, 1970.

[66] R J Schultz. Reactive plasma etching. In S. M. Sze, editor, *VLSI Technology*, page 184. McGraw-Hill, 1988.

[67] C J Mogab. The loading effect in plasma etching. *J. Electrochem. Soc.: Solid-State Science and Technology*, 124:1262, Aug, 1977.

[68] S J Fonash. An overview of dry etching damage and contamination effects. *J. Electrochem. Soc.*, 137:3885, Dec, 1990.

[69] L M Ephrath and D J DiMaria. Review of RIE induced radiation damage in silicon dioxide. *Solid State Technology*, 24:182, April, 1981.

[70] S W Pang. Dry etching induced damage in Si and GaAs. *Solid State Technology*, 27:249, April, 1984.

[71] R A Gdula. The effects of processing on radiation damage in SiO_2. *IEEE Transactions on Electron Devices*, ED-26:644, April, 1979.

[72] T Watanabe and Y Yoshida. Dielectric breakdown of gate insulator due to reactive ion etching. *Solid State Technology*, 27:263, April, 1984.

[73] D L Flamm. Trends in plasma sources and etching. *Solid State Technology*, 34(3):47, March, 1991.

[74] K Suzuki, S Okudaira, and I Kanomata. The role of ions and neutral active species in microwave plasma etching. *J. Electrochem. Soc.: Solid-State Science and Technology*, 126:1024, June, 1979.

[75] I H Hutchinson. *Principles of Plasma Diagnostics.* Cambridge University Press, 1987.

[76] E Metcalfe. *Atomic Absorption and Emission Spectroscopy.* John Wiley & Sons, 1987.

[77] R W B Pearse and A G Gaydon. *The Identification of Molecular Spectra.* Chapman and Hall, London, 1965.

[78] P J Marcoux and P D Foo. Methods of end point detection for plasma etching. *Solid State Technology*, 24(4):115, April, 1981.

[79] J G Shabushnig, P R Demko, and R N Savage. Applications of optical emission spectroscopy to semiconductor processing. *Mat. Res. Soc. Symp. Proc.*, 38:77, 1985.

[80] B J Curtis. Optical end-point detection for the plasma etching of aluminium. *Solid State Technology*, 23:129, April, 1980.

[81] W R Harshbarger, R A Porter, T A Miller, and P Norton. A study of the optical emission from a RF plasma during semiconductor etching. *J. Applied Spectroscopy*, 31(3):201, 1977.

[82] O Krogh, H Slomowitz, Y Melaku, and H Blom. Summary abstract: Spectroscopic diagnostics of photoresist erosion in an aluminium etch plasma. *J. Vac. Sci. Technol. A*, 5(4):1929, Jul/Aug, 1987.

[83] J Felts and E Lopata. Measurements of electron temperature in a capacitively coupled plasma using emission spectroscopy. *J. Vac. Sci. Technol. A*, 6(3):2051, May/June 1988.

[84] J E Greene. Abstract: Optical spectroscopy for glow discharge sputtering diagnostics and process control. *J. Vac. Sci. Technol.*, 15(2):203, 1978.

[85] J W Coburn and M Chen. Optical emission spectroscopy of reactive plasmas: A method for correlating emission intensities to reactive particle density. *J Appl. Phys.*, 51(6):3134, June, 1980.

[86] R W Dreyfus, J M Jasinski, R E Walkup, and G S Selwyn. Optical diagnostics of low pressure plasmas. *Pure & Appl. Chem.*, 57(9):1265, 1985.

[87] R A Gottscho and V M Donnelly. Optical emission actinometry and spectral line shapes in RF glow discharges. *J. Appl. Phys.*, 56(2):245, July, 1984.

[88] A P Day, D Field, D F Klemperer, and Y P Song. Re-examine mass spectrometry for endpoint detection. *Semiconductor International*, 12(12):110, Nov, 1989.

[89] H L Brown, G B Bunyard, and K C Lin. Applications of mass spectrometers to plasma process monitoring and control. *Solid State Technology*, 21:35, July, 1978.

[90] A P Webb and J A Smith. Applications of in-situ SIMS during processing of electronic materials. *Surface and Interface Analysis*, 12:303, 1988.

[91] J W Coburn. Mass spectrometric studies of positive ions in RF glow discharges. *Thin Solid Films*, 171:65–80, 1989.

[92] J F O'Hanlon. *A User's Guide to Vacuum Technology.* Wiley Interscience, New York, 1989.

[93] B A Raby. Mass spectrometric study of plasma etching. *J. Vac. Sci. Technol.*, 15(2):205, March/April, 1978.

[94] H W Lehmann, E Heeb, and K Frick. Plasma diagnosis by time resolved mass spectrometry. *Solid State Technology*, 24:69, Oct, 1981.

[95] F F Chen. Electric probes. In R H Huddlestone and S L Leonard, editors, *Plasma Diagnostic Techniques.* Academic Press, New York, 1965.

[96] J D Swift and M J R Schwar. *Electrical probes for plasma diagnostics.* Iliffe Books Ltd, London, 1970.

[97] J G Laframboise. Theory of spherical and cylindrical Langmuir probes in a collisionless, Maxwellian plasma at rest. In *University of Toronto, Institute for Aerospace Studies, report no. 100*, June, 1966.

[98] B E Cherrington. The use of electrostatic probes for plasma diagnostics: A review. *Plasma Chemistry and Plasma Processing*, 2(2):113, 1982.

[99] R M Clements. Plasma diagnostics with electric probes. *J. Vac. Sci. Technol.*, 15:193, Mar/Apr, 1978.

[100] N St J Braithwaite, N M P Benjamin, and J E Allen. The plasma parameters of an RF argon discharge. In *I. Symp. Plasma Chem.*, Eindhoven, 1985.

[101] M J Kushner. A kinetic study of the plasma etching process: Probe measurements of electron properties in an RF plasma etching reactor. *J. Appl. Phys.*, 53(4):2939, April, 1982.

[102] N. St. J. Braithwaite. Plasma parameters and the use of Langmuir probes. In *IEE Summer School*, 1986.

[103] R R J Gagne and A Cantin. Investigation of an RF plasma with symmetrical and assymetrical electrostatic probes. *J. Appl. Phys.*, 43(6):2639, June, 1972.

[104] E Eser, R E Ogilvie, and K A Taylor. Plasma characterisation in sputtering processes using the Langmuir probe technique. *Thin Solid Films*, 68:381, 1980.

[105] N St J Braithwaite, N M P Benjamin, and J E Allen. An electrostatic probe technique for RF plasma. *J. Phys. E:Sci Instrum.*, 20:1046, 1987.

[106] M W Allen, B M Annaratone, and J E Allen. The positive ion characteristics of Langmuir probes in an RF argon plasma. In *9th Conference on Gas Discharges and their Applications*, Venice, Sept 19th-23rd, 1988.

[107] T I Cox, V G I Deshmukh, D A O Hope, A J Hydes, N St J Braithewaite, and N M P Benjamin. The use of Langmuir probes and optical emission spectroscopy to measure electron energy distribution functions in RF-generated argon plasmas. *J. Phys. D: Appl. Phys.*, 20:820, 1987.

[108] Ch Steinbruchel. Langmuir probe measurements on CHF_3 and CF_4 plasmas: The role of ions in the reactive sputter etching of SiO_2 and Si. *Journal Electrochem. Soc.:Solid State Science and Technology*, 130(3):648, March, 1983.

[109] D Maundrill, J Slatter, A I Spiers, and C C Welch. Electrical measurements of RF-generated plasmas using a driven electrostatic probe technique. *J. Phys. D: Appl. Phys.*, 20:815, 1987.

[110] D I C Pearson, G A Campbell, C W Domier, and P C Efthimion. A microwave interferometer for density measurement and stabilisation in process plasmas. In *Mat. Res. Soc. Symp. Proc.*, volume 117, page 311. Materials Research Society, 1988.

[111] H H Busta, R E Lajos, and D A Kiewit. Plasma etch monitoring with laser interferometry. *Solid State Technology*, 22:61, Feb, 1979.

[112] P Banks, W Pilz, I Hussla, G Lorenz, and G Castrischer. *In-situ diagnostics for plasma processing.* SPIE meeting: Monitoring and control of plasma-enhanced processing of semiconductors, Santa Clara, USA, 1-2 Nov, 1988.

[113] K Ukai and K Hanazawa. End-point determination of aluminium reactive ion etching by dischage impedance monitoring. *J. Vac. Sci. Technol.*, 16(2):385, Mar/Apr, 1979.

[114] R A Gottscho and T A Miller. Optical techniques in plasma diagnostics. *Pure & Appl. Chem.*, 56(2):189–208, 1984.

[115] W J Harshbarger. Plasma diagnostics and end-point detection. In *VLSI Electronics: Microstructure Science*, volume 8, page 411. Academic Press, 1984.

[116] J Speight. Overview. In S J Moss and A Ledwith, editors, *The Chemistry of the Semiconductor Industry.* Blackie & Son Ltd, Glasgow, 1987.

[117] G E P Box, W G Hunter, and J S Hunter. *Statistics for experimenters: an introduction to design, data analysis, and model building.* Wiley & Sons, New York, 1978.

[118] G E P Box and N R Draper. *Empirical Model-Building and Response Surfaces.* John Wiley & Sons, New York, 1987.

[119] G Z Yin and D W Jillie. Orthogonal design for process optimisation and its application in plasma etching. *Solid State Technology*, 29(5):127, May, 1987.

[120] *RS/Discover Statistical Appendices.* BBN Software Products Corporation.

[121] V Hegemann and J Fitch. Statistical strategies for optimising processes: Part II. In *TI Technical Journal*, page 69, Mar/Apr 1987.

[122] K-K Lin and C J Spanos. Statistical equipment modelling for VLSI manufacturing: an application for LPCVD. *IEEE Trans. Semiconductor Manufacturing*, 3(4):216, Nov, 1990.

[123] J R Hannah, R J Holwill, P N Kember, and R Grimwood. Characterisation of a production single step planarisation technique using ECR deposition. In *180th Electrochemical Society Proceedings*, Phoenix, USA, Oct 13-17, 1991.

[124] S F Bergeron and B F Duncan. Controlled anisotropic etching of polysilicon. *Solid State Technology*, 25:98, Aug, 1982.

[125] M T Mocella, M W Jenkins, H H Sawin, and K D Allen. Parametric characterisation of plasma etching. *Mat. Res. Soc. Symp. Proc.*, 38:227, 1985.

[126] X Feng and G Ruan. The modelling and simulation of reactive ion etching rate using statistical method. In *ESSDERC*, Berlin, 1989. Springer-Verlag.

[127] P E Riley, M Chang, S G Ghanayem, and A Mak. Development of a magnetron-enhanced plasma process for tungsten etchback with response surface methodology. *IEEE Trans. on Semiconductor Manufacturing*, 3(3):142, Aug, 1990.

[128] D J Thomas and S J Clements. A parametric investigation of the reactive ion etching of InP in CH_4/H_2 plasmas using response surface methodology. In *ESSDERC*, page 121, Nottingham, Sept, 1990. IOP Publishing.

[129] K J McLaughlin, S W Butler, T F Edgar, and I Trachtenberg. Development of techniques for real-time monitoring and control in plasma etching. *J. Electrochem Soc.*, 138(3):789, March, 1991.

[130] M Meyyappan and J P Kreskovsky. Glow discharge simulation through solutions to the moments of the Boltzmann transport equation. *J. Appl. Phys.*, 68(4):1506, August, 1990.

[131] M Dalvie, K F Jensen, and D B Graves. Modelling of reactors for plasma processing 1: Silicon etching by CF_4 in a radial flow reactor. *Chemical Engineering Science*, 41(4):653–660, 1986.

[132] D E Edelson and D L Flamm. Computer simulation of a CF_4 plasma etching silicon. *J. Appl. Phys.*, 56:1522, Sept, 1984.

[133] S-K Park and D J Economou. A mathematical model for etching of silicon using CF_4 in a radial flow plasma reactor. *J. Electrochem. Soc.*, 138:1499, May, 1991.

[134] A Cantin and R R J Gagne. Pressure dependence of electron temperature using RF-floated electrostatic probes in RF plasmas. *Applied Physics Letters*, 30(7):316, April, 1977.

[135] P A Chatterton, J A Rees, W L Wu, and K Al-Assadi. A self-compensating Langmuir probe for use in RF (13.56MHz) plasma systems. *Vacuum*, 42(7):489, 1991.

[136] Robert C Weast, editor. *Handbook of Chemistry and Physics: 56th Edition.* CRC Press Inc., Cleveland, Ohio, USA, 1975.

[137] J L Franklin. *Ionisation potentials, appearance potentials and heats of formation of gaseous positive ions.* National standard reference data series. US National Bureau of Standards, Washington, 1969.

[138] A Von Engel. *Ionised Gases.* Oxford Clarenden Press, 2nd edition, 1965.

[139] J R Hannah, J J de Lima, and R J Holwill. Real time process monitoring for RIE using in-situ SIMS.

[140] D W Daniel, R Bloom, and J E Reece. Identifying an etch process window using response surface methodology. *Solid State Technology*, 31:117, Sept, 1988.

[141] J R Hannah and R J Holwill. The statistical modelling of an aluminium reactive ion etch process. In *Nutech 1991: Workshop on Numerical Simulation for Technology Development.*, Sept 23/24 1991. Bad Tolz, Germany.

Appendix A

Statistical Notes

An analysis of variance and definition of terms used within the RS/1 statistical software package is given below, where the mean sum of squares is the sum of squares divided by its degrees of freedom.

Source of variation	Mean sum of squares
S_L^2 = Lack of fit (about regression)	$= \sum_{i=1}^{m} \frac{r_i(\bar{\eta}_i - \hat{\eta}_i)^2}{(m-p)}$
S_e^2 = Pure (experimental) error	$= \sum_{i=1}^{m} \sum_{j=1}^{r_j} \frac{(\eta_{ij} - \bar{\eta}_i)^2}{(n-m)}$
S_R^2 = Residual	$= \sum_{i=1}^{m} \sum_{j=1}^{r_j} \frac{(\eta_{ij} - \hat{\eta}_i)^2}{(n-p)}$
S_T^2 = Total	$= \sum_{i=1}^{m} \sum_{j=1}^{r_j} \frac{(\eta_{ij} - \bar{\eta}_i)^2}{(n-1)}$

where:

m	number of unique x_i locations
n	total number of data points $n = \sum_{i=1}^{m} r_i$
p	total number of parameters in model
r_i	number of data points at $\boldsymbol{\xi}_i$ (replicates)
$\boldsymbol{\xi}_i$	set of values of all independent variables (ξ_i) for data point i
η_{ij}	measured value of dependent variable at $\boldsymbol{\xi}_i$ and replicate r_j
$\hat{\eta}_i$	fitted value of η_i at $\boldsymbol{\xi}_i$ (from model)
$\bar{\eta}_i$	mean measured value of dependent variable at $\boldsymbol{\xi}_i$
$\hat{\eta}$	grand mean of all measured values

In addition to the ANOVA calculations, a number of tests were carried out to test the quality of model fit:

Hypothesis	Statistical test
Goodness of Fit of model	$\frac{S_L^2}{S_e^2}$
Adjusted squared multiple correlation coefficient	$R_{adj}^2 = 1 - \frac{S_R^2}{S_T^2}$

The Goodness of Fit test determines whether the model is an adequate fit for the experimental data i.e., whether the empirical model is a good approximation for the mechanistic model. The test determines whether the model predicted variance in η is larger than the experimentally determined variance.

The adjusted squared multiple correlation coefficient R_{adj}^2 is the proportion of the total variation about the grand mean $\hat{\eta}$ that is explained by the fitted model and has been adjusted to account for the number of parameters in the model.